AFRL-HE-WP-TR-2005-0002

United States Air Force
Air Force Materiel Command
Air Force Research Laboratory

Application of Data Mining and Knowledge Discovery Techniques to Enhance Binary Target Detection and Decision-making for Compromised Visual Images

D. W. Repperger
Air Force Research Laboratory
Human Effectiveness Directorate
Wright-Patterson AFB OH

C. A. Phillips
C. D. Schrider
E. A. Smith
Department of Biomedical
Industrial and Human Factors Engineering
Wright State University
Dayton OH

November 2004

Final Report for February 1990 To November 2004

Human Effectiveness Directorate
Warfighter Interface Division
Collaborative Interfaces Branch
2255 H Street
Wright-Patterson AFB OH 45433-7022

NOTICES

When US Government drawings, specifications, or other data are used for any purpose other than a definitely related Government procurement operation, the Government thereby incurs no responsibility nor any obligation whatsoever, and the fact that the Government may have formulated, furnished, or in any way supplied the said drawings, specifications, or other data, is not to be regarded by implication or otherwise, as in any manner licensing the holder or any other person or corporation, or conveying any rights or permission to manufacture, use, or sell any patented invention that may in any way be related thereto.

Please do not request copies of this report from the Air Force Research Laboratory. Additional copies may be purchased from:

National Technical Information Service
5285 Port Royal Road
Springfield, Virginia 22161

Federal Government agencies and their contractors registered with the Defense Technical Information Center should direct requests for copies of this report to:

Defense Technical Information Center
8725 John J. Kingman Road, Suite 0944
Ft. Belvoir, Virginia 22060-6218

TECHNICAL REVIEW AND APPROVAL

AFRL-HE-WP-TR-2005-0002

This report has been reviewed by the Office of Public Affairs (PA) and is releasable to the National Technical Information Service (NTIS). At NTIS, it will be available to the general public.

This technical report has been reviewed and is approved for publication.

FOR THE COMMANDER

//Signed//

MARIS M. VIKMANIS
Chief, Warfighter Interface Division
Air Force Research Laboratory

REPORT DOCUMENTATION PAGE

Form Approved
OMB No. 074-0188

PLEASE DO NOT RETURN YOUR FORM TO THE ABOVE ADDRESS.

1. REPORT DATE (DD-MMM-YYYY)	2. REPORT TYPE	3. DATES COVERED (From – To)
November 2004	Final Report	February 1990 to November 2004

4. TITLE AND SUBTITLE

Application of Data Mining and Knowledge Discovery Techniques to Enhance Binary Target Detection and Decision-making for Compromised Visual Images

5a. CONTRACT NUMBER

5b. GRANT NUMBER

5c. PROGRAM ELEMENT NUMBER
62202F

6. AUTHOR(S)

*D. W. Repperger
**C. A. Phillips, C D. Schrider, E. A. Smith

5d. PROJECT NUMBER
7184

5e. TASK NUMBER
08

5f. WORKUNIT NUMBER
69

7. PERFORMING ORGANIZATION NAME(S) AND ADDRESS(ES)

**Department of Biomedical, Industrial and Human Factors Engineering
Wright State University, Dayton OH

8. PERFORMING ORGANIZATION REPORT NUMBER

9. SPONSORING / MONITORING AGENCY NAME(S) AND ADDRESS(ES)

*Air Force Research Laboratory
Human Effectiveness Directorate
Warfighter Interface Division
Air Force Materiel Command
Wright-Patterson AFB OH 45433-7022

10. SPONSOR / MONITOR'S ACRONYM
AFRL-HE-WP-TR-2005-0002

11. SPONSOR/MONITOR'S REPORT NUMBER(S)

12. DISTRIBUTION / AVAILABILITY STATEMENT

Approved for public release; distribution is unlimited.

13. SUPPLEMENTARY NOTES

14. ABSTRACT

In an effort to improve decision-making on the identity of unknown objects appearing in visual images when the surrounding environment may be noisy and cluttered, a highly sensitive target detection scheme is developed employing nonlinear dynamical equations. It is first shown that the signal to noise ratio of this particular operation on rudimentary signals can be amplified by a factor of over one million. This means (for elementary signals) that it is possible to effectively magnify the ***"quality of information"*** in an input signal. This procedure affords exciting opportunities in target detection. The input signal may be a sum of sine waves, it could be an auditory signal, or possibly a visual rendering of a scene. Since image processing is an area in which the original data are stationary in some sense (auditory signals suffer from nonstationary effects), the algorithm is applied to a visual rendering scene in a noisy environment.

A description of the mathematical details of the algorithm used for the image enhancement is described in the appendix for completeness. The algorithm is based on a concept from nonlinear dynamics, termed "stochastic resonance." Such a procedure has a biological basis, and may be termed "biomimicry" or "biologically inspired."

15. SUBJECT TERMS

Improved decision-making, image enhancement, nonlinear dynamics, stochastic resonance, biologically inspired systems

16. SECURITY CLASSIFICATION OF:			17. LIMITATION OF ABSTRACT	18. NUMBER OF PAGES	19a. NAME OF RESPONSIBLE PERSON:
a. REPORT	b. ABSTRACT	c. THIS PAGE			Daniel W. Repperger
UNCLAS	UNCLAS	UNCLAS	UNLIMITED	102	19b. TELEPHONE NUMBER *(Include area code)* (937) 255-8765

Standard Form 298 (Rev. 8/98)
Prescribed by ANSI Std. Z39-18

THIS PAGE IS INTENTIONALLY LEFT BLANK

PREFACE

A study was conducted on image processing using a computational method from nonlinear dynamics. This approach has similarities to biological systems and may be considered "bio inspired".

THIS PAGE IS INTENTIONALLY LEFT BLANK

TABLE OF CONTENTS

THIS PAGE IS INTENTIONALLY LEFT BLANK

INTRODUCTION

Decision-making provides the basis for much of our behavior and actions in our environment. There are generally two types of errors that can be made. When a human takes an action, this response may be too aggressive or possibly too conservative depending on his perception of the environment. This perception can be altered prior to the decision-making process. In any event, the two types of errors that result can lead to significantly different cost penalties associated with making each type of error. One simple application of decision-making occurs in the area of Biomedical Engineering. For example, the goal in this case may be to correctly detect the presence of a tumor in a human, when it ***may*** or ***may not*** be present. Based on data from an x-ray or other source, if the decision-making process of the detection is too aggressive (presuming the tumor is at hand when it is really not existent), the results may precipitate an early surgery (exploratory), when it is not needed. This is not desired. However, if the decision-making process is too conservative, then the conclusion would be that the tumor does not exist. If, indeed, a tumor was actually present and growing, the penalty to the human would also be very costly, in a health sense, to ignore this critical information.

In the military application, the effects of being too aggressive or too conservative in decision-making have similar costs and risks. For the military application related to this scenario, the decision maker approaches a tree in a foreign country. In the tree is a camouflaged soldier (cf. Figure 1). The soldier may be either friendly or hostile. An immediate action of the decision maker is required. If the decision-making process is too aggressive, the soldier on the ground will shoot at the object in the tree. If the soldier in the tree is friendly (not hostile), this "friendly fire" incident has a great penalty to the decision maker. On the other hand, if the object in the tree is a hostile (enemy) soldier, the conservative decision to not fire at the object may result in the enemy soldier shooting the decision maker. Thus the error in ignoring the information (much like the tumor example in Biomedical Engineering) is even more costly to the person making the action who is required to elicit a binary choice prior to his response.

Certain attributes that occur in biological systems are going to be employed herein for the target detection problem to synthesize a nonlinear system which will work in a

Hostile Person Hiding in a Tree-Binary Decision-Making Process

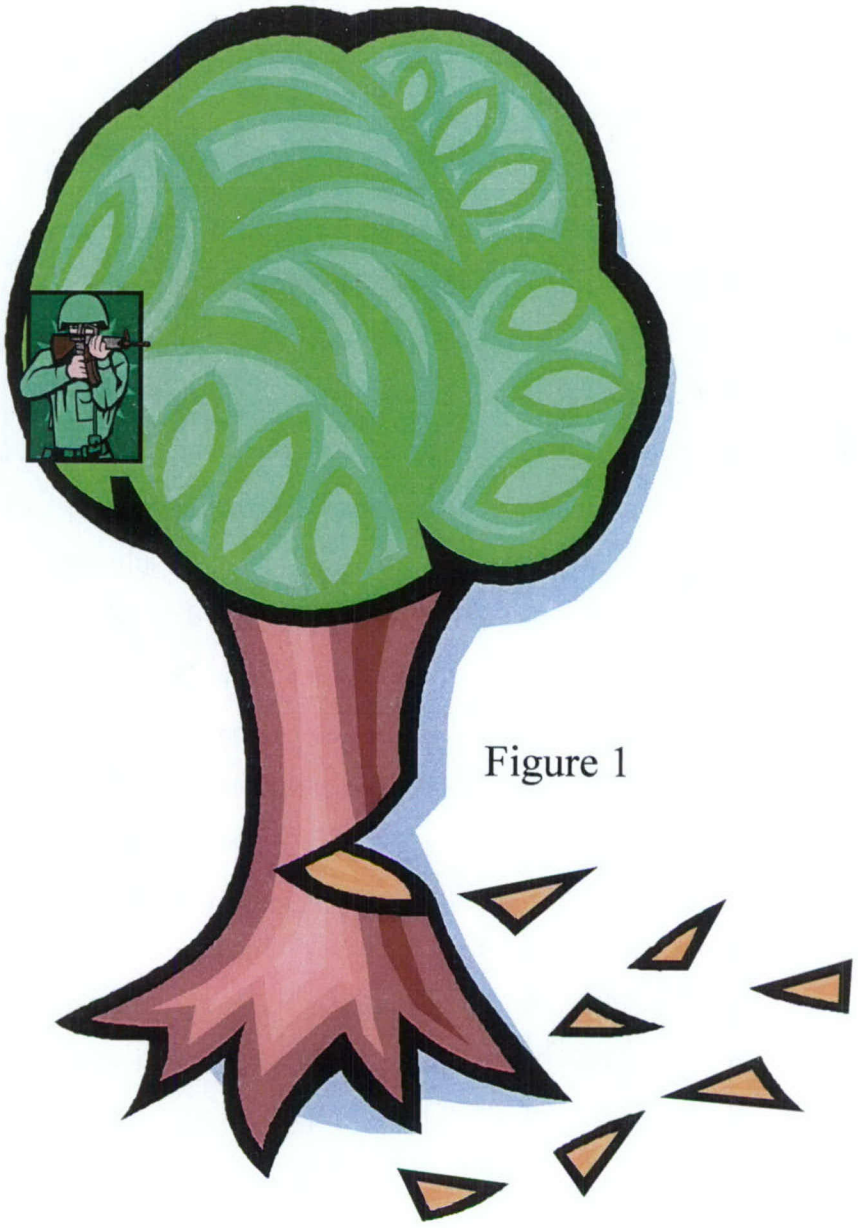

Figure 1

manner to improve target detectability and also increase the signal to noise ratio of the perceived target. It will be shown in the sequel that when the signal to noise ratio increases in a target detection task, both types of errors in decision-making will decrease, accordingly. This method will be shown to be "bioinspired." The strong rationale for emulating biological systems is that, in nature, there are many unexplained phenomenon which have not presently been used for sensing and decision-making. For example, it is well known that when birds migrate annually

from South America to Alaska, they are able to identify precise (and repeatable) locations where they rest on the journey. The position location schemes of these birds are far better than any GPS (global positioning system) derived by humans using linear models and sensors. Another biological analogy involves certain insects which can detect the presence of their opposite gender via smell for a distance over 2 miles. The signal to noise ratio for the detection of such a target stimulus is so small, it must be completely masked by the noise in the environment. Such processes must be nonlinear to have this enhanced sensitivity because no linear system would effectively have the capability to operate functionally in this low signal to noise environment. Hence emulation of biological systems ("bioinspired" or "biomimicry") provides a powerful platform to construct analytic methods to improve decision-making since their existence in nature is proof positive that such a modus operandi can be devised.

This report will study a means of improving decision-making with humans when the data provided may be of very poor quality. The assumptions that are being made are:

(1) Every decision process has some error.

(2) For a binary decision (two choices), there are two types of errors.

(3) The human must respond with an action within a limited time frame.

(4) Our goal will be to simultaneously minimize both types of error described above.

(5) A nonlinear assistive device will enable us to make improved decisions.

(6) We will emulate certain aspects from Biological Systems.

The techniques developed herein will be applied to an image processing problem to show the efficacy of the proposed method. Various types of literature will now be reviewed to set the stage for a methodology to improve decision-making. The first literature review will discuss a related topic, data mining, or means of gleaning information from data.

LITERATURE REVIEW

In order to completely examine a wide range of data relevant to this problem of enhanced target detection, there exists a host of pertinent literature in the area of data mining and knowledge discovery in data, which is applicable to the problem at hand.

Relationship to Data Mining and Knowledge Discovery in Data

Data mining and knowledge discovery in data is now a prevalent problem in our modern information age [1]. In industry, government, academia and elsewhere, there is significant interest in gleaning the relevant knowledge from an overload of information and data that are available. Key research problems include: (1) How to warehouse the data, how to reduce data, (e.g. via feature selection, association, and clustering), how to visualize the data, and how to interpret the reliability of the data? The overall goal is to make predictions or discovery in the data which has different meanings to distinct users [2].

There are a number of analytical means of addressing problems in data mining using, e.g. statistics, pattern recognition, database management and artificial intelligence. The applications include security and criminal detection [3], and in business/marketing for industries [4,5] to assess carefully their competitors and customers. Decisions have to be made on finite and limited use of resources with the ultimate goal of achieving the best information quality decisions based on the available data that can be obtained. In criminal detection, interest exists in classifying and correctly detecting certain patterns [3]. The data may be in the form of text, pictures, or from alternative sources. Developing profiles of high-risk people is of significant interest to enhance law enforcement. A powerful tool used in this context is a decision tree which is a graphical representation of the relationship between a dependent variable (output) and a set of independent variables (inputs) usually in the form of a tree-shaped structure that represents a set of decisions (cf. Figure 2).

For example, to describe a decision tree, in Figure 2, the objective is to determine likely factors that are related to the incidence of high blood pressure. The data are first grouped by those individuals considered as having high or low (normal) blood pressure. From those individuals with high blood pressure, they are further grouped into an age category as being either old or young. If the preponderance of the individuals which are still considered as having high blood pressure are further grouped by weight, the heavy individuals seem to predominant. The tree is the node (round circle) where that category of individuals is being considered. The branches indicate the choices of categories (more than two choices are possible), and the plus or minus sign indicates that the factor under consideration is relevant (+) or not relevant (-).

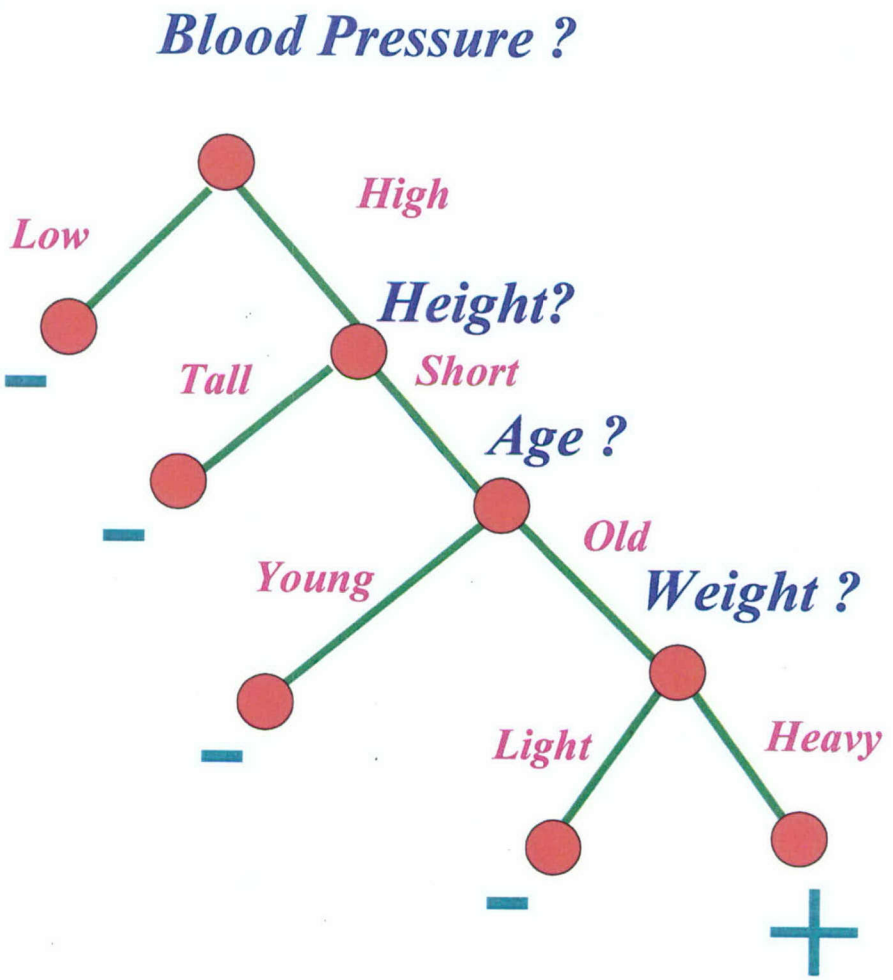

Figure 2 - A Decision Tree for Detecting the Causes of High Blood Pressure

Thus going down the tree in a direction in which the minus signs do not appear indicates that the individuals who have a propensity for high blood pressure are those who are short, older, and of high weight. This decision tree structure has the advantage that computer code can automatically be written, e.g. in pseudo code:

```
If Blood Pressure is = High
  & If height is  = short
    & If age is = old
     &  If weight is = heavy
          Then Blood pressure is high = True
         end
       end
    end
end
```

The business applications of data mining are widely eclectic. This includes building models on which customers may respond to a direct-mail campaign, reducing the number of fraudulent claims with insurance, improving the ability to predict the likely fluctuations in financial markets and in general developing more intelligent and successful strategies for investments [4]. In counter-terrorism applications [5], keeping valuable data both private from hostile groups yet usable to those in the intelligence community provides a great challenge.

Many new technologies now exist for data mining applications [6]. The technologies are sometimes classified as database management and warehousing, machine learning, statistics, decision support, parallel processing, and visualization. The means of projecting data in a visual sense is the most powerful procedure [7] and is the most applied in the field today. Some of the analytical techniques include Bayesian methods (Bayesian nets and adaptive Bayesian), fuzzy sets, and evolutionary computing [8]. Neural networks and preprocessing algorithms can be invaluable in the formation of databases in which the data mining tools can be implemented. Models can be used in the data [9] as a high-level, global description of a data set. Models built in this way may be descriptive (summarizing key points in the data) or inferential (allowing one to make some statement about the population from which the data were drawn or about likely future data values). Score functions can be used as metrics to discern the efficacy of a model. Certainly all evaluations of data mining tools are implicit in statistical methods in the data [10]. We now discuss the concept of SR (stochastic resonance), which can be viewed as a data mining tool when used within the context of enhancing visual images.

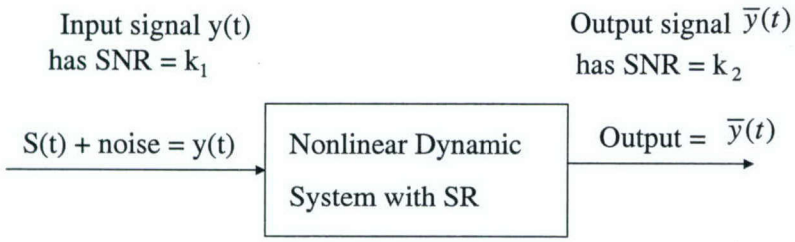

Note: $k_2 / k_1 >> 1$

Figure 3 – Viewing the SR Dynamic Filter as A Signal/Noise Amplifier

The Historical Application of SR (Stochastic Resonance) for Amplification of "Information Quality" in an Input Signal.

Discovered in the early 1980's [11] to explain the abnormal periodicity of ice ages, physicists for the next 20 years used this concept to model and elucidate phenomenon from a variety of physical processes. In more recent times [12-15], it has been shown that the method described as "Stochastic Resonance" will yield an amplification of signal to noise ratio (SNR). Figure 3 portrays this concept using a block diagram. In Figure 3 the input to the block is the signal y(t) = *S(t)* plus a noise source. The two signals (*S(t)* and the noise) are added together to form y(t) which is then transformed by the SR filter. This block in Figure 3 can also be viewed as a coordinate transformation. The output signal from the block is y_bar(t). The SNR in the input signal y(t) is k_1. The SNR in the output signal y_bar(t) is k_2. The overall gain (information quality) of this process is the ratio of k_2 to k_1 which can turn out to be larger than unity. At first this seems to be an incredible result, i.e. we have *improved the information quality* of the input signal (*S(t)* + noise) by processing the data through this special filter. This has analogies to data mining or knowledge discovery since we can now uncover key elements in the data by processing the signals through the coordinate transformation as shown in Figure 3. More quantitatively:

$$\text{SNR gain} = k_2 / k_1 >> 1 \qquad (1)$$

where it is shown, later, that this SNR gain may be six orders of magnitude or more for certain elementary signals. Related to this work, others have noted, theoretically, [16] that target detection, by itself, can be enhanced for the case of certain classes of nonlinear systems with the addition of random disturbances.

An Early Application to Image Enhancement Using the SR Technique

In early 1995, some evidence surfaced in the Biomedical and image processing community to suggest that certain nonlinear operations on image data can enhance detectability of hidden objects. More recently, [17] has shown that the signal to noise ratio can be improved in certain types of image processing by the application of just the noise alone. In their application a hierarchical cluster analysis was employed with a stochastic disturbance (noise) which improved the signal-to-noise ratio for the identification of functional MRI patterns. Similarly, in [18-32], there now exists a wide range of evidence that patterns and images are enhanced by the addition of certain types of noise. To show an example of how SR can enhance the contrast of an image, Figure 4 from [28] is used as an instance. In Figure 4, moving to the right, the intensity of the white Gaussian noise is increased. The goal is to identify the object in the diagram. Obviously too much noise or too little noise degrades the identification of the object.

Too little noise Optimum noise level Too much noise

Direction of increasing noise intensity

Figure 4 from [28] illustrating how SR can enhance a visual image.

The ultimate step in this process would be to develop image-processing algorithms using some of the techniques from SR. First we will investigate this improvement of target detectability within a framework involving decision-making.

THE BASIC CONCEPTS OF DECISION-MAKING– TYPE 1 AND TYPE 2 ERRORS

Figures 5a-b facilitate the discussion on how the procedure described herein will assist in the improvement of decision making. Present day methods will either reduce type 1 error ***or*** type 2 error (***but not both simultaneously***). With reference to the problem of detecting the object in the tree in Figure 1, let us denote the truth is H_0 if the object in the tree is friendly. Alternatively, the hypothesis H_1 is that the object is hostile. If the decision maker decides to shoot at the object (and it is friendly or H_0), this is termed a Type 1 error. In Figure 5a the area A_1 represents all these Type 1 errors. If, however, the object (or target in the tree) is hostile and the decision is to not shoot at the object, this is a second type of error (Type 2 error) and is

denoted by the area A_2 in Figure 5a. Both types of errors have significant consequences on the mission. The goal is to minimize both Type 1 and Type 2 errors. Figure 5b can be compared to Figure 5a. Figure 5b

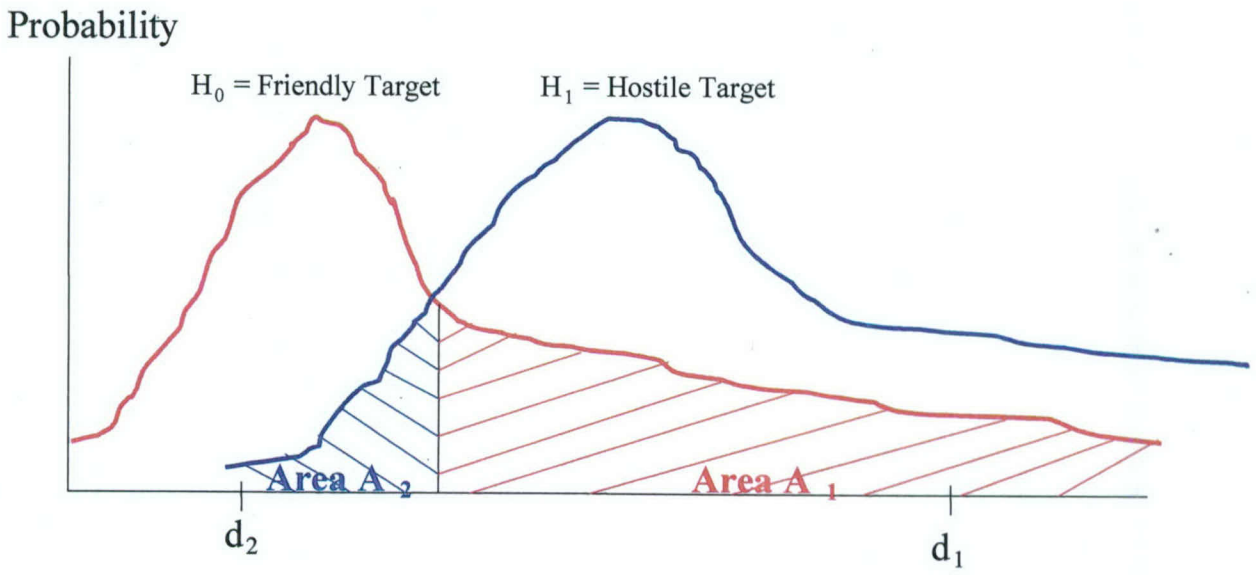

Figure 5a - Decision Making Process

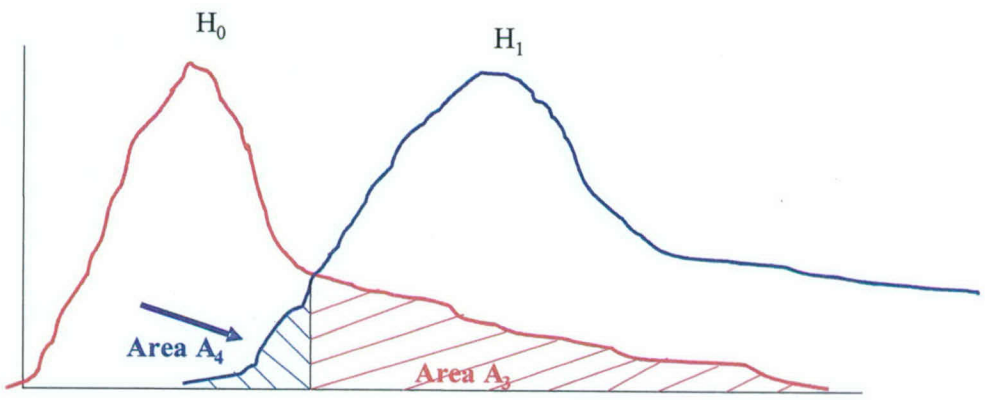

Figure 5b - Improved Decision Making Process

represents a better decision making process because both the Type 1 and Type 2 errors are reduced. That is, $A_3 < A_1$ and $A_4 < A_2$. Thus both types of error are reduced simultaneously. Typically what is accomplished in the modern day assessment processes is that decision makers

work with the x-axis of Figure 5a. They make a binary choice on a measured variable (d_1 or d_2) and will select either H_0 or H_1 according to how aggressive or conservative they wish to be in identifying the unknown object in the tree. By sliding along on the x axis of Figure 5a, either the Type 1 ***or*** the Type 2 error is reduced. If one is reduced, the other is correspondingly increased.

What will be different in the approach taken here is that ***both*** the Type 1 and Type 2 error will simultaneously be reduced. Before this methodology is explained, a quantitative description of signal to noise (SNR) will be reviewed.

THE CONCEPT OF SNR WHEN USED IN TARGET DETECTION

In this section we generalize the discussion so far to describe a quantitative description of the SNR and the underlying assumptions required to characterize the ability to detect targets correctly. For a straightforward binary decision, Figure 6 shows a simplified description of a decision making process for two distributions, analogous to Figures 5a-5b. The distribution H_0 has mean of μ_0 and standard deviation σ_0. The distribution H_1 has a mean of μ_1 and standard

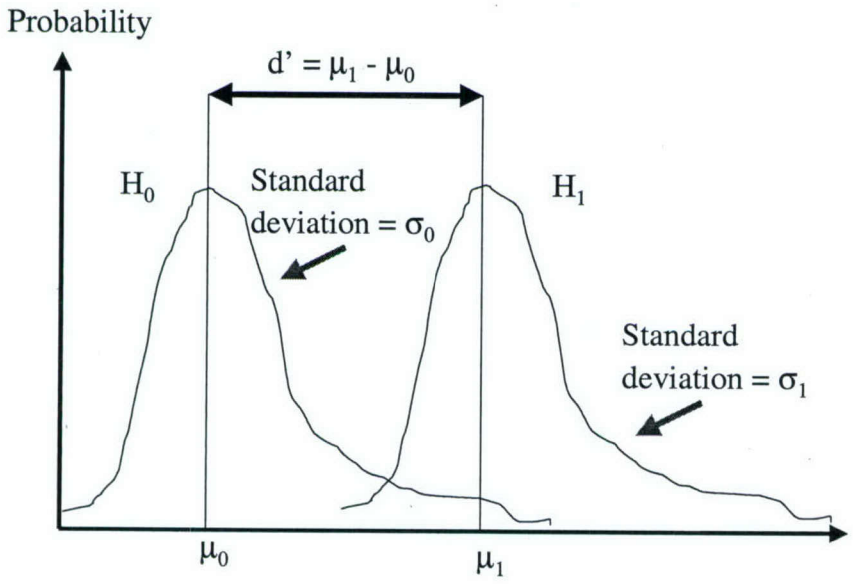

Figure 6 - Defining SNR for Detection in a Binary Decision Process

deviation σ_1. If an approximation can be made that $\sigma_0 = \sigma_1 = \sigma$, and a sensitivity parameter d' is defined via:

$$d' = \mu_1 - \mu_0 \quad (2)$$

Then the SNR is typically defined via:

$$SNR = d' / \sigma \quad (3)$$

Thus if the two distributions in Figure 6 are far apart, then d' is large and this enhances the distinction between the two distributions and the SNR is large. If the σ is small (or made smaller), then the SNR also increases and, again, it is easier to discern the two distributions. Figure 7 shows the ROC (Receiver Operator Characteristic) curve that summarizes the main points in Figure 6 into an easy to understand diagram.

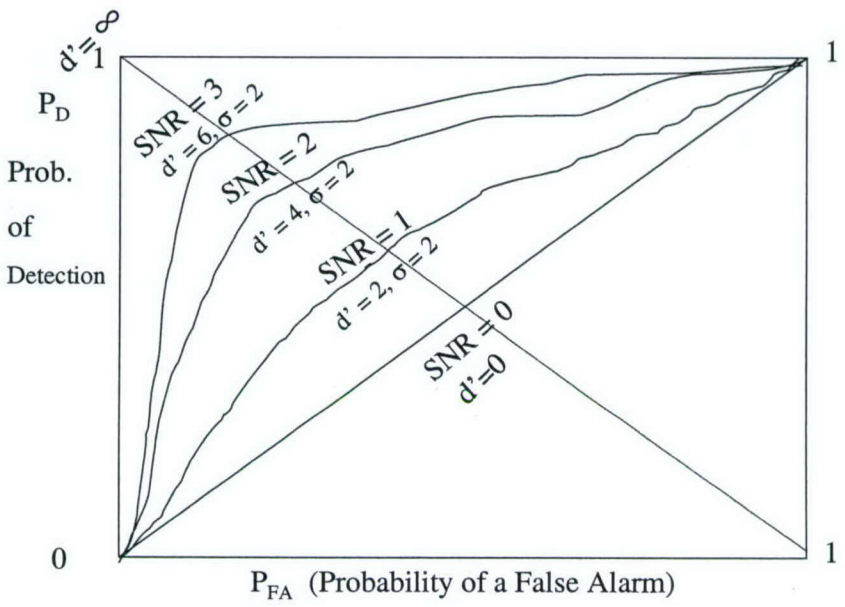

Figure 7 – The ROC (receiver operating characteristic) Curve

In Figure 7, the ROC curve is a plot of probability of detection (P_D) on the y axis versus Probability of a False Alarm (P_{FA}) on the x axis. This plot is sometimes termed sensitivity (y axis) versus 1-specificity (x axis). In Figure 7, the diagonal denoted as SNR = 0 represents random guessing on one of the binary choices. In this case the distribution functions in Figure 6 completely overlap (d' = 0). As the signal to noise ratio increases, however, (d' increases), the operating curves in Figure 7 tend to move to the upper left-hand corner of the diagram. The best plot would occur if the curves of operation would start at the origin and to go directly up to the top left point (0,1) and then transverse right to the point (1,1). The area enclosed under this ROC

curve is sometimes used as a measure of the efficacy of the decision making process. The Type 1 and Type 2 errors can also be easily defined in the ROC curve in Figure 7.

It will be shown in the sequel that the SR procedure will actually increase the SNR and thus improve the propensity to make a correct detection of targets in obscure environments. Before this can be presented, two examples from Physics will be discussed to illustrate why SR can improve sensitivity to the detectability of faint targets, when they are not immediately apparent.

EXAMPLE 1 OF SR – IDENTIFICATION OF A SUBLIMINAL SIGNAL BELOW A THRESHOLD.

Figure 8 shows one physical example of how SR can provide some advantage in the detection of faint or weak signals.

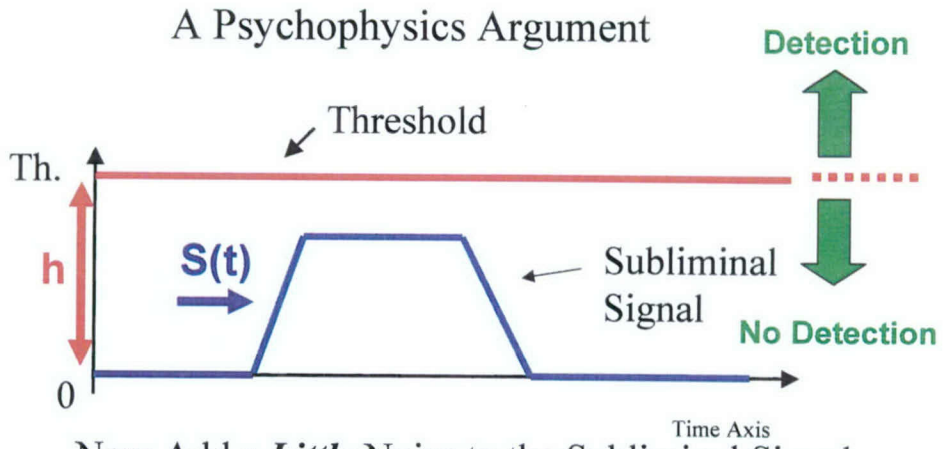

Now Add a ***Little*** Noise to the Subliminal Signal

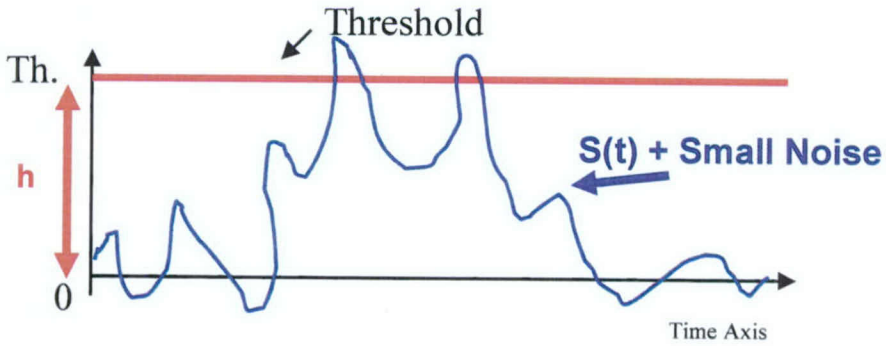

Now Add ***a Lot of*** Noise to the Subliminal Signal

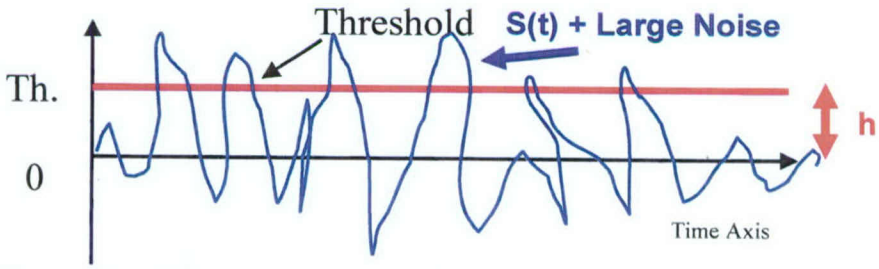

Figure 8 – SR Viewed as Detecting a Subliminal Signal

Figure 9 summarizes the discussion so far on how one can interpret the SR effect.

Figure 9 – Statistical Interpretation of SR

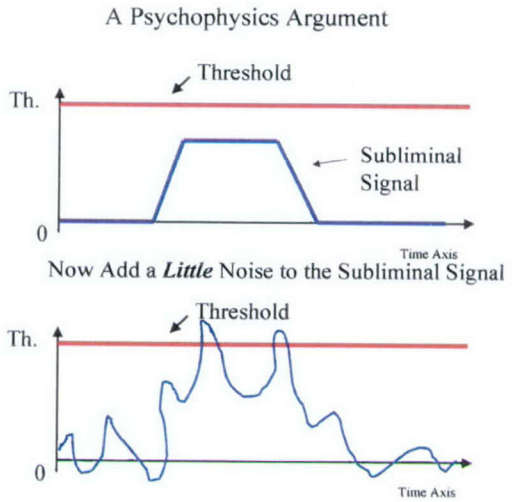

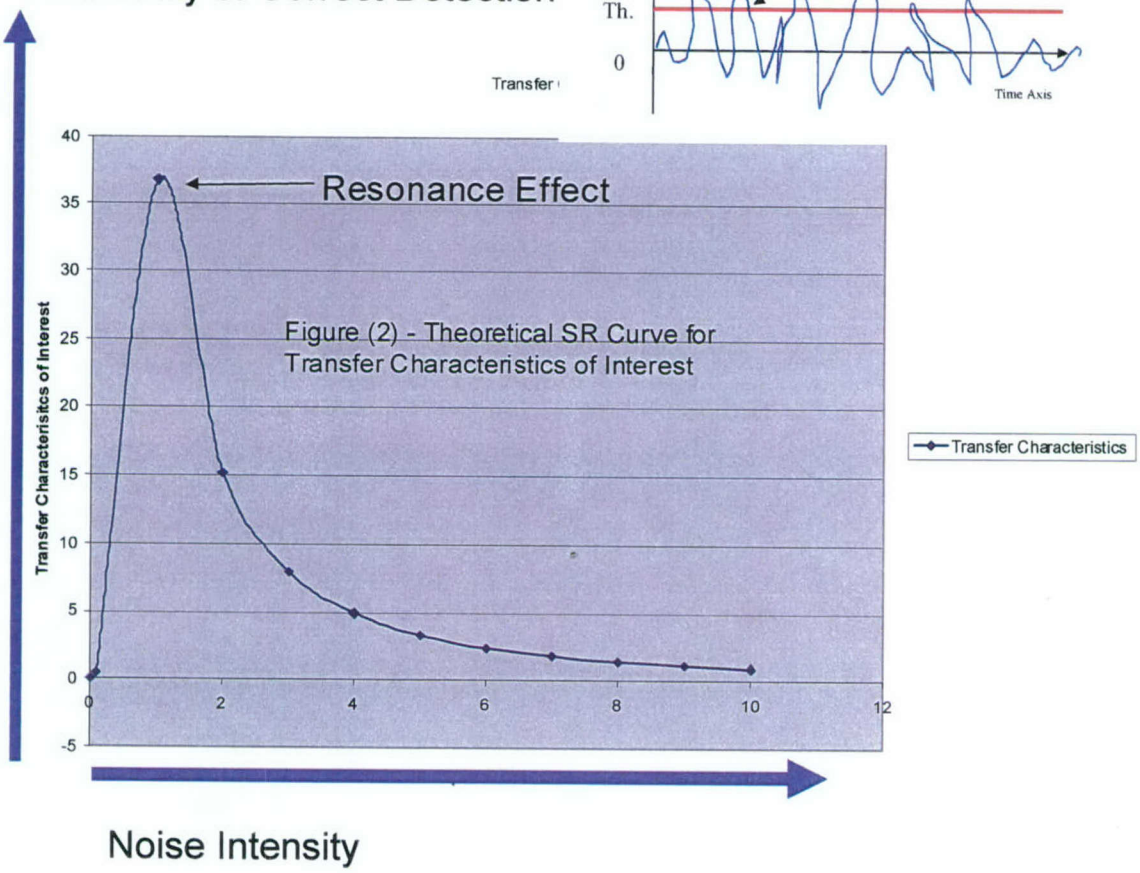

To explain Figures 8 and 9, it is seen in Figure 8 that it is desired to correctly detect the subliminal signal *S(t)* when it is in the high state (high level of the trapezoidal signal), yet submersed below the threshold of value h. In Figure 8, top plot, even when the subliminal signal

is in the high state, it cannot be detected because all signals are below the threshold. In the middle plot of Figure 8, a small amount of noise has been added to *S(t)*. It is now seen that when the trapezoid is in the high state, it occasionally pierces through the threshold and appears above the threshold. Thus it is correctly detected as being in the high state. Hence the number of missed negatives (detecting *S(t)* when it is really high) is reduced somewhat. In the bottom plot of Figure 8, the intensity of the added noise is still further increased. Here it is seen that the combined signal *S(t)* + noise pierces through the threshold even when it is in the low state. This leads to a false positive (we think *S(t)* is high, when it is really low). Thus the number of missed negatives is less by increasing the noise as we go down the graphs of Figure 8, however, the number of false positives increases, causing a reduced number of correct detections. In Figure 9, this discussion is summarized. Here is seen the stochastic resonance curve. The y axis of this curve is proportional to the probability of correct detection of *S(t)* when it is really high. The x axis is the intensity of the noise (power or variance). The SR resonance curve acts similar to what was shown in Figure 8, when increasing noise tends to first help the decision-making process and then tends to hurt the process of correctly classifying *S(t)* when it is in its high state. To describe this curve, starting at the origin in the bottom graph in Figure 9, the curve must start at the origin. This is because if the subliminal signal is below the threshold (no noise added), then the probability of correct detection of *S(t)* in the high state is zero. Moving to the right from the origin in this diagram, the curve rises because as the intensity of the noise increases, the number of missed negatives quickly decreases and the number of false positives slowly increases. The curve rises until a resonance point is reach as denoted in Figure 9. To the right of the resonance point on the SR curve, the number of missed negatives still is decreasing but the increasing of the number of false positives makes the overall decision process less effective. Thus the curve drops to the right of the resonance point as the noise intensity continues to increase. The curve gradually returns to zero, just as in Figure 9, when the substantial increase of the noise produces so many false positives, that the overall decision making process is compromised.

The second example from Physics is very analogous to the first example in the sense that the detectability of a high state of a subliminal signal will be enhanced by the addition of the noise. The advantage of the second example is that the dynamical equations of motion can now be obtained which will help in the numerical integration of a filter to process signals.

EXAMPLE 2 OF SR – THE BIPOTENTIAL WELL PROBLEM

Figures 10a-b portrays a second example which describes the SR effect. This example is very popular within the Physics community.

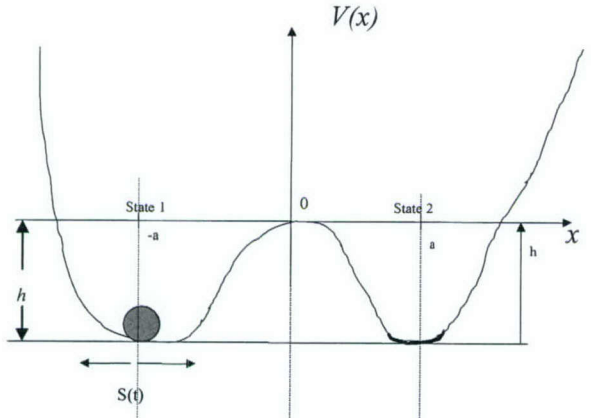

Figure 10a – The Bi-Potential Well Problem

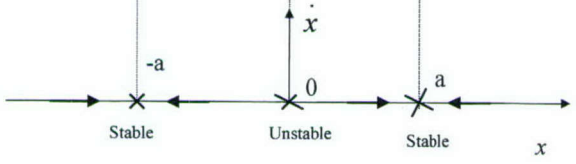

Figure 10b – Equilibrium Points for the Physical System

To explain Figures 10a-b, the green ball is trapped in one or two potential wells. The signal *S(t)* represents the subliminal signal. The signal *S(t)* could represent the trapezoid of Figure 8, which can be in either a high or low state. The height of the potential well in Figure 10a is h units. This is analogous to the threshold of h units in Figure 8. Again, since *S(t)* is always below h units, it cannot transverse the threshold and change states. The right state (x = a) will be denoted as the high state; the left state (x = - a) will be denoted as the low state. White Gaussian noise is now added to *S(t)*. The combined signal *S(t)* + noise will now overcome the potential barrier of h units (analogous to piercing the threshold in Figure 8) and switch states (or equilibrium points). If too much noise is added (high intensity), the signal *S(t)* will continue to switch equilibrium points, even when it does not toggle between the low and high state. Thus the correlation

between *S(t)* switching states and toggling between the right and left potential wells starts to degrade with the addition of too much noise. Figure 10b displays the physical equilibrium points of the Physics example in Figure 10a. It is noted that the potential well is characterized by two stable equilibrium points interlaced between an unstable equilibrium point. In Figure 10b, when x = -a is called a stable equilibrium point. This is true because if the ball is resting in this potential well and is perturbed slightly, the motion always returns to the original equilibrium point. This is also true when x = a. Here, again, if the ball is perturbed slightly, it returns to the equilibrium point x = a. The point x = 0, however, is an unstable equilibrium point. It is observed that small perturbations about the point x = 0 results in the ball moving either right or left away from the original equilibrium point. This is characteristic of an unstable equilibrium point.

Now the efficacy of this work, it will be demonstrated. The ability of the SR filter to amplify the signal to noise ratio in an input signal (consisting of elementary signals) to extreme amounts will be demonstrated. This computer simulation study will now be presented to show the extent of this gain. For elementary signal analysis (two sine waves), it was demonstrated [33] that the signal to noise amplification for a block similar to Figure 3 could exceed 1 million or more, hence substantially increasing the likelihood of a correct detection of a target, especially when it is subliminal.

COMPUTER SIMULATION OF IMPROVED SNR FOR ELEMENTARY SIGNALS

To fairly test the SR process, an input signal *S(t)* will be selected to be the sum of two sine waves (with unity amplitude and having frequencies of 1 and 4 hertz (Hz)) denoted as follows:

$$S(t) = \sin(2 \pi (1) t) + \sin (2 \pi (4) t) \qquad (4)$$

Rationale for Selecting *S(t)* to be the Sum of Two Basic Sinusoids

The selection of *S(t)* in equation (4) is to consist of two sinusoids of different frequencies and equal amplitude. The rationale for this selection of a target signal is derived from studies in

signal analysis where a measured signal is typically decomposed into its Fourier components as described in equation (5) as an inverse transform:

$$y(t) \approx \text{ Inverse Fourier Transform of } \{Y(j\omega)\} \approx \sum_{i=1}^{N} a_i \sin(\omega_i t + \phi) + b_i \cos(\omega_i t + \phi) \quad (5)$$

where the Fourier components (amplitude coefficients a_i and b_i of equation (5)) occur at the frequencies ω_i as the significantly important components of the signal *y(t)*. In equation (5), only *N* frequencies are considered, which is an approximation to the original signal *y(t)*. Since most signals in nature have a substantial portion of their spectral power at low frequencies, the approximation of the first *N* components seems pragmatic. The task of target detection can be formulated as the role of identifying a single (or multiple) sinusoid(s) in noise or possibly distinguishing two different target signals. The task is then to identify the signature of each target (sets of a_i, b_i and ω_i values from the Fourier analysis that make the targets different) when buried in noise. The goal here is to clearly distinguish the Fourier components of *S(t)* as being different from the adjacent noise signals that appear in the power spectral analysis of the signals *y(t)* or *y_bar(t)*. In real time, Figure (11) displays a plot of $S(t) = \sin(2\pi t)+\sin(8\pi t)$ versus time in seconds over a four second time period.

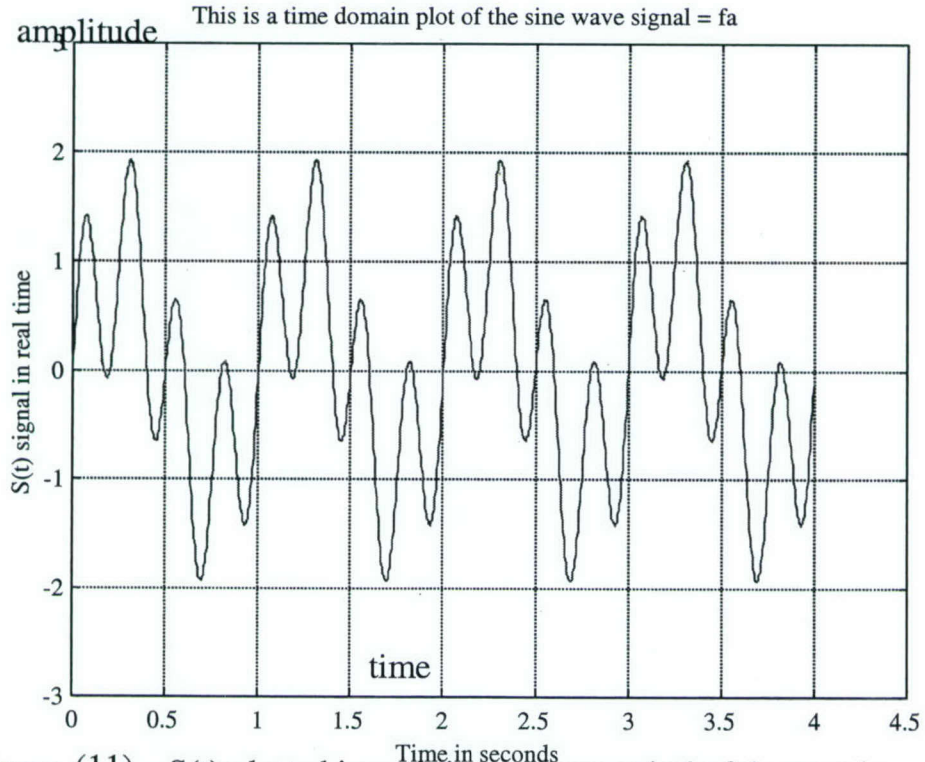

Figure (11) – S(t) plotted in real time over a period of 4 seconds.

It is seen that the components of 1 Hz and 4 Hz are very apparent in the signal in Figure (11). To see this effect even more clearly, a fast Fourier transform (FFT) operation of the signal *S(t)* is displayed in Figure (12). In Figure (12) it is observed, for this two sine wave signal, that the power in *S(t)*, in the frequency domain, is equally concentrated at the points1 Hz and 4 Hz on the x axis of Figure (12).

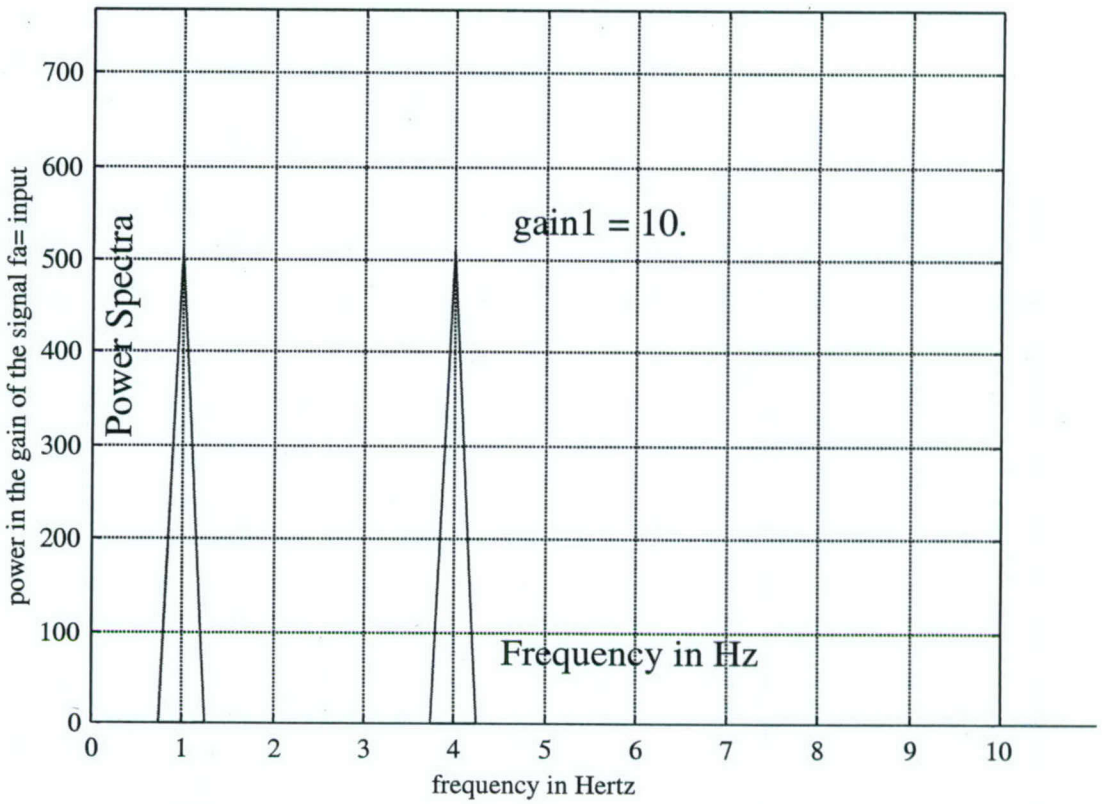

Figure (12) - An Fast Fourier Transform of *S(t)* in Figure (11)

From Figure (12), it is extremely easy to distinguish the two constituent components that make up *S(t)* (the peak power at 1 and 4 Hz).

With the addition of noise, however, the lucid diagram in Figure (12) now becomes quite muddled. The input signal to now be analyzed is *y(t)* which contains the sum of *S(t)* and white-Gaussian noise, i.e. *y(t)* satisfies:

$$y(t) = S(t) + \eta(t) \qquad (6)$$

and the fast Fourier transform is now performed on *y(t)* rather than *S(t)*. As the power of the noise ($\eta(t)$) term increases, the goal is to still attempt to identify (and distinguish) the two peaks of *S(t)* in the frequency domain at 1 Hz and 4 Hz from the power spectra plots of *y(t)* or from its

transformed counterpart *y_bar*(t) illustrated in Figure (3). It is noted that the zero mean Gaussian (normal) noise source $\eta(t)$ has a density function specified via:

$$\text{density function} = g(x) = \frac{1}{\sigma\sqrt{2\pi}} e^{-x^2/2\sigma^2} \qquad (7)$$

where σ is the standard deviation of the zero mean Gaussian random process $\eta(t)$ in equation (6). For simulation purposes, to compare conventional detection methods to those of the SR nonlinear dynamical system, the pure, deterministic signal $S(t)$ was slightly modified to be of the form:

$$S(t) = \text{gain1} * [\sin(2\pi(1)t) + \sin(2\pi(4)t)] \qquad (8)$$

and the noise term is describe via

$$\eta(t) = \text{gain1} * \text{gain2} * \text{randn}(.) \qquad (9)$$

where the function randn(.) is used in MATLAB™ to call the white-Gaussian noise generator. Noting that the constant, gain1, multiplies both $S(t)$ and $\eta(t)$, then the remaining variable in equation (9) (gain2) is the only influence on the SNR with the standard deviation of the noise source σ set = 1. The calculation of the SNR in the frequency domain is proportional to the square of the magnitudes of the Fourier components of $S(t)$ to the corresponding values for $\eta(t)$. Thus, it can be shown that the relative comparison of any numerical simulation in terms of SNR is proportional to $(1/(\text{gain2}))^2$ compared to the baseline condition (gain2=1)). The gain1 term has no effect on the SNR but sets up a baseline or standard for all relative measurements of both the signal and the noise. A series of plots of the output variable are now displayed for:

$$y(t) = S(t) + \eta(t) \qquad (10)$$

with their fast Fourier transform sketches provided for this method which will be termed the "conventional method".

Conventional Method (Not Using the SR Nonlinear Dynamical Filter)

The conventional method will deal with the analysis of the signal $y(t)$ (before the filtering) using Fourier analysis. Figure (13) illustrates the FFT plot of $y(t)$ for the case of gain1=10 and gain2=1. This corresponds to a baseline condition to study the SNR as gain2 is manipulated. It is seen in Figures (13-15) that the power in the spectral components of the noise (normal, Gaussian) appears at all frequencies and slowly creeps upward as gain2 increases in

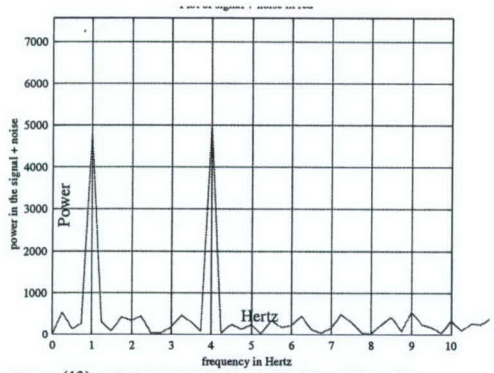

Figure (13) – Gain1=10, Gain 2 = 1 Traditional Detection

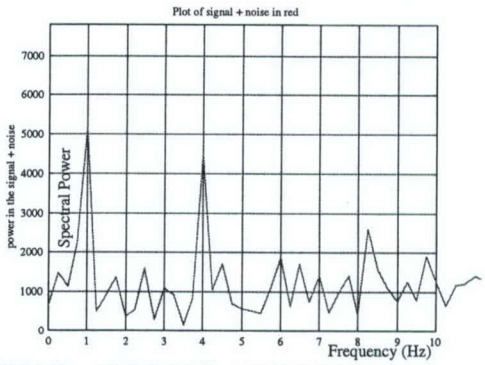

Figure (14) – Gain1=10, Gain 2 = 4 Traditional Detection

Figures (13-15) to the point that it will eventually cause confusion in the identification of the target signals at 1 Hz and 4 Hz. Figure (15) portrays the FFT of *y(t)* when the variable gain2 = 7.

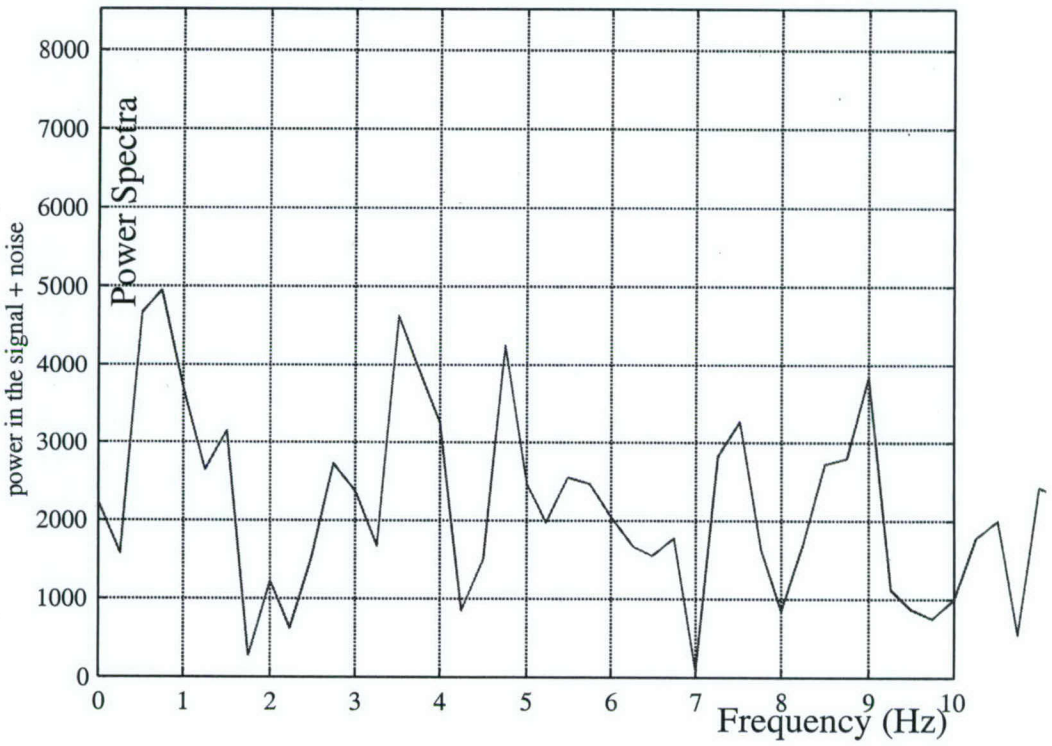

Figure (15) – Gain1=10, Gain 2 = 7 Traditional Detection

From Figure (15), it is obvious that it is now much more difficult to discern the peaks of the 1Hz and 4 Hz signal because of the masking introduced by the noise. The actual SNR in Figure (15) is proportional to $1/(7)^2$ compared to the baseline condition in Figure (13). From observing Figure (15), it is obvious that if gain2 > 7, it becomes increasingly difficult to accurately detect a target comprised of the deterministic (sine waves at 1 Hz and 4 Hz) signals contained in *S(t)*.

The next step is to now pass the y(t) signal through the SR filter. This method, using y_bar(t) rather than y(t), will be termed the "nonconventional method".

Nonconventional Methods (Using the SR Nonlinear Dynamical Filter)

The new or nonconventional method will now deal with the signal *y_bar(t)* after it has been transformed by passing *y(t)* through the nonlinear SR filter in Figure (3). Power spectral analysis will also be performed on the signals *y_bar(t)* and contrasted to those similar analyzes performed on *y(t)*. As a comparison to the data presented in Figures (13- 15), the real time noisy data *y(t)* are now transformed by the nonlinear dynamic system of Figure (3). The FFT analysis was then conducted on the output signal *y_bar(t)* as described in Figure (3). The gain2 variable was adjusted upward to take on situations in which gain2 >> 7. We illustrate, for comparison, some extreme examples. Recall from the conventional method (Figure (15)), if gain2 $\geq$ 7 (with a SNR of $1/(7)^2$ as compared to Figure (13)), the conventional method in distinguishing the two input signals fails at about gain2 $\geq$ 7. Figure (16) illustrates the output (*y_bar(t)*) of the SR nonlinear filter in real time when the value of gain2 = 200, gain1 = 10, and $h = 0.1$ for the potential barrier height of the SR filter described in the appendix.

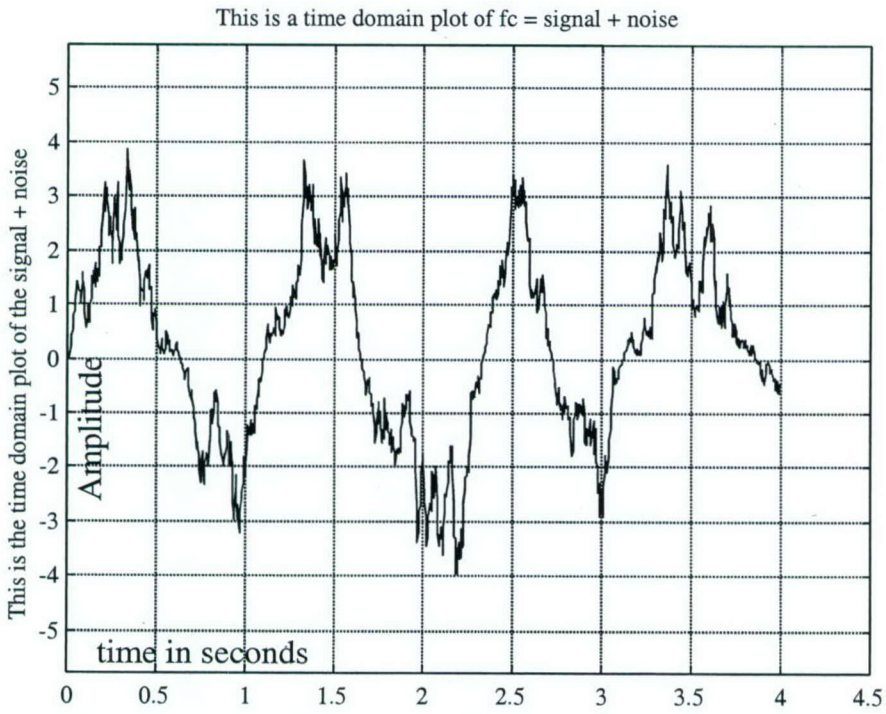

Figure (16)-Output of SR filter with h=0.1, gain1 = 10, gain2 = 200

A comparison should be made between Figures (16) and (11), the latter of which consists of noise-free data (in real time). It is seen in Figure (17) (FFT of Figure (16)) that even with a significantly reduced SNR (comparing $1/(7)^2$ to $1/(200)^2$) it is still possible in Figure (17) to discern, ***in a spectral sense***, that a significant event occurs at a 1 Hz component and at a 4 Hz component of the input signal. This seems plausible in comparing Figure (16) to Figure (11) where the output seems periodic and somewhat in phase with the true deterministic signal.

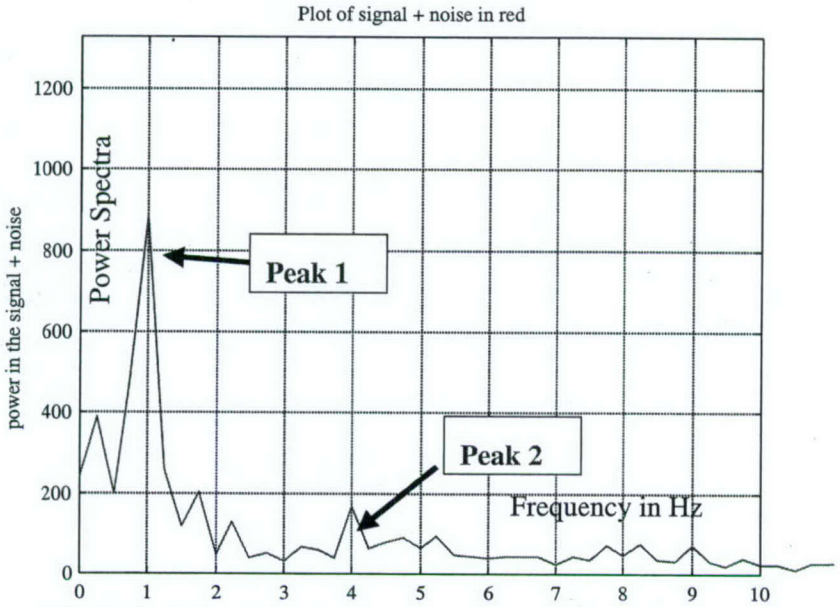

Figure (17)- FFT of Figure D.7 using SR output, h = 0.1, gain1 = 10 and gain2 = 200.

From Figure (17), it is clear that it is possible to discern the two frequencies in the input signal $S(t)$, even when the SNR has been compromised by a factor of $(1/(7)^2) / (1/(200))^2$ which represents an amplification of the SNR (in the spirit of Figure (17) to over 800 to 1) by using the SR filter. There are, of course, several shortcomings with this procedure, which need to be discussed.

Shortcomings of the SR Nonlinear Dynamic Filter

There are two ways the filter thus described can have inferior performance:

(1) Computational complexity can increase in a substantial manner.

(2) Distortion of the original signal can occur.

(1) For the computational complexity issue, runs have been conducted for values of gain2 at levels of 900 or more. Figure (18) illustrates a plot of the number of FLOPS (Floating Point Operations) necessary to compute the SR filter output *y_bar(t)*.

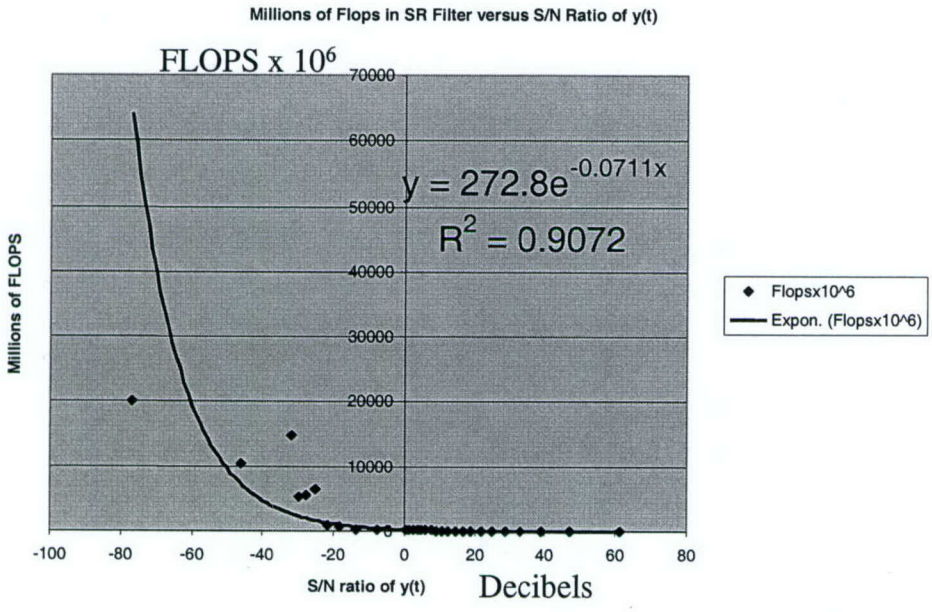

Figure (18) – Millions of FLOPS versus SNR ratio (dB) for the SR Filter

It should be noted that the significant number of FLOPS which are required at high noise levels (negative values of SNR) is due to the nature of the integration subroutine employed in MATLAB™. The most accurate method was engaged. It utilized fourth order Runge-Kutta predictor corrector methods. Such methods require a significant number of iterations before convergence. The way that Runge-Kutta works is that the integration will not be complete until certain convergence criteria are met and the error between adjacent estimates of the derivative terms is below a specified bound. This prolongs the time and multiplications necessary to perform the numerical integration, since a high accuracy and numerical iterations are required before each step is considered solved by the integration subroutine. The high noise, when added to *S(t)*, acts like a "stiff" differential equation (sudden change in the value of the x variable), which takes substantial time for the integration subroutine to be satisfied that the accuracy of the method has been achieved. This may be ameliorated if hardware could perform this task in lieu of a software method. For example, in the case of gain2 at a level of 900 requires approximately

$2x10^{10}$ FLOPS or 20 Giga FLOPS which can be computationally excessive. In some applications, however, when it is essential to detect an extremely weak signal in noise, it is still possible to use the method as described in this appendix to glean out information if computation time is not a critical issue.

(2) Figure (19) displays how distorted the output signal *y_bar(t)* for the SR filter in Figure (3) may become as gain2 approaches values of 900 or more. Superimposed on the plot for *y_bar(t)* is the original signal *S(t)* in real time (gain1 = 10). The transformed signal *y_bar(t)* in Figure (19) (for gain2 = 900) does not even complete a full four cycles over the 4 seconds of data which introduces a nonzero mean(dc) component. This distorts *y_bar(t)* from the original signal *S(t)* both in phase and in amplitude. When the FFTs are run, a resulting dc component (bias) is obtained which influences whether an accurate detection may occur, especially at low frequencies.

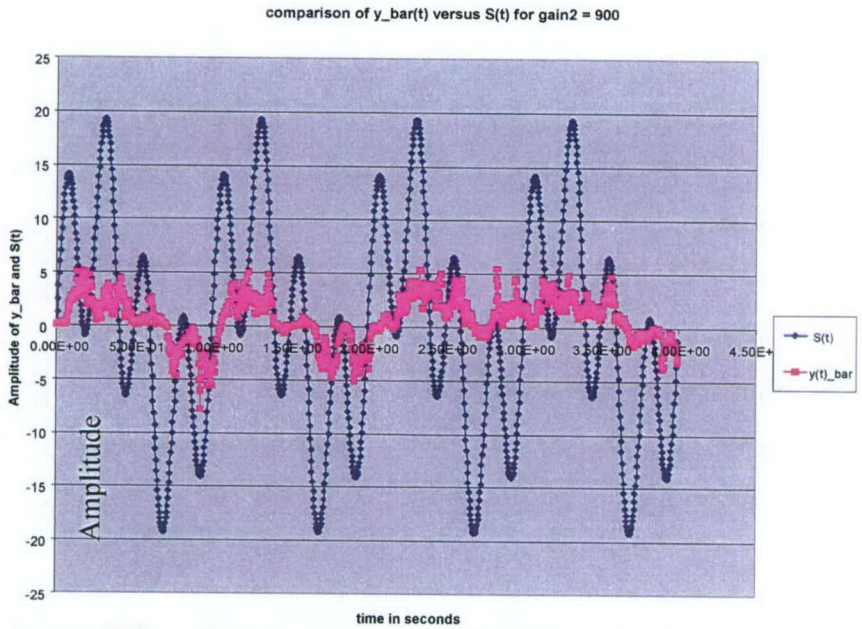

Figure (19) - Overlay of *y_bar(t)* and *S(t)* for gain2=900

This is to not an unusual result to expect since a nonlinear system has transformed the data from *y(t)* to *y_bar(t)* which will normally produce distortion of this type to a sine wave input. It is interesting to note that the FFT of Figure (19) for *y_bar(t)* shows the peaks of *S(t)* as demonstrated in Figure (20). Recall that the noise factor is now gain2 = 900, which translates

into a SNR of approximately - 55 dB. This is an incredible result considering the intensity of the noise relative to the power in the target signal $S(t)$.

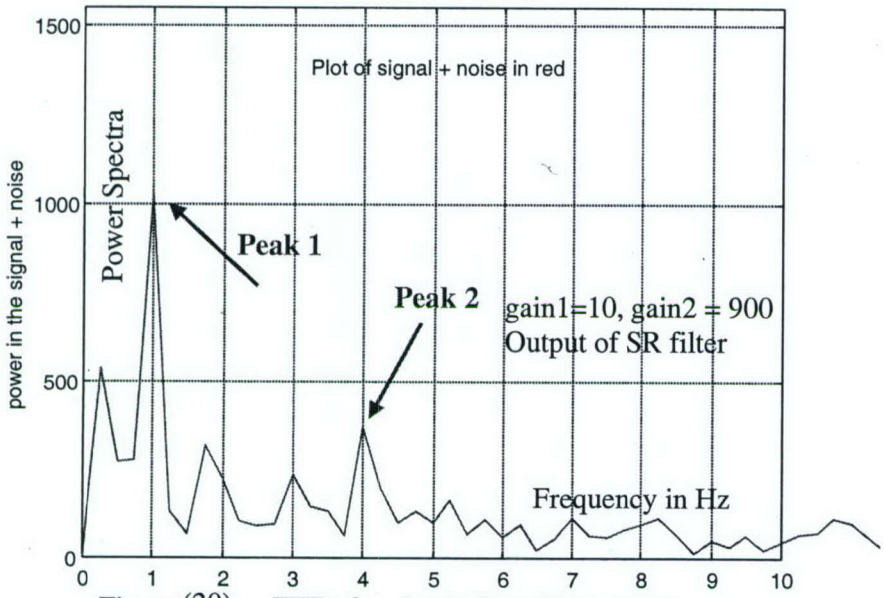

Figure (20) - FFT of $y\_bar(t)$ from Figure (19)

Finally we conclude with an overall signal to noise ratio comparison of the conventional methods (using $y(t)$) versus the SR filter procedure (using $y\_bar(t)$) thus far discussed in terms of the information quality gain of the input signal $y(t) = S(t) + \eta(t)$.

NUMERICAL COMPARISON OF THE CONVENTIONAL METHOD TO THE SR FILTER

Figure (21) illustrates the overall comparison of the performance of the SR filter to the conventional methods as discussed previously. The performance of both systems in

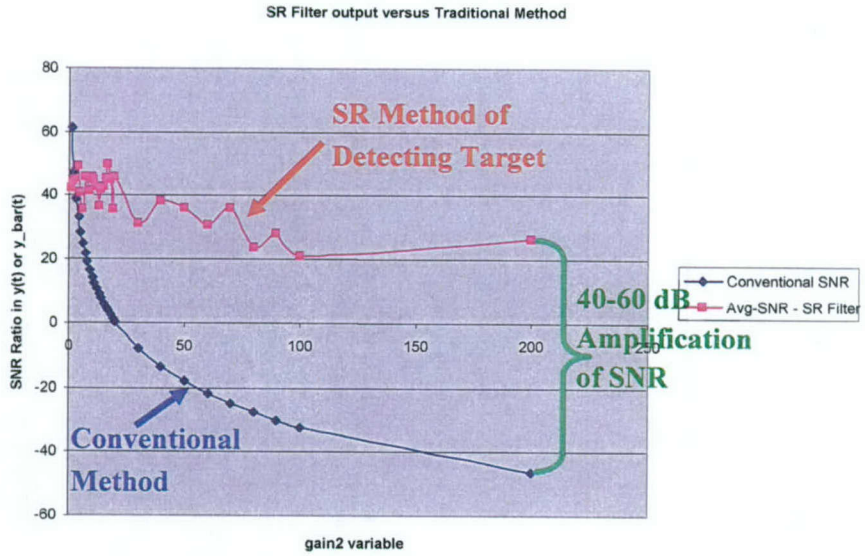

Figure (21)– Comparison of Conventional Method to the SR Transformed Data

estimating a target is based on a procedure [34] to deal with detecting targets when passed through nonlinear transformations such as portrayed in Figure (3). The definition of SNR (in decibels or dB- a devised unit for amplification of information quality) is specified via:

$$\text{SNR} = 10 \log_{10} \frac{S(\omega_0)}{N(\omega_0)} \tag{11}$$

Where, at the frequency ω_0, the power in the target signal $S(\omega_0)$ is determined as well as the noise power $N(\omega_0)$. Since it is desired to have a power measure, to determine $S(\omega_0)$, it can be further defined via the spectral power estimate at the frequency ω_0 of interest, where:

$$S(\omega_0) = |Y(\omega_0)|^2 \tag{12}$$

is the square of the magnitude (volts^2) of the output spectral signal. Thus the SNR given in equation (12) is a true power measure and 10 $\log_{10}$ is the appropriate conversion to obtain the terms in units of decibels. For the noise term, the noise power was estimated at adjacent frequencies to the frequency of interest (1 Hz or 4 Hz) and then averaged over adjacent frequencies. For Figure (20), the SNR of the output *y(t)* or *y_bar(t)* was computed for both the 1 Hz signal and the 4 Hz signal and then averaged.

Results of the Comparison of the Conventional to the SR Method

In studying Figures (18,21) some interesting results appear:

(1) For low values of noise (high levels of SNR, e.g. SNR = 1 on the left side of Figure (21)) the conventional methods perform better than the SR filter. This is because the distortion introduced by the filter provides a disadvantage on the ability of the system to identify a target. Thus the SR methods provide advantages only for cases in which the targets have to be detected in environments with high uncertainty.

(2) For increased levels of noise power (much lower levels of SNR on the right side of Figure (21)), however, which corresponds to high levels of gain2, the nonconventional method introduced in this report yields a gain in the SNR of over 40 dB (approaching 60 dB) as compared to standard procedures. Since this is a power gain, the 60 dB SNR amplification gain translates into the ability to significantly detect a target better using this new system, which is proportional to 10^6 or provides a 1,000,000 amplification of the SNR ratio. This can only dramatically improve the ability to detect certain targets, especially when they are buried in extremely high levels of noise.

The No Free Lunch Theorem for Image Enhancement

With reference to the prior discussion it is seen that a trade off exists between the SNR gain and the number of FLOPS necessary to perform the numerical integration in an accurate manner. Table 1 shows some of these values with the appropriate conversions:

Table 1 – SNR Ratio versus FLOPS

SNR defined by equation (11)	FLOPS for convergence
-80 dB	2×10^{10} FLOPS
-50 dB	1×10^{10} FLOPS
-30 dB	5×10^{9} FLOPS
-20 dB	1×10^{8} FLOPS

Comparing the first two rows of Table 1, it is seen that approximately 4-5 db gain in SNR corresponds to 1 G FLOP of computation. Since a 3 dB power gain corresponding to a doubling of a variable, a crude rule of thumb can be stated as:

Rule of Thumb: 1 G FLOP of computation = a doubling in SNR (13)

This is an example of the "No Free Lunch" theorem. In order to gain signal to noise information quality gain (via performing integration on signals with large negative SNR values), it is necessary to perform a great deal of computations (perform many G FLOPS to achieve accuracy of the integration of the resulting stiff differential equations.)

In the next section, a more thorough description of how the method synthesized to this point will assist in decision making is presented. The goal will be to minimize ***both*** Type 1 and Type 2 error discussed previously.

AN EXPLANATION WHY THE SR APPROACH HELPS IN THE DECISION-MAKING PROCESS

Returning to the basics of decision making from the earlier Figures 5a-b, Figures 22a-b represents an interesting means of describing why the true decision making can be enhanced for a binary process.

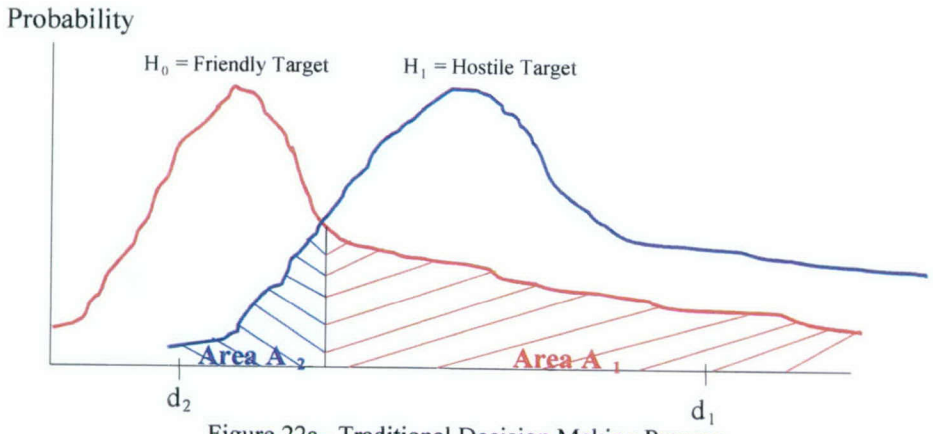

Figure 22a– Traditional Decision Making Process

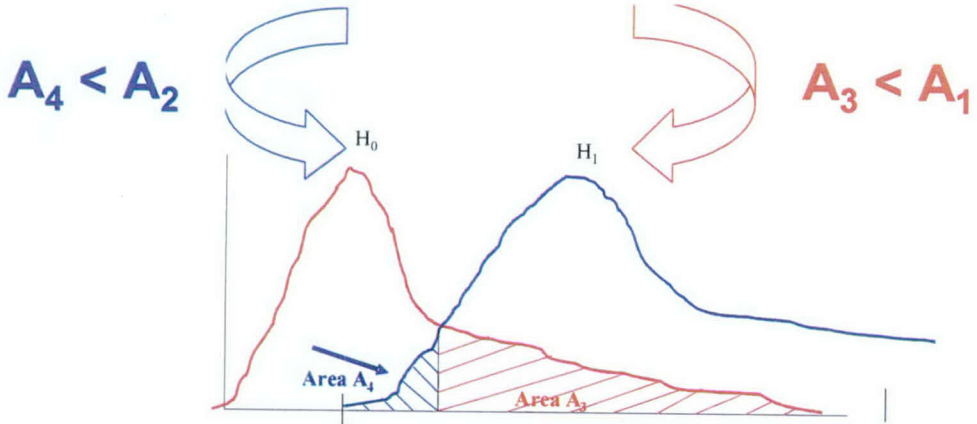

Figure 22b– Revised Decision Making Process

To describe what is occurring in Figures 22a-b with respect to the SR method to improve decision making it is necessary to compare Figure 22a to Figure 22b. Referring back to the example of the identification of the man in the tree, the true situation H_0 is that the man in the tree is friendly; the true situation H_1 is that the man in the tree is hostile. The Type 1 error (friendly fire) in Figure 22a is denoted as A_1 and the same Type 1 error in Figure 22b is denoted as A_3, Note that $A_3 < A_1$. A similar argument holds for the Type 2 error. In Figure 22a, the area A_2 (Type 2 error) is that the man in the tree is hostile, but we erroneously select H_1. In Figure 22b A_4 the area has the same interpretation but the area $A_4 < A_2$. Hence the revised decision making process in Figure 22b is better than the traditional method in Figure 22a.

To explain how the decision-making process is enhanced, in the overlap area of Figure 22a (in the areas A_1 and A_2), a random selection of points is made. For example, suppose, for a fixed value of the x axis (in the area A_1), the value of the H_0 function was 0.4 and the value of the H_1 function was 0.1. We then select 5 points in the area A_2. Using the SR method, four of

the points are then assigned to the H_0 and one point is assigned to the H_1 distribution. The area A_2 now drops. Relating this method to the identification of the subliminal signal *S(t)* under a threshold in Figure 8, this would translate into whenever the subliminal signal pierced through the threshold, the assignment would be made that *S(t)* was in the high state. There are two interesting analogies to this process which add further credence.

(1) The flu shot analogy explains this abstract concept within a medical context. If 100,000 people take a flu shot, it is known that not taking the flu shot will result in 20 deaths due to flu. However, after taking the flu shot, only 8 deaths now occur. Some of these deaths are due to the adverse interaction of the shot and not the flu. However, the overall risk is reduced from 20/100,000 to 8/100,000 which benefits the general population. This type of risk reduction is well understood in making intelligent decisions in the medical community. The SR method makes decisions (assigns random pixels to either H_0 or H_1 based on the most likely probability). Obviously the SR method makes errors, similar to the flu shot analogy, however what is similar is that the overall risk is reduced (both Type 1 and Type 2 error are mitigated, accordingly).

(2) The second analogy involves the gaming industry. Players who attempt to bet against the house (the casino) may experience good luck streaks for short periods of time. However, the house eventually wins because in the long run, the odds are against the player. In this SR process described here, the odds are being improved by the reassignment of the pixels to either H_0 or the H_1 population. It is still possible to make an error, but on the average, over a long period of time, this procedure will prevail, much like the success of the gambling house over the player.

To now go into much more detail on the process, the SR method will be examined for the case of a visual image that has been compromised. First the technique is verbally described and then applied to example 1.

EMPIRICAL DEMONSTRATIONS THAT AN IMPROVED SIGNAL TO NOISE RATIO WILL ENHANCE TARGET DETECTION AND DECISION-MAKING

About 10 year ago, it was first noticed that certain visual images could be enhanced (objects could be identified more clearly) if noise were added. Figure 23 showed this effect quite vividly. In Figure 23 (earlier discussed as Figure 4), random white Gaussian noise is added of increasing intensity in going to the right. For the middle picture, the object is most easily

Figure 23 from [28] illustrating how SR can enhance a visual image.

identified. Too little or too much noise works against the process of accurately identifying the object in the picture. This effect should be compared to the SR curve in Figure 9 which shows a resonance at an optimum amount of noise to enhance the image. Here the goal is the identification of a key object. In Figure 23, the only way the image was manipulated was through the addition of the noise. In the next section we discuss all the details requisite to the enhancement of the image using the analogy in Figures 22a-b. First the procedure is outlined for jpeg images.

PROCEDURE FOR SR ENHANCEMENT (FOR JPEG IMAGES)

(1) Divide the image up into the three primary colors (Red, Green, and Blue).

(2) Within a color, plot a histogram of frequency versus gray scale index. Since the jpeg images considered are 8 bit, the gray level may go from 0 (black) to 255 (white). On other graphs the gray level may go from 0 (black) to 1.0 (white).

(3) Perform a black and white rendering of the within color image. Take the ratio of number of black pixels versus the total number of pixels from this rendering. This ratio represents a centroid of area of the histogram distribution.

(4) Fit a parabola with the vertex of the parabola at the centroid point, the area under the parabola exactly matches or is slightly larger than the area under the histogram plot in step 2.

(5) Now plot the true histogram plot from step 2 over the template of the parabola from step 4. The excess pixels are defined as those above the template.

(6) It is now required to adjust the number of gray levels of the image. Choose N pixels to be adjusted (N to the left and N to the right). For a given gray level (x axis), we move the excess pixels either left (to zero or black) or right (to the white).

Only N pixels are affected.

(7) The resulting image is the enhanced image. The level of enhancement is a function of N, the number of pixels that are affected.

(8) Repeat steps 2-7 for each color and now fuse all three enhanced images.

Figure 24 portrays how the pictures are originally decomposed. Figure 25 shows the overlap of the parabolic template and the actual histogram distribution.

In Figure 24, the three primary colors (red, green, and blue) are individually sliced from the original image. A plot of the histograms (frequency of occurrence) versus gray level is given within each color. A parabola is fit for each color with the vertex at the appropriate centroid.

Real Data - .jpg File

Figure 24 –

Breaking the Original Image up into the constituent colors.

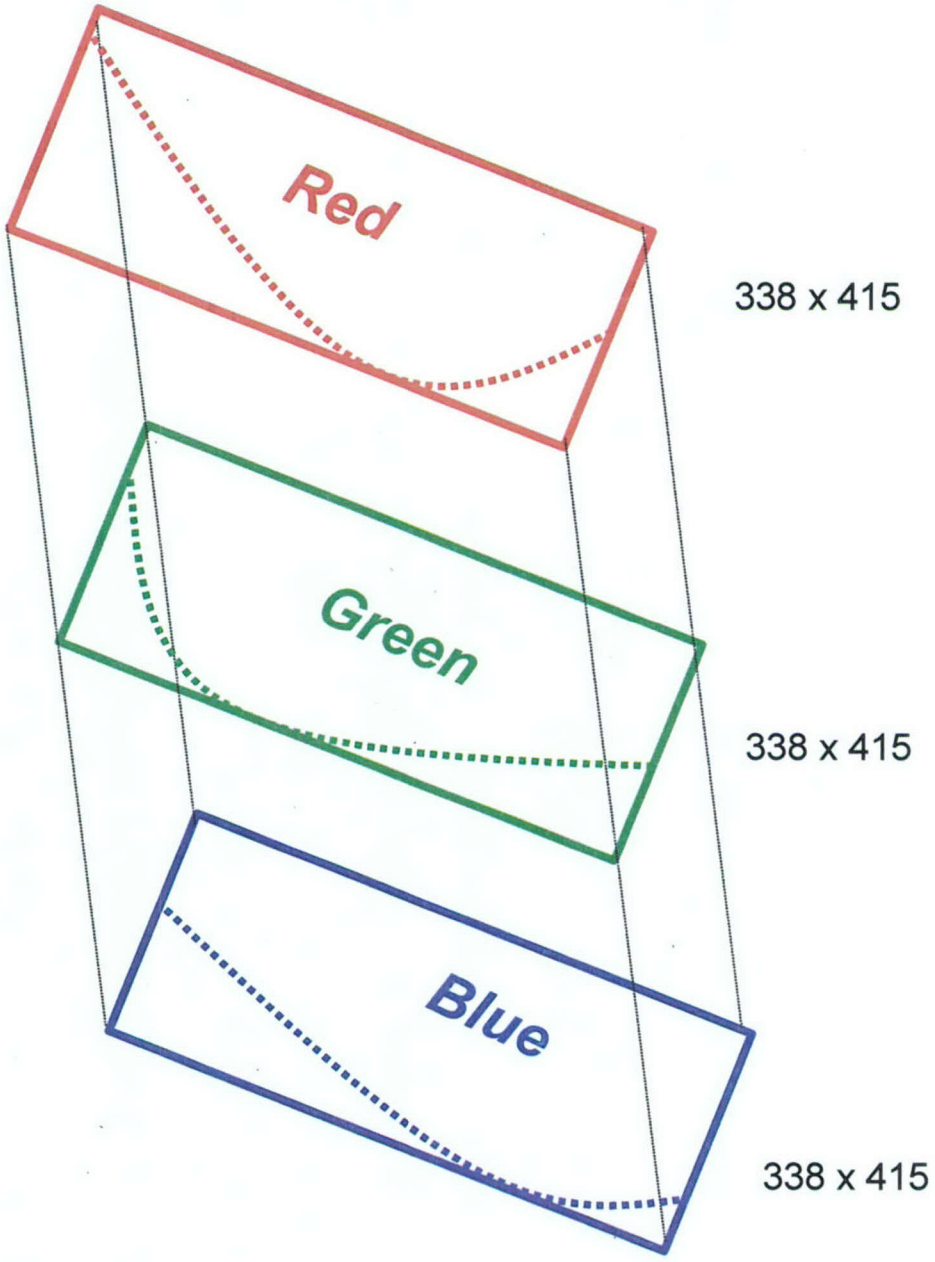

This parabola represents a template in which the pixels should appear if normally viewed. The next step will be to plot the actual histogram diagram on top of this template. Those excess gray levels will then be moved left (left is darker for this color or set to 0) or right (right (set = 1) or

white for this color). Thus the SR method is making a decision on the confused pixels via this assignment, much like occurs in Figures 22a-b where the distinction is between two distributions (binary decision).

The next step is to move those pixels above the template. This will reduce the Type 1 and Type 2 error. Figure 25 displays this action for an example of the man in the tree. Here the pixels are either moved directly left or directly right.

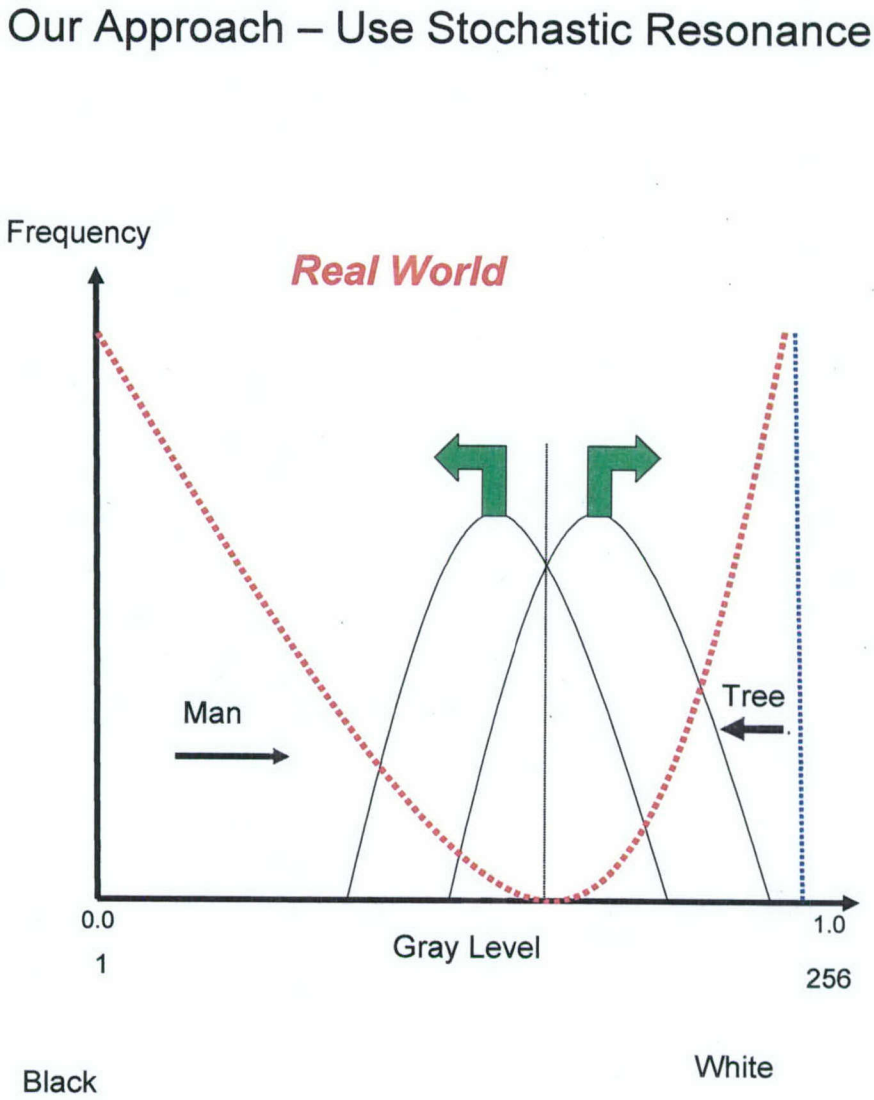

Figure 25 – Overlaying the parabola and the histogram distribution.

Recall that only N points will be moved. Much like the SR curve in Figure 9, it is presumed that moving too many points (or too few points) will not enhance the image. Finally after this

process is conducted for each of the three colors, the three enhanced color images are then recombined together to realize the overall enhanced image.

To better illustrate the seven step procedure with a real world example, Figure 26 will be the first example we will consider. The picture was taken from a TV or other source and the goal is to find out if additional information or objects could be identified from the image.

Image Processing Example 1 with A SR Approach

Figure 26 shows the original image we wish to enhance using the SR method. Such an image was taken from a TV camera. We wish to learn or discover details in the image using the principal of SR. It is obvious this is a poor image and the recognition of objects is difficult. Note that all 3 of the primary colors appear in this original image.

Figure 26 – Original Image to be Enhanced by the SR Process

The next portrayal of Figure 26 will be the green layer, only, that can be gleaned from this diagram. Since the original image has a high green content, the green slice represents a substantial representation of the visual energy in the original image in Figure 26.

Second column non zero - Pure green slice of the data rendering

Figure 27 – The Green Slice from the Original Image

This is the first of the three slices involving the primary colors.

The next slice from the original image is derived from only the red slice which is portrayed next.

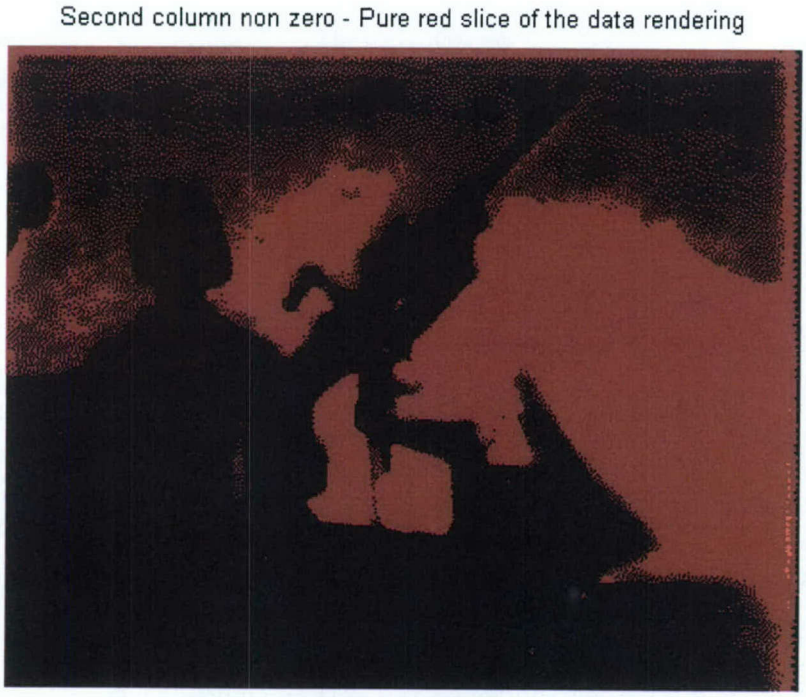

Figure 28 – The Red Slice from the Original Image

The remaining slice is the blue portion of the original Figure 6 which is now displayed:

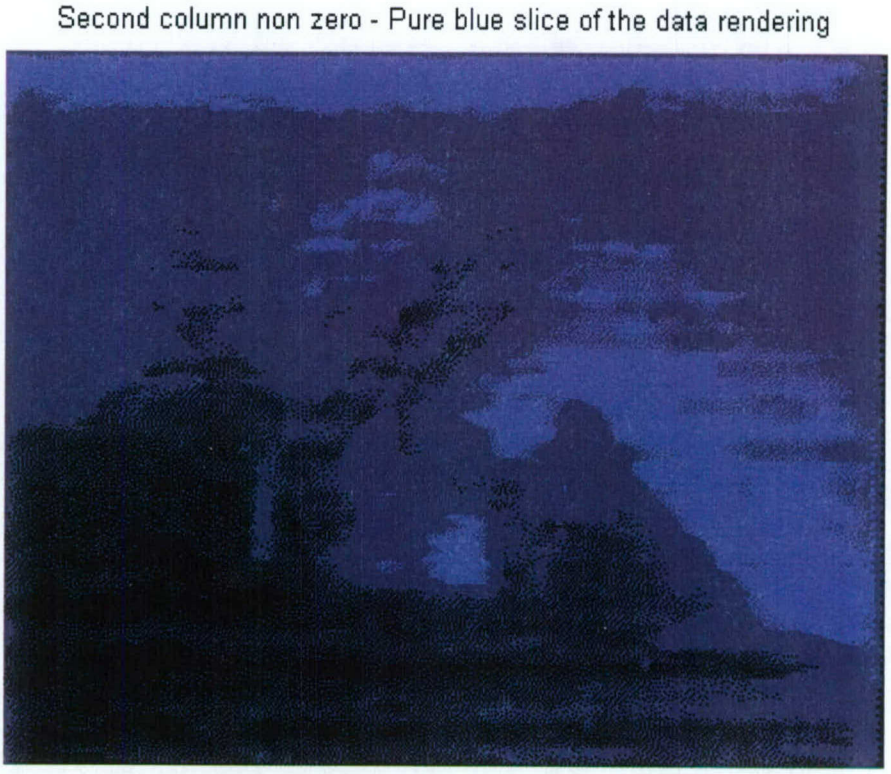

Figure 29 – The Blue Slice from the Original Image

Since the blue image is the most confused (contains the least information), the next effort will focus on Figure 29 and how we can best enhance the visual information it contains. The next rendering is a black and white representation of Figure 29.

In Figure 30, the black portions correspond to zero blue (black) or 100% blue (white). The gray versions of the next picture are various levels of blue that appear in the blue slice in Figure 29.

Figure 30 – A Black and White Rendering of the Blue Slice

The goal of the next few steps will be to demonstrate that Figure 30 can be enhanced significantly by the SR method and aid in the detection of objects appearing in the original image.

A histogram of the Figure 30 image will now be displayed.

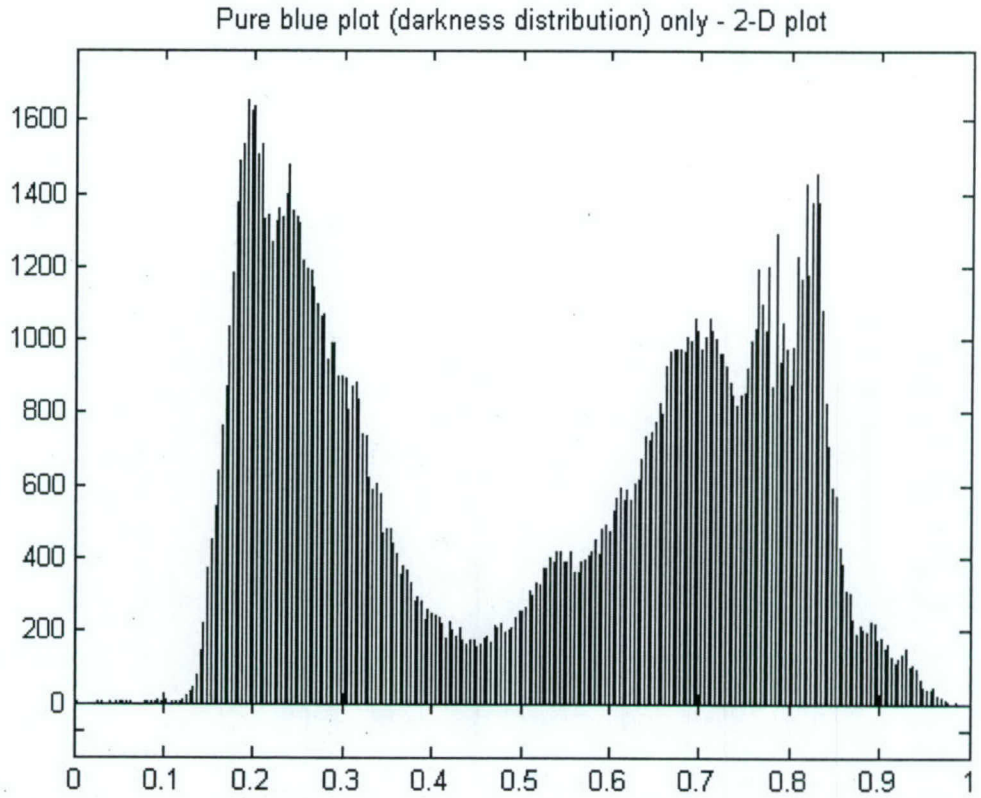

Figure 31 – The Histograms of the Blue Slice from Figure 30

To overlay this diagram with a parabola template, Figure 31 will be redrawn in MATLAB™ to better represent the histogram distribution of this blue layer.

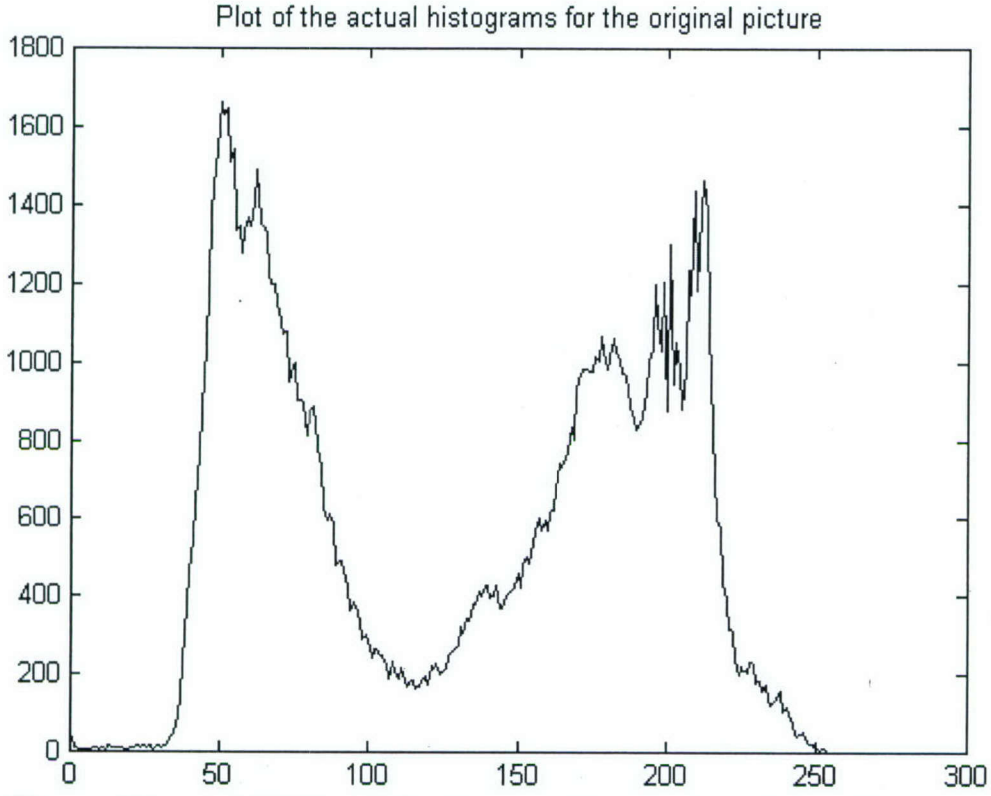

Figure 32 – A MATLAB Histogram Rendering of the Blue Slice

The template consisting of the parabola needs to be constructed next. From the black and white rendering of Figure 30, the parabola is constructed such that the area under the parabola is equal to (or slightly greater than) the area under the histogram illustrated in Figure 32 and with its vertex located at the centroid of areas in Figure 32. Figure 33 shows this parabola constructed via MATLAB™.

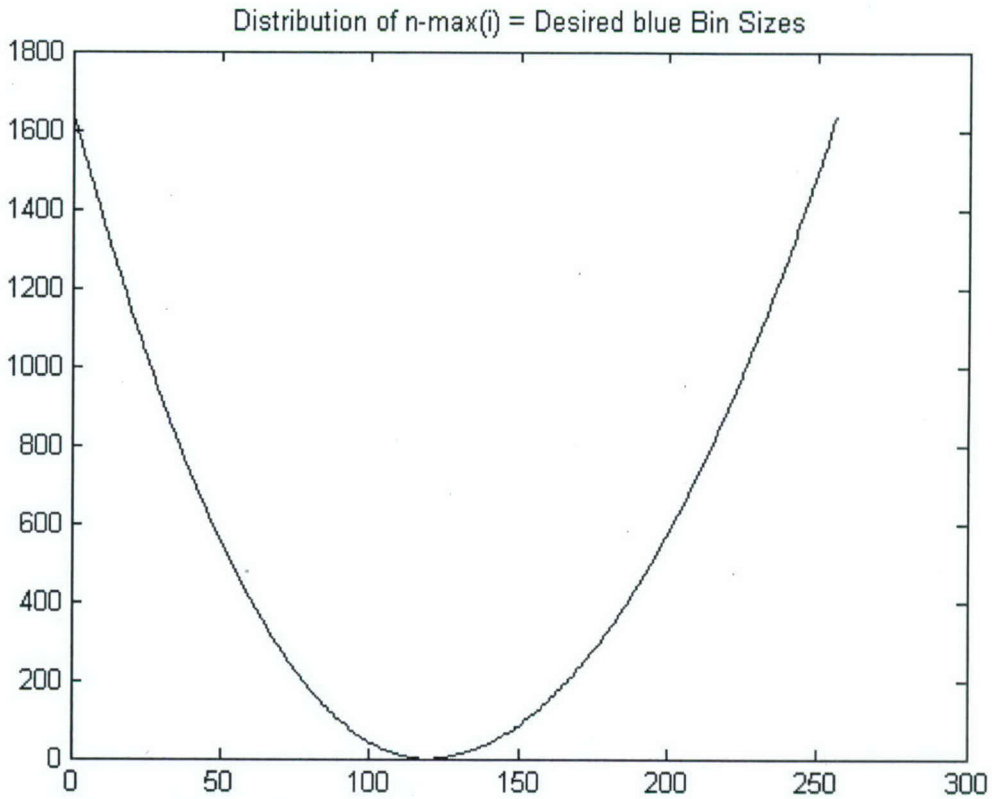

Figure 33 – The Parabola Template for the Blue Slice

Next, Figures 32 and 33 will simultaneously be plotted to show how the original histogram distribution is at variance with the template in Figure 33.

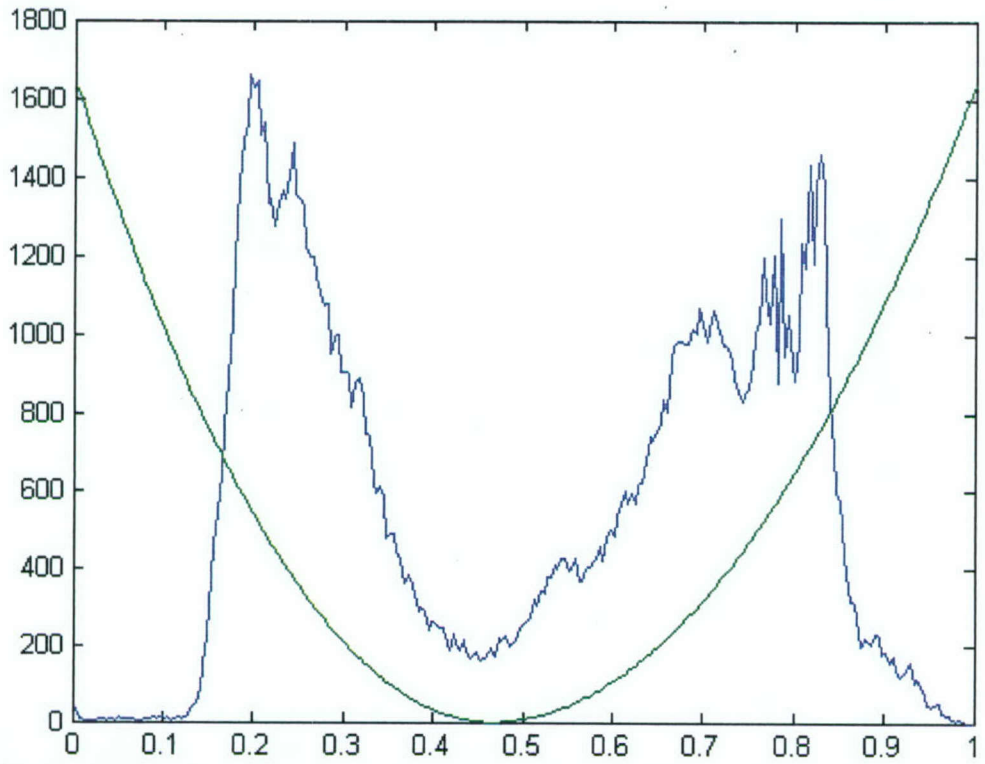

Figure 34 – The Overlap of Histograms and Template – Blue Slice

In Figure 34 it is seen where the histograms are above the template. These are the candidate pixels to be adjusted to the left or the right. These are the "confused pixels" and are analogous to the areas A_1 and A_2 in Figure 22a. To the left of the vertex of the parabola, the excess pixels are sent directly left (made black or no blue color). To the right of the vertex of the parabola, the excess pixels are sent directly right (made white or full blue color). In this case the black means "no blue color" and white means "full blue color". It is more convenient to develop a function of the excess pixels. This is a distribution of the difference between the actual histograms and the template. Figure 35 shows this difference function which is a plot of the difference between the two curves in Figure 34.

Whenever this difference function in Figure 35 is positive, pixels should be moved either left or right according to the location of the vertex of the parabola in Figures 33, 34.

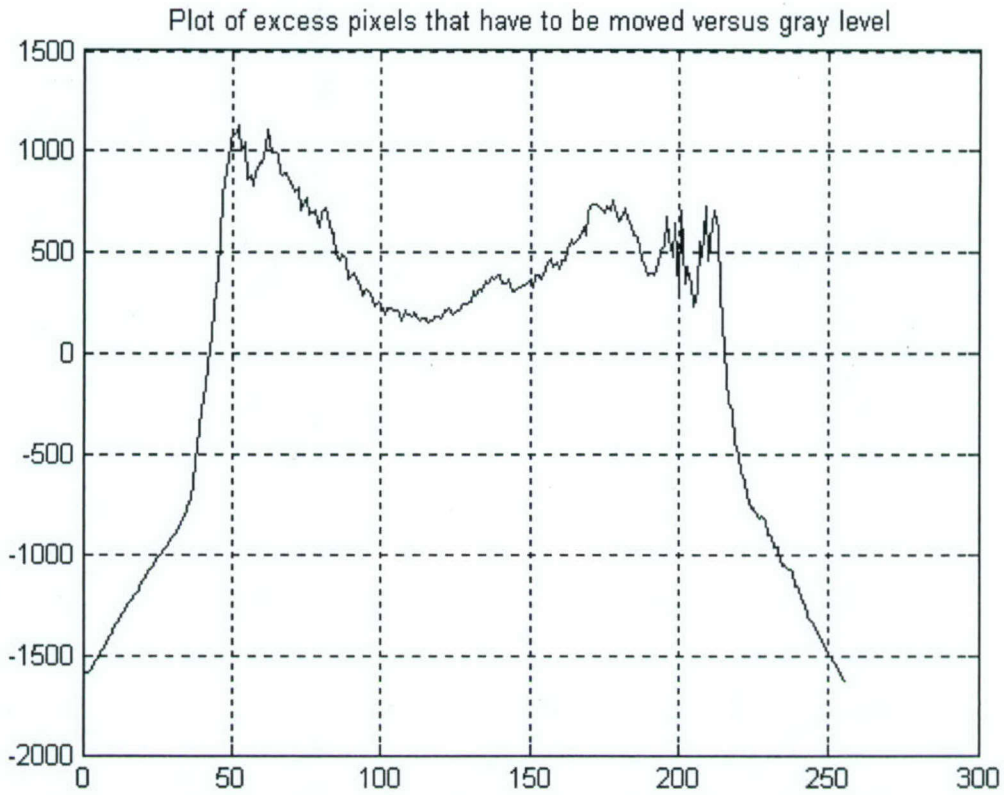

Figure 35 – A Plot of the Excess Pixels to be Moved

To now see the full effect of the image processing algorithm, let us review its effect on the blue image. Figure 36 will portray the evolution of the blue slice as this technique is applied to this picture.

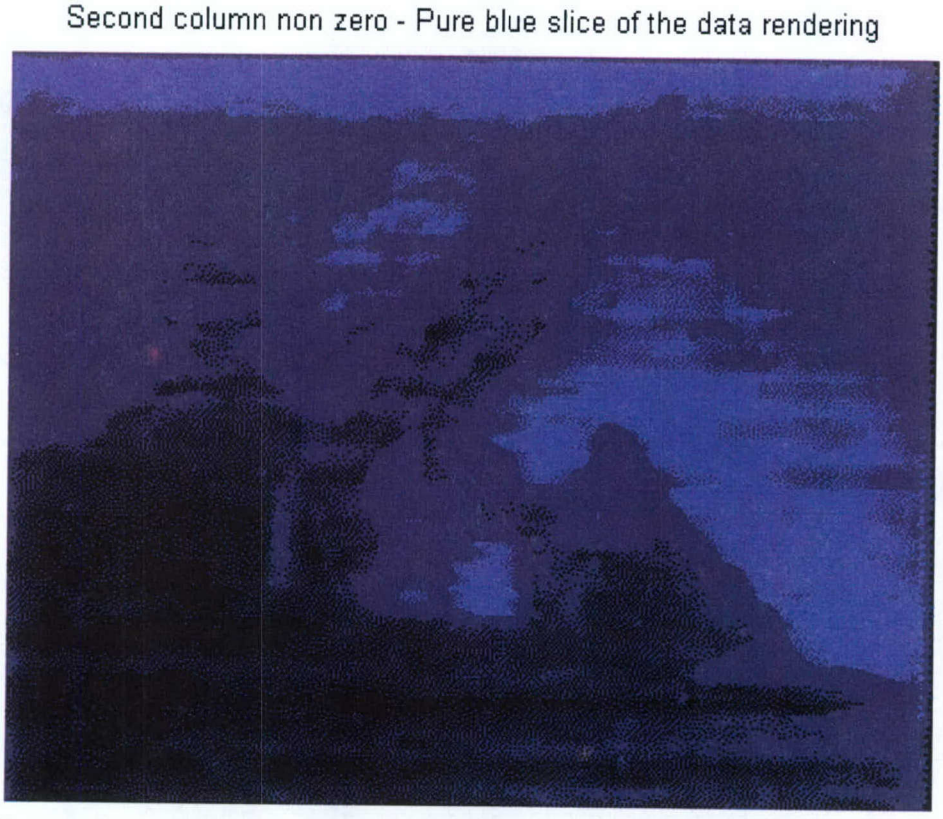

Figure 36 – The Original Blue Slice with no Enhancement

The next image is Figure 37, which is a black and white rendering of this diagram.

This is the fundamental image we wish to manipulate. Note how murky the objects appear in Figure 37. Our goal in this exercise is to improve upon this image in the ability to discern objects in the image.

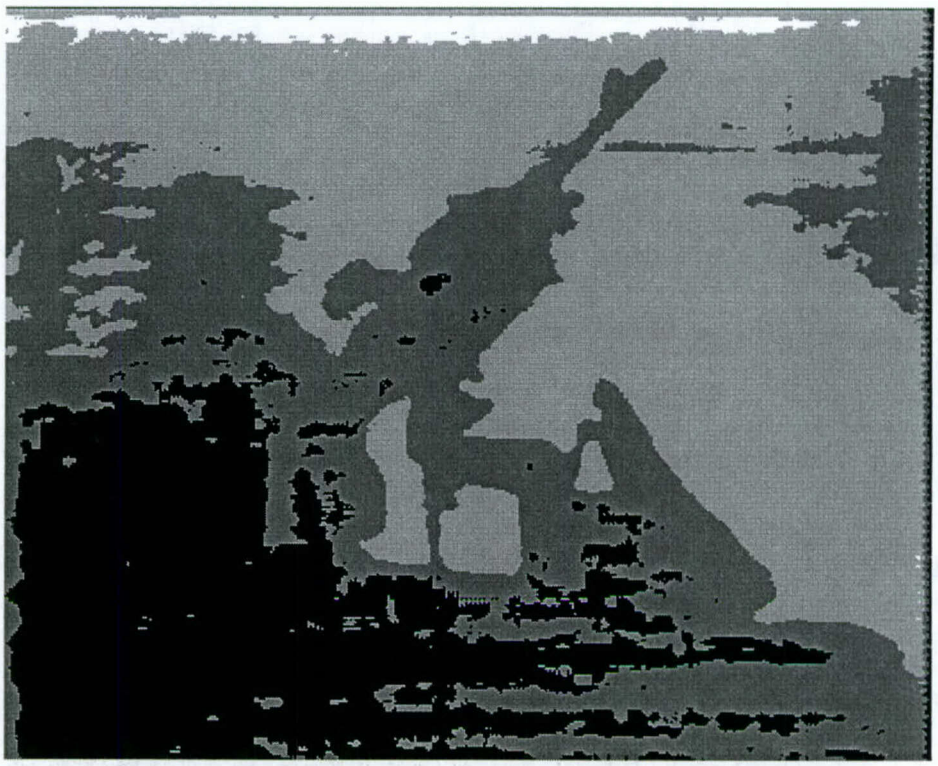

Figure 37 – The Blue Slice as a Black and White Image – N = 0

Figure 38 will be the first SR enhancement of Figure 37. Here we have enhanced N= 500 pixels to the right and N = 500 pixels to the left for this blue slice.

Here is the blue picture

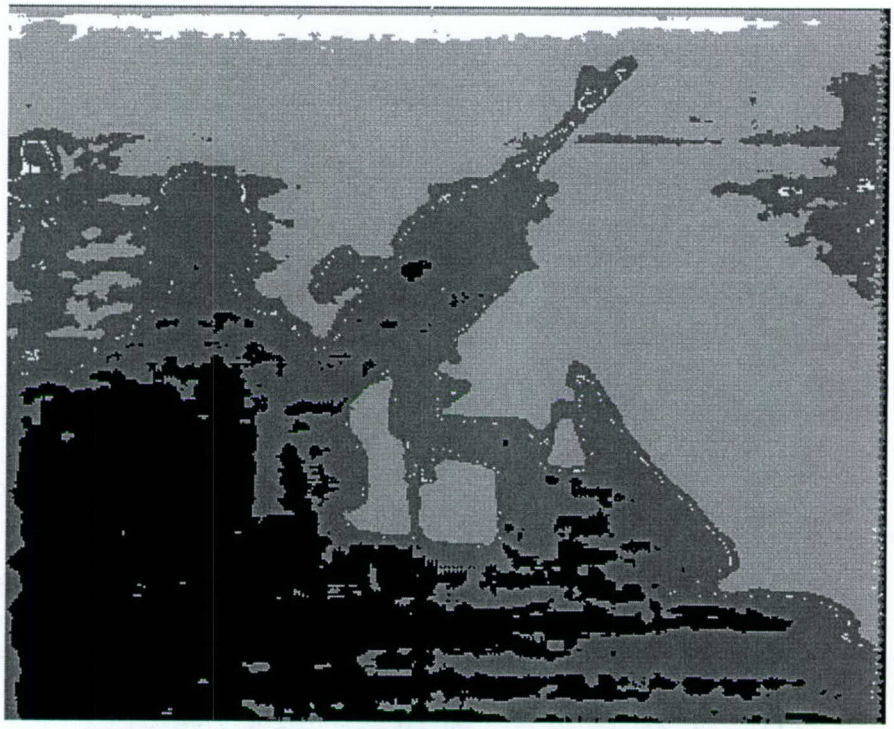

Figure 38 – The Blue Slice as a Black and White Image – N=500

Note the white dots appearing around the key objects- the soldier, the gun, and various other objects adjacent to the soldier. Figure 39 will be the next SR enhancement of Figure 38 by increasing N to 1,000.

In Figure 39 we have enhanced N = 1000 pixels to the right and N = 1000 pixels to the left for this blue slice.

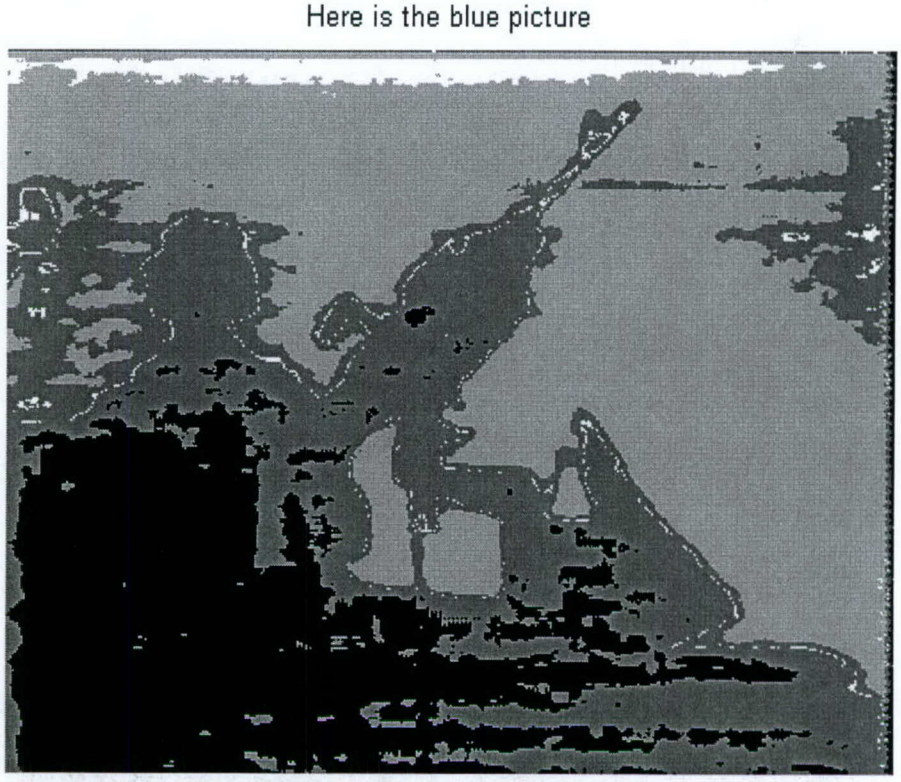

Figure 39 – The Blue Slice as a Black and White Image – N=1000

Figure 40 will be the next SR enhancement of Figure 39.

In Figure 40 we have enhanced N = 2000 pixels to the right and N = 2000 pixels to the left for this blue slice.

Here is the blue picture

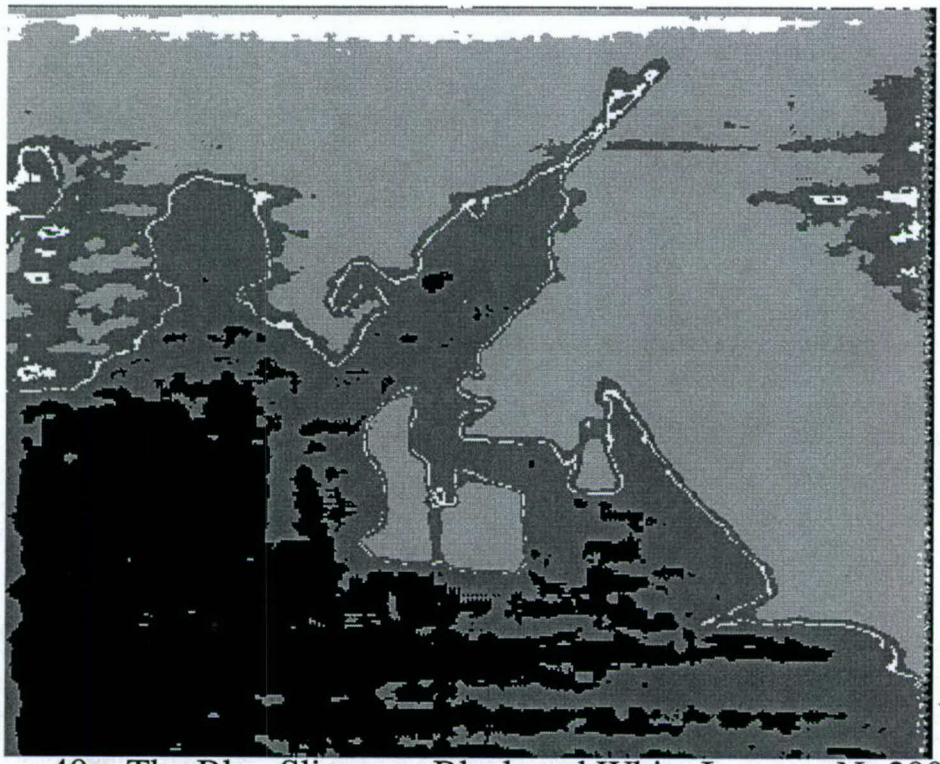

Figure 40 – The Blue Slice as a Black and White Image – N=2000

Figure 41 will be the next SR enhancement of Figure 40.

In Figure 41 we have enhanced N = 3000 pixels to the right and N= 3000 pixels to the left for this blue slice.

Here is the blue picture

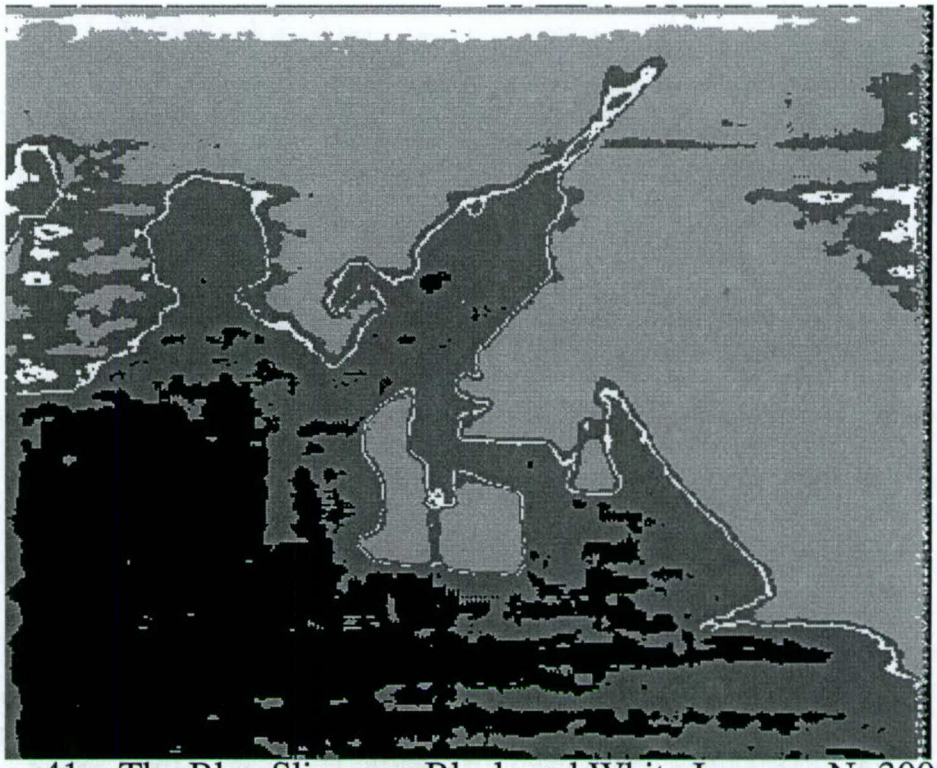

Figure 41 – The Blue Slice as a Black and White Image – N=3000

Figure 42 will be the next SR enhancement of Figure 40.

In Figure 42 we have enhanced N = 5000 pixels to the right and N= 5000 pixels to the left for this blue slice.

Here is the blue picture

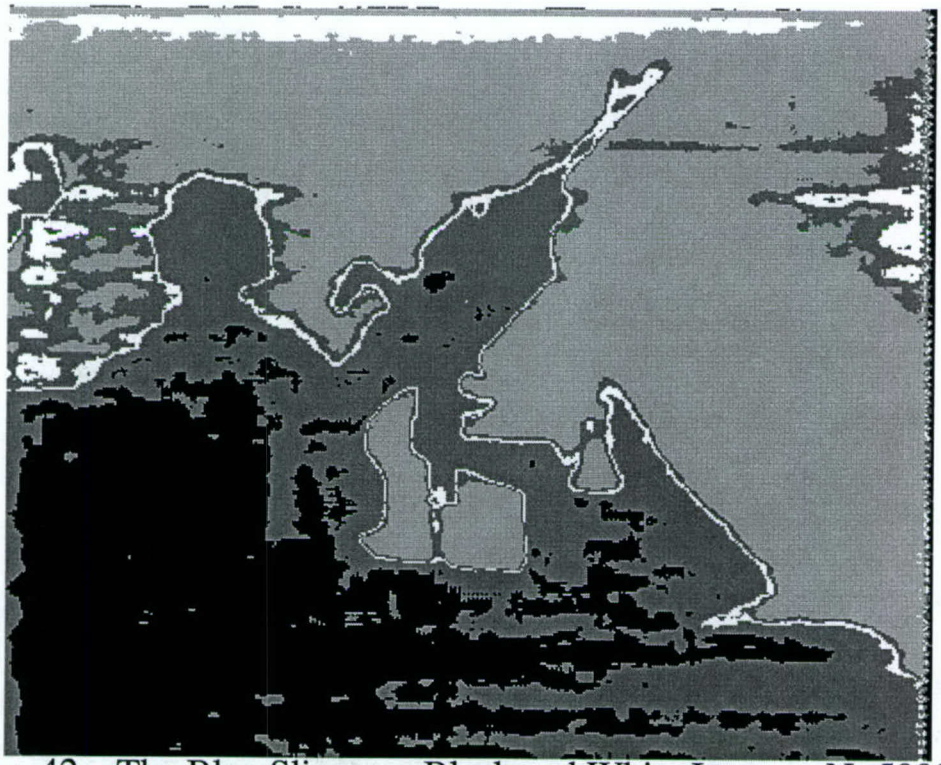

Figure 42 – The Blue Slice as a Black and White Image – N=5000

Figure 43 will be the next SR enhancement of Figure 40.

In Figure 43 we have enhanced N = 10,000 pixels to the right and N= 10,000 pixels to the left for this blue slice.

Here is the blue picture

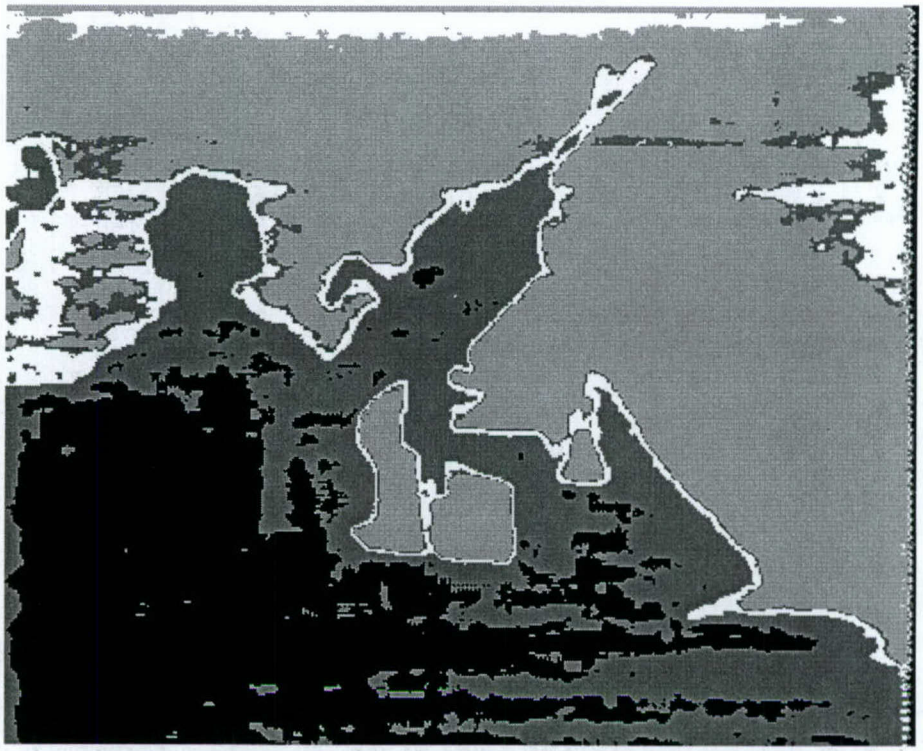

Figure 43 – The Blue Slice as a Black and White Image – N=10,000

In Figure 43, note the large amount of white (presence of the full blue color) now appears around the key objects (the soldier's head, the gun base and differently in the upper part of the gun). Now to continue on to the next color slice, Figure 44 represents this green slice of the original picture.

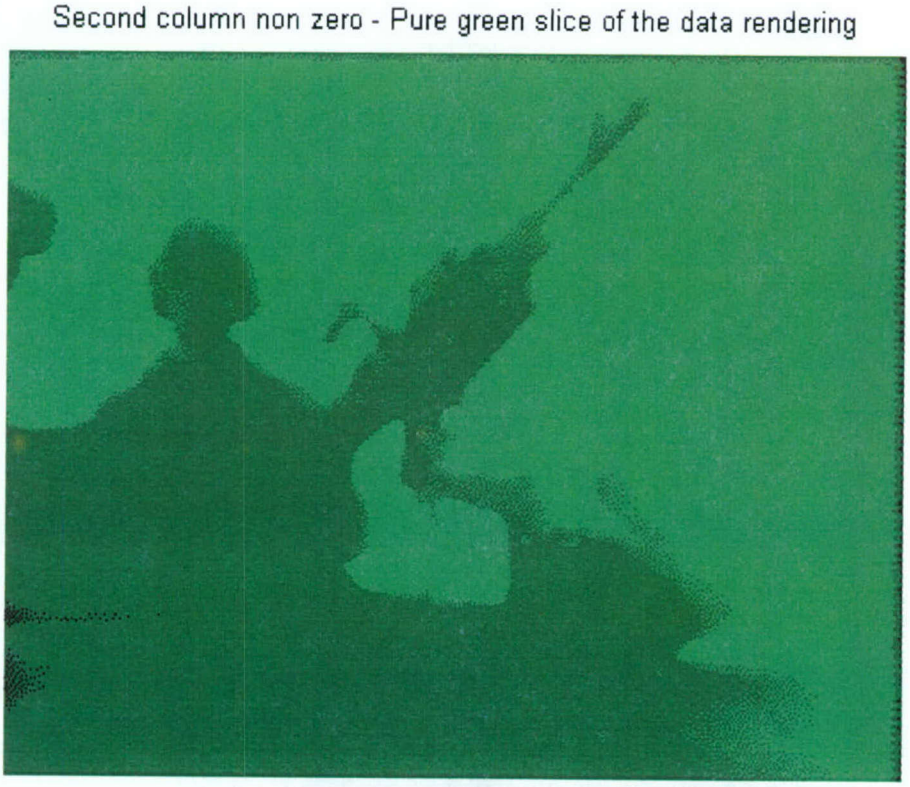

Figure 44 – The Green Slice of the Original Image

Figure 45 is the black and white rendering of Figure 44, which will now be manipulated.

It is noted in Figure 45 that the presence of the plentiful white color means that high levels of the green color appear throughout the picture.

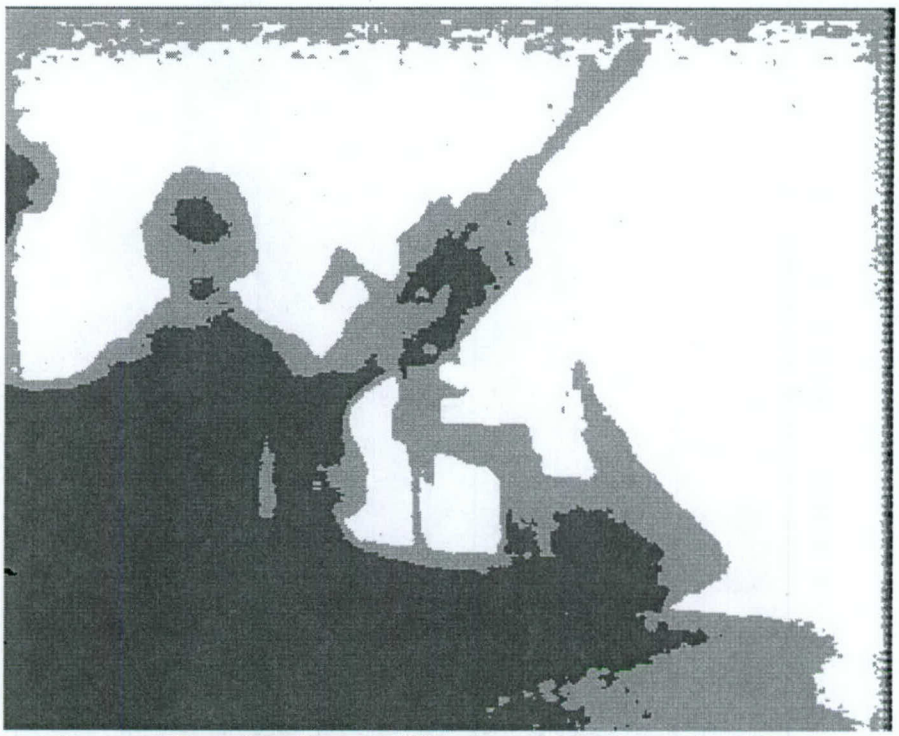

Figure 45– The Green Slice as a Black and White Image

Figure 46 will be the first SR enhancement of Figure 45.

In Figure 46 we have enhanced N = 500 pixels to the right and N= 500 pixels to the left for this green slice.

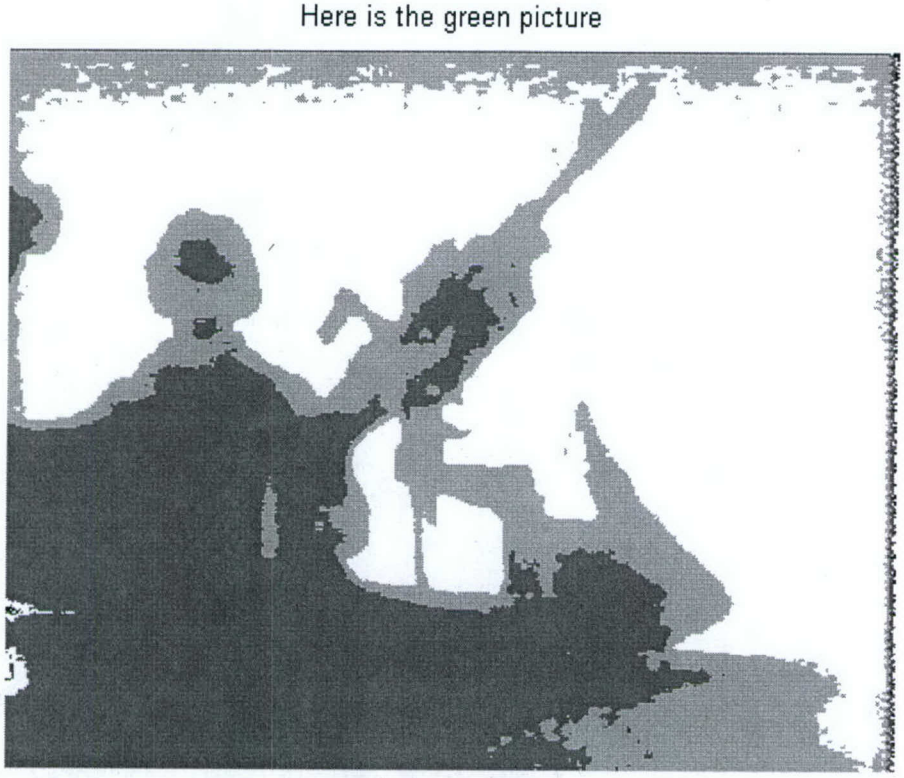

Figure 46– The Green Slice as a Black and White Image – N = 500

Figure 47 will be the next SR enhancement of Figure 45.

In Figure 47 we have enhanced N = 1000 pixels to the right and N= 1000 pixels to the left for this green slice.

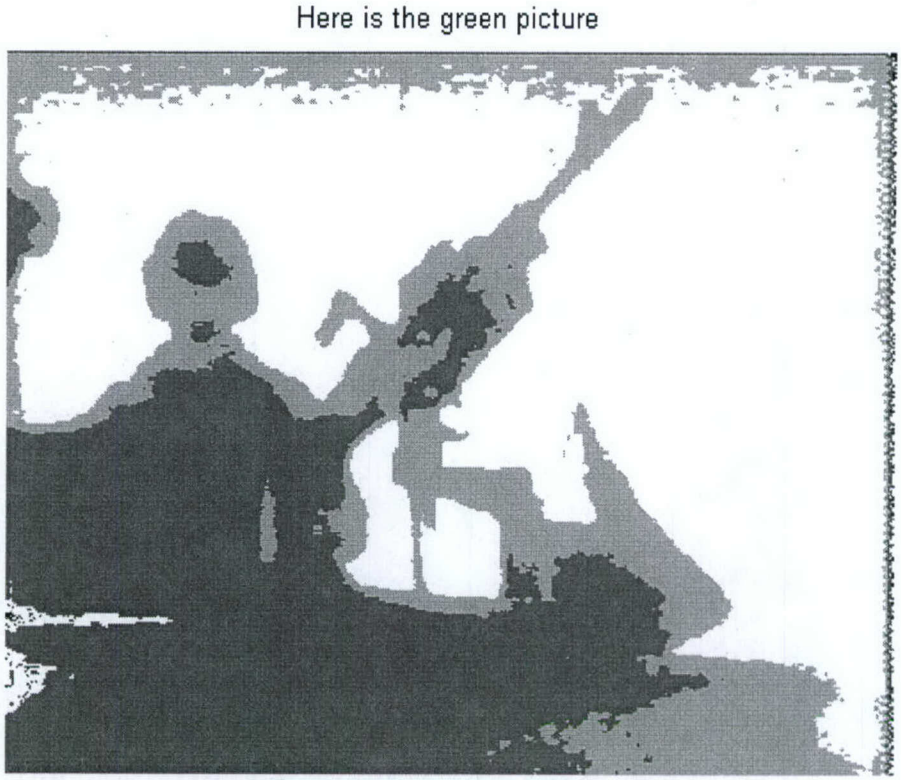

Figure 47– The Green Slice as a Black and White Image – N = 1000

Figure 48 will be the next SR enhancement of Figure 45.

In Figure 48 we have enhanced N = 2000 pixels to the right and N= 2000 pixels to the left for this green slice.

Figure 48– The Green Slice as a Black and White Image – N = 2000

Figure 49 will be the next SR enhancement of Figure 45.

In Figure 49 we have enhanced N = 3000 pixels to the right and N= 3000 pixels to the left for this green slice.

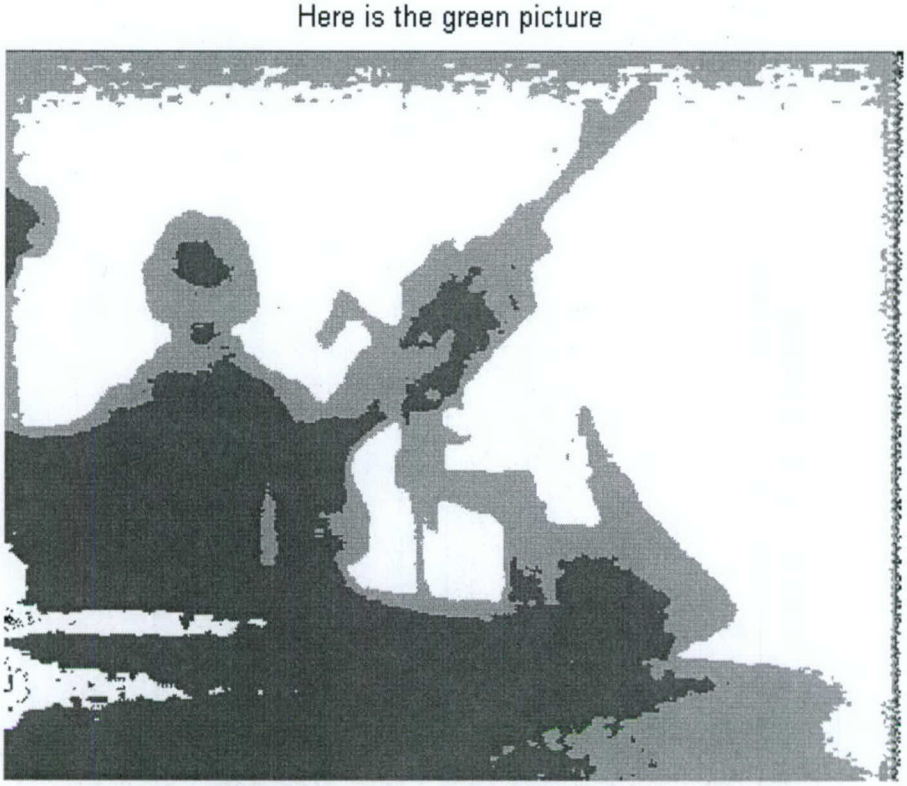

Figure 49– The Green Slice as a Black and White Image – N = 3000

Figure 50 will be the next SR enhancement of Figure 45.

In Figure 50 we have enhanced N = 5000 pixels to the right and N= 5000 pixels to the left for this green slice.

Figure 50– The Green Slice as a Black and White Image – N = 5000

It is mentioned that for this green color, there was not a lot of change from the original picture as a result of this SR result.

Figure 51 is the red slice of the original picture.

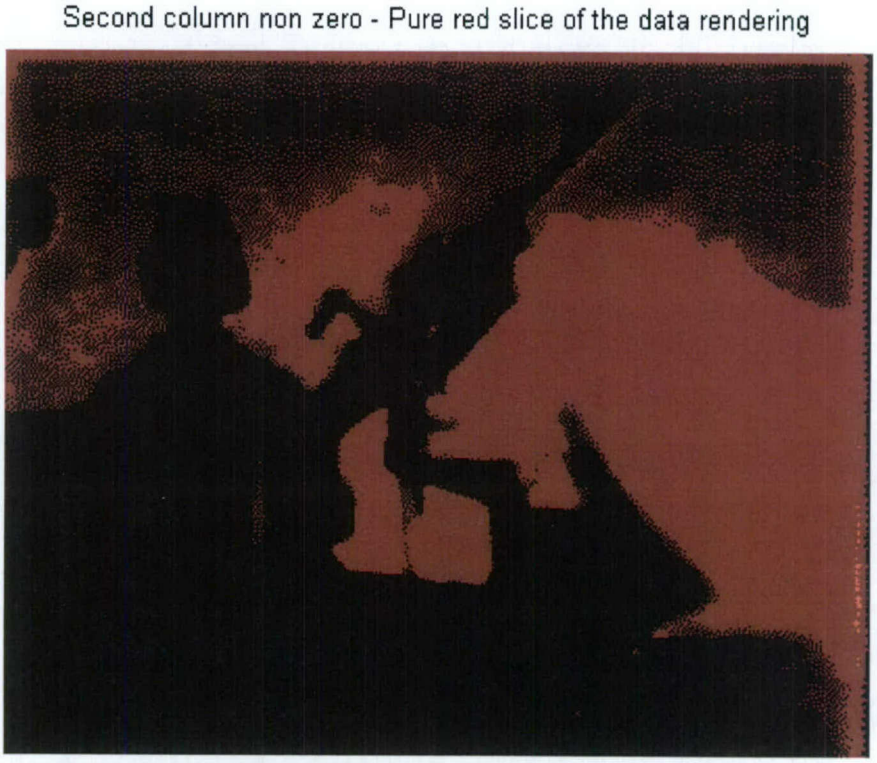

Figure 51– The Red Slice of the Original Image

Figure 52 is a black and white rendering of Figure 51, which will be manipulated.

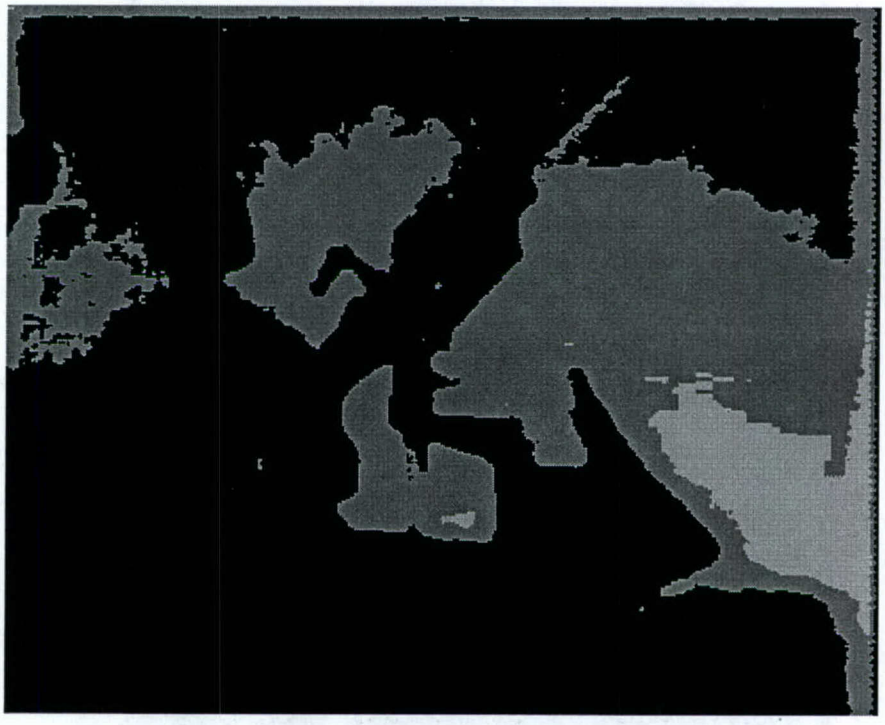

Figure 52– The Red Slice as a Black and White Image

Figure 53 will be the first SR enhancement of Figure 51. Here we have enhanced N = 500 pixels to the right and N= 500 pixels to the left for this red slice.

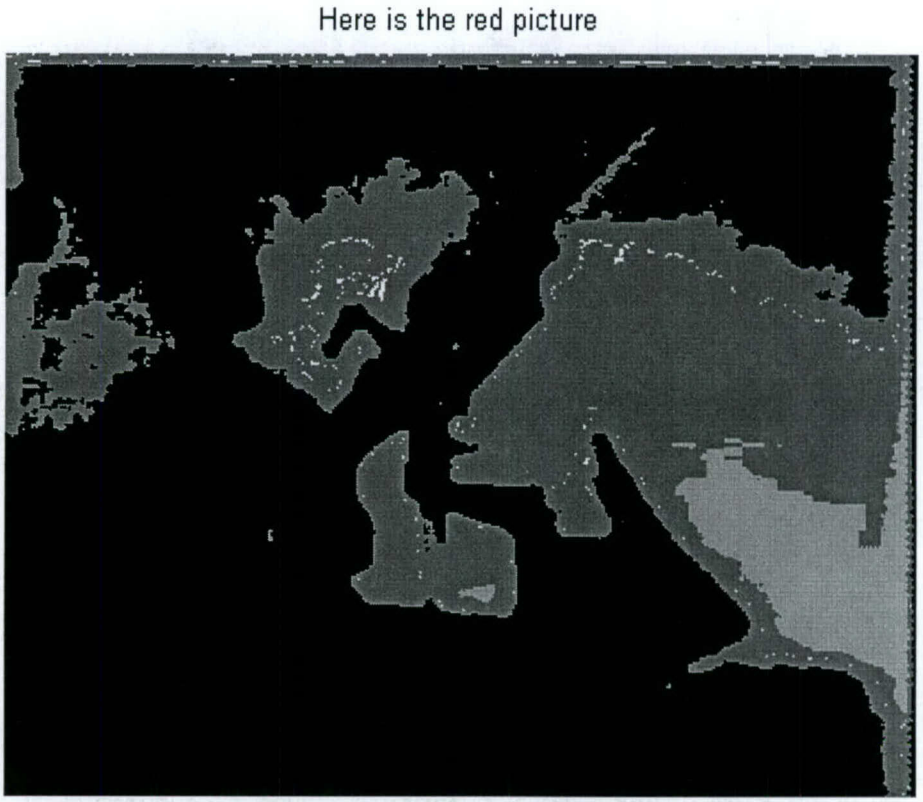

Figure 53– The Red Slice as a Black and White Image – N = 500

Figure 54 will be the next SR enhancement of Figure 51. Here we have enhanced N = 1000 pixels to the right and N= 1000 pixels to the left for this red slice.

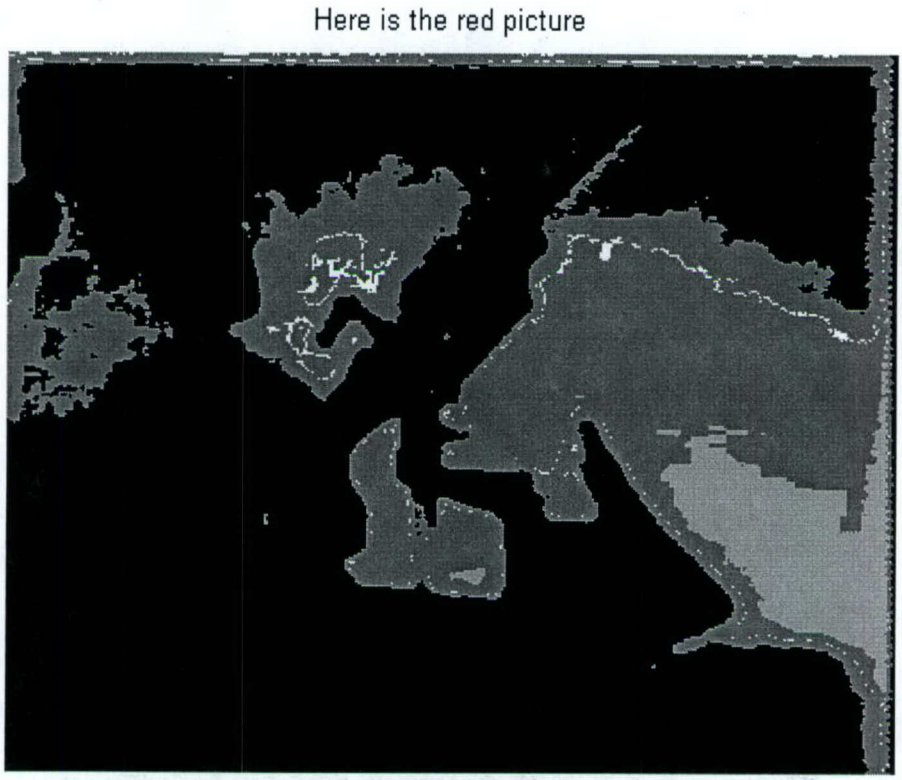

Figure 54– The Red Slice as a Black and White Image – N = 1000

Figure 55 will be the next SR enhancement of Figure 51. Here we have enhanced N = 2000 pixels to the right and N= 2000 pixels to the left for this red slice.

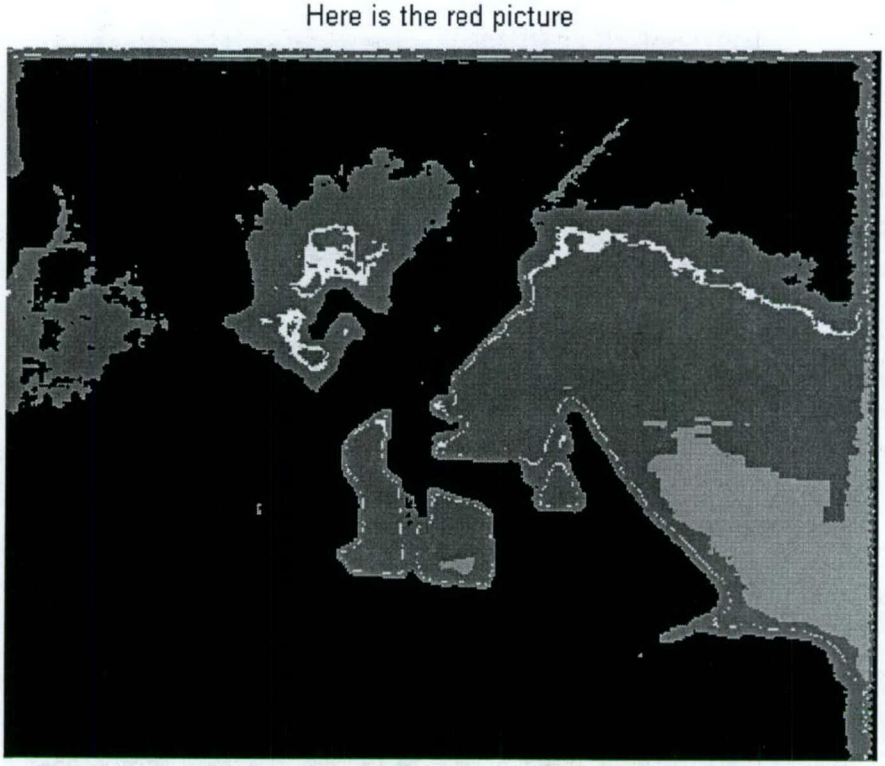

Figure 55– The Red Slice as a Black and White Image – N = 2000

Figure 56 will be the next SR enhancement of Figure 51. Here we have enhanced N = 3000 pixels to the right and N= 3000 pixels to the left for this red slice.

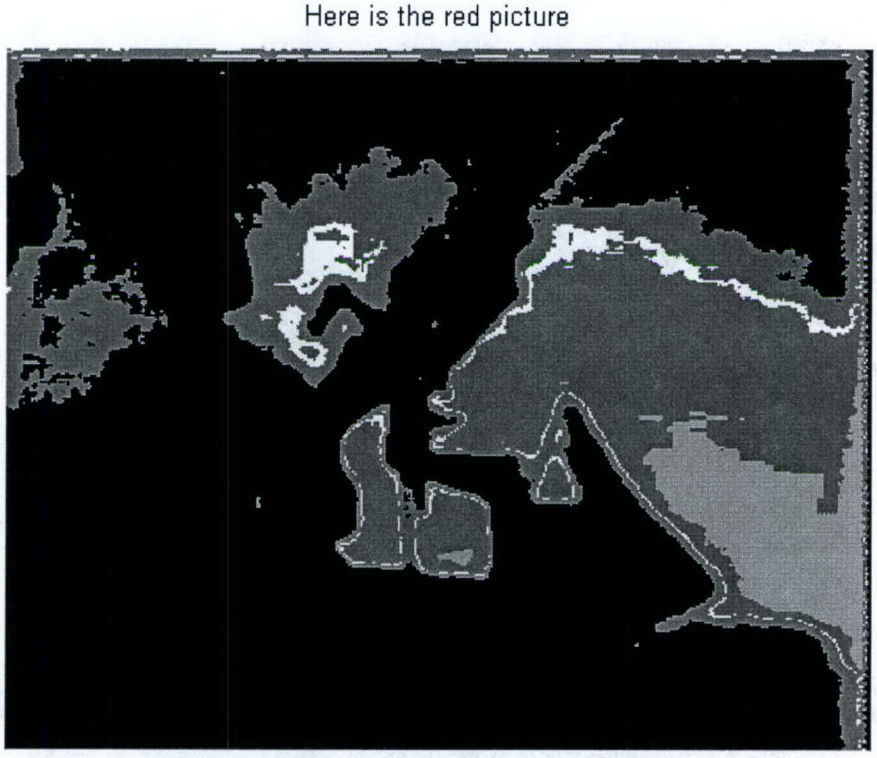

Figure 56– The Red Slice as a Black and White Image – N = 3000

Figure 57 will be the next SR enhancement of Figure 51. Here we have enhanced N = 5000 pixels to the right and N= 5000 pixels to the left for this red slice.

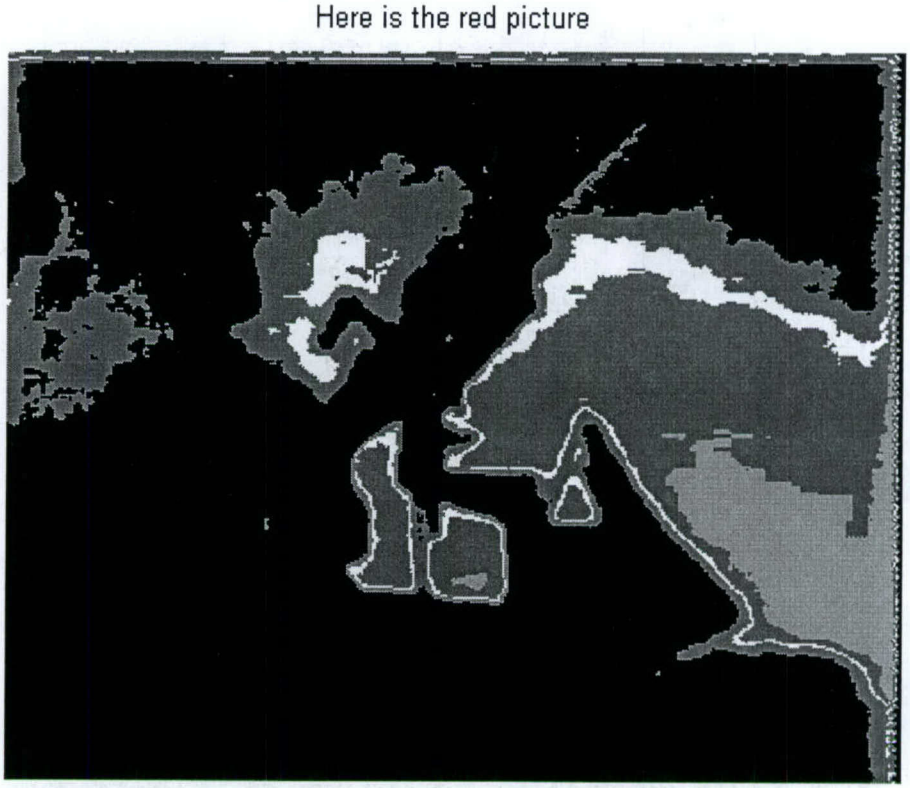

Figure 57– The Red Slice as a Black and White Image – N = 5000

Figure 58 will be the next SR enhancement of Figure 51. Here we have enhanced N = 10,000 pixels to the right and N= 10,000 pixels to the left for this red slice.

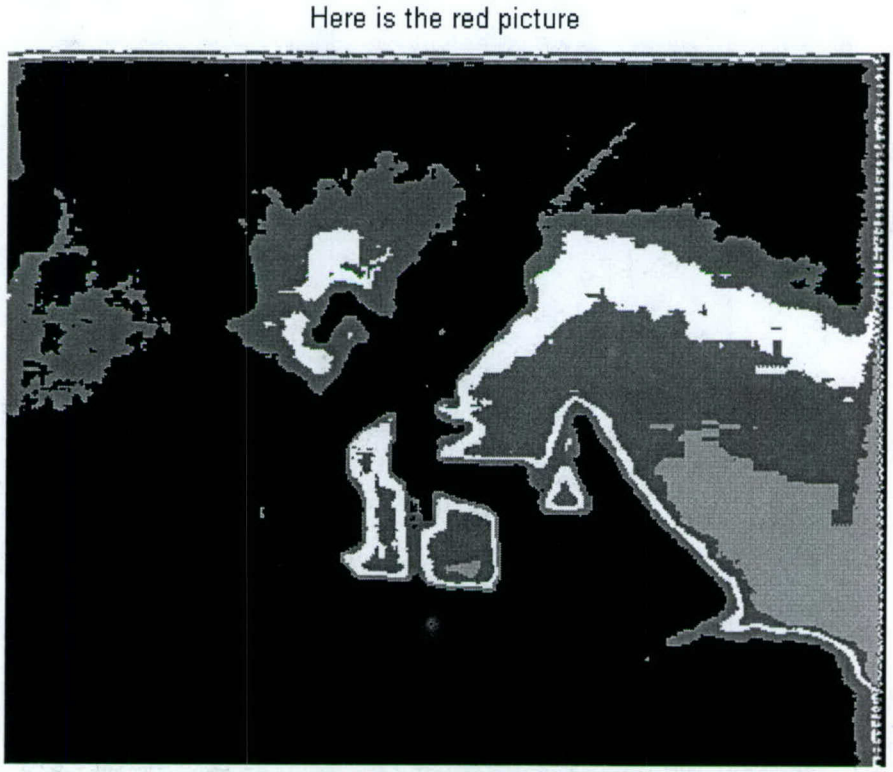

Figure 58– The Red Slice as a Black and White Image – N = 10,000

Figure 59 will be the basis for the overall fusion of the three color enhancement. This is the original image repeated for comparison purposes.

Figure 59– The Original Image – No Enhancement

Figure 60 will be the first SR enhancement of Figure 59. Here we have enhanced N = 500 pixels to the right and N= 500 pixels to the left for this fused image consisting of all three enhanced colors.

Figure 60– The Original Fused Image – N = 500

Figure 61 will be the next SR enhancement of Figure 59. Here we have enhanced N = 1000 pixels to the right and N= 1000 pixels to the left for this fused image consisting of all three enhanced colors.

Figure 61– The Original Fused Image – N = 1000

Figure 62 will be the next SR enhancement of Figure 59. Here we have enhanced N = 2000 pixels to the right and N= 2000 pixels to the left for this fused image consisting of all three enhanced colors.

Figure 62– The Original Fused Image – N = 2000

Figure 63 will be the next SR enhancement of Figure 59. Here we have enhanced N = 3000 pixels to the right and N= 3000 pixels to the left for this fused image consisting of all three enhanced colors.

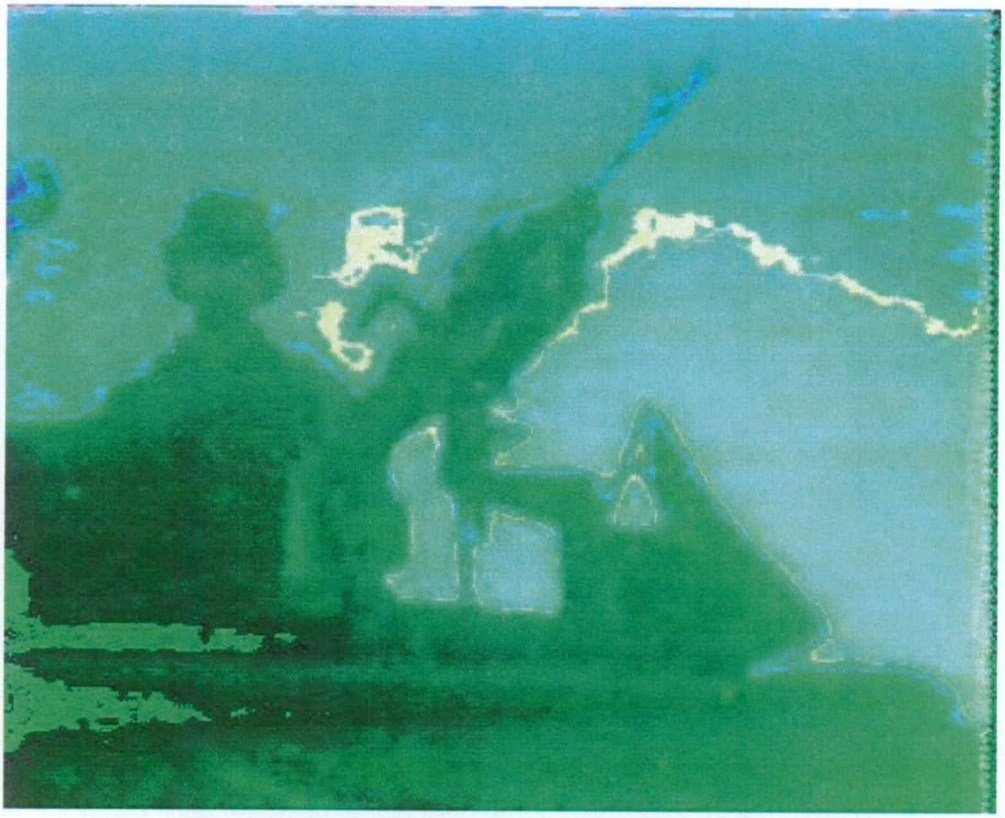

Figure 63– The Original Fused Image – N = 3000

Figure 64 will be the next SR enhancement of Figure 59. Here we have enhanced N = 5000 pixels to the right and N= 5000 pixels to the left for this fused image consisting of all three enhanced colors.

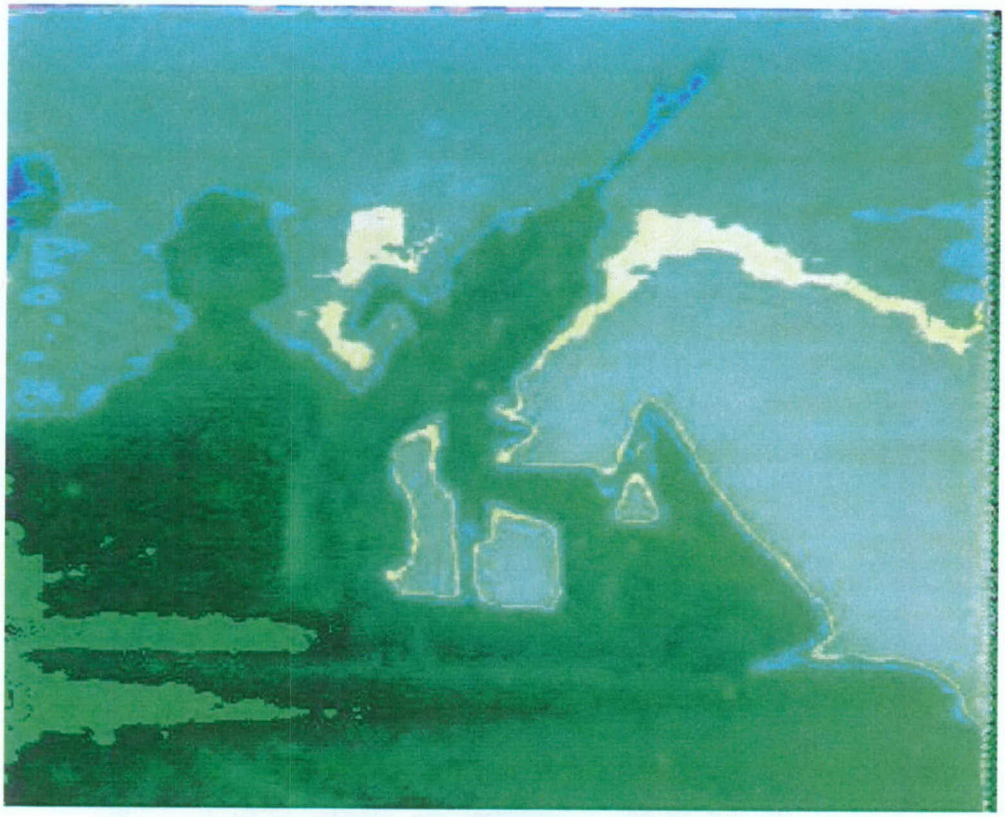

Figure 64– The Original Fused Image – N = 5000

Since the technique for manipulation of images seems to depend on how the histograms of the pixels are manipulated, the next step will be to consider the SR method developed so far with standards in the image processing industry.

Image Processing Example 2 with A RetineX Approach

In the early 1960's, Edwin Land [35-37] discovered an algorithm to enhance images called the RetineX method. A RetineX contains all mechanisms from retina to cortex necessary to form images in terms of lightness. In short, it brought out the idea that vision is the result of image processing of spatial information found in the image. This method is widely accepted [38] as a baseline standard to compare alternative algorithms. A study was conducted to better understand how this baseline algorithm excels in its ability to improve image quality by

lightening images, yet preserving their original integrity. Figure 65 shows a picture taken with a camera in which the light from the window makes the rendering of the remainder of the picture to be difficult. This is a common problem in which large amounts of light (from the window) saturate the camera, thus producing dark images on the right hand side of the picture. The goal will be to improve the rendering of this picture by lighting the image to enable better identification of the objects in the picture.

Dad - Girl - Original Image

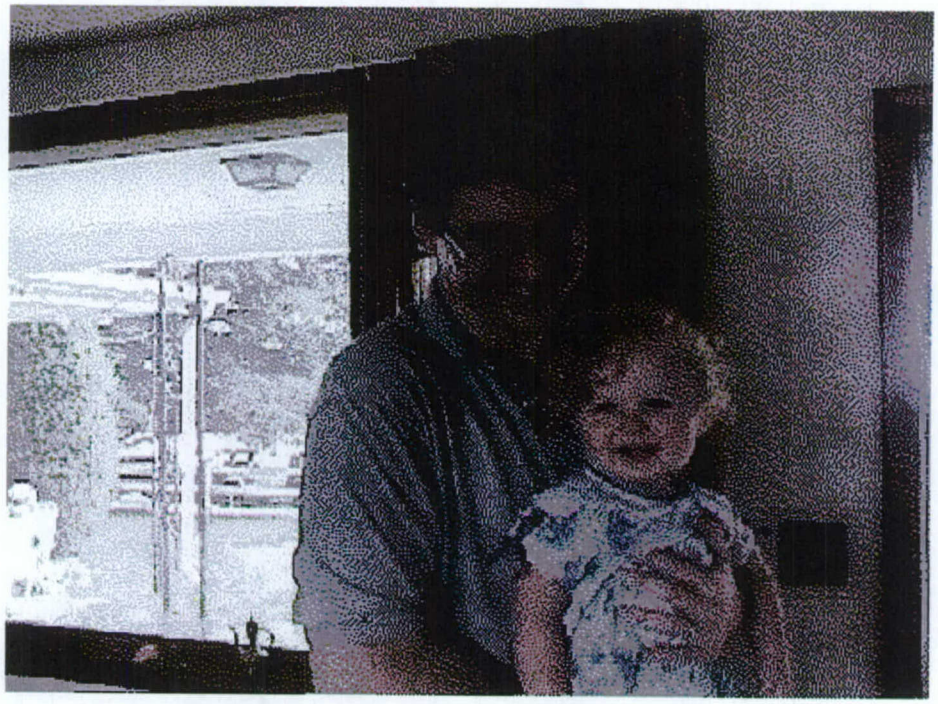

Figure 65 – Original Image

The RetineX algorithm was applied to the image in Figure 65. The resulting image is shown in Figure 66.

Dad_girl_RetinaX image

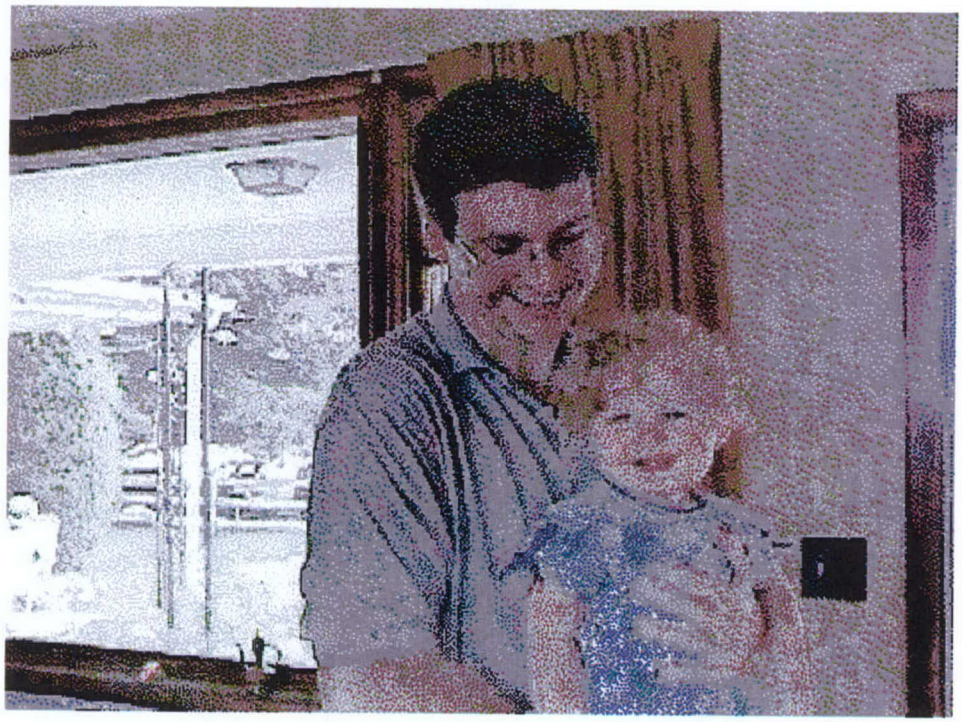

Figure 66 – The Image Processed by the RetinaX Algorithm

It is clear that the right hand side of the picture has been significantly clarified. To understand the reason why the image can be enhanced, we next examine the distributions of the histograms of the two pictures, Figures 65 and 66. Both histograms are plotted in Figure 67.

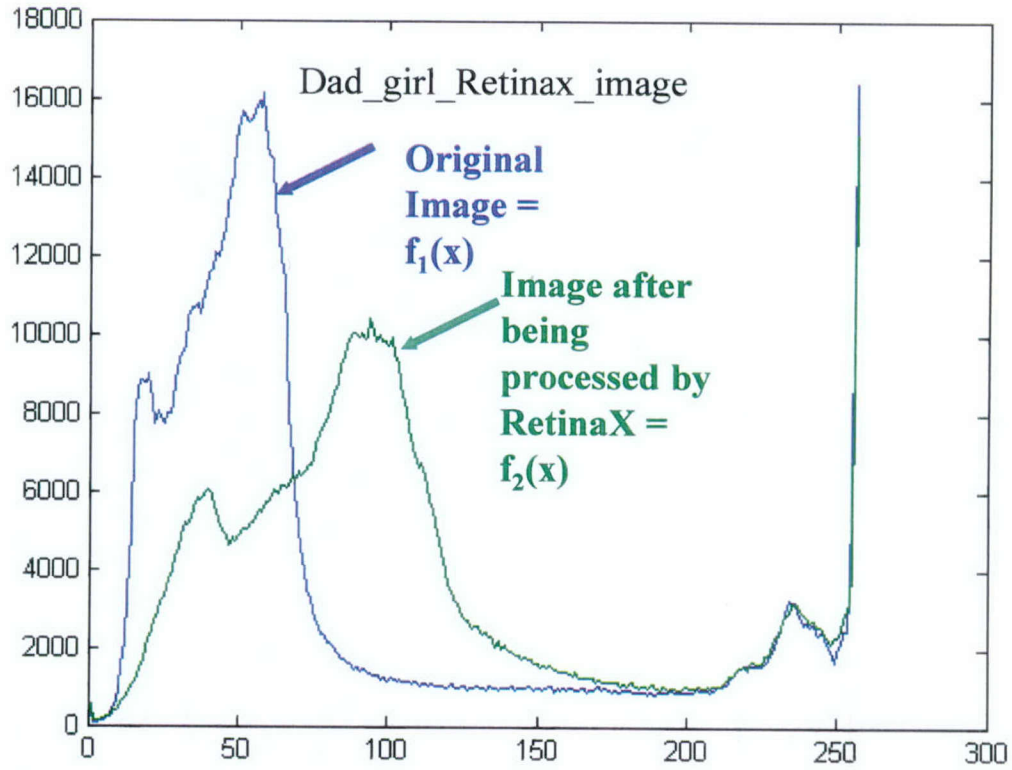

Figure 67 – Histogram Plot of the Original and RetineX Image

In Figure 67, it is noted that the original histogram distribution (called $f_1(x)$) where the x axis is the darkness level running from 0 (black) to 256 (white) for this 8 bit word representation of the darkness level of the picture. For the original image $f_1(x)$, the darkness level is too highly concentrated between the range of 10-80 gray levels. Since 0 is black, this means the original image is too dark. The image, after being processed by RetineX, however, is denoted as $f_2(x)$ and shows some similarities to the shape of $f_1(x)$, however, it is more spread out to keep the visual energy in the mid band of sensitivity (gray level $\approx$ 100 or larger). One can view the RetineX algorithm as an operation on the function $f_1(x)$ such that:

$$f_2(x) = T\,[\,f_1(x)\,] \qquad (14)$$

Where T [.] is a transformation of coordinates and $f_1(x)$ is the input function (original image) and $f_2(x)$ is the output (transformed image).

To further understand the difference induced by the RetineX transformation we now plot the difference function which is a portrayal of the difference between the two histogram functions in Figure 67.

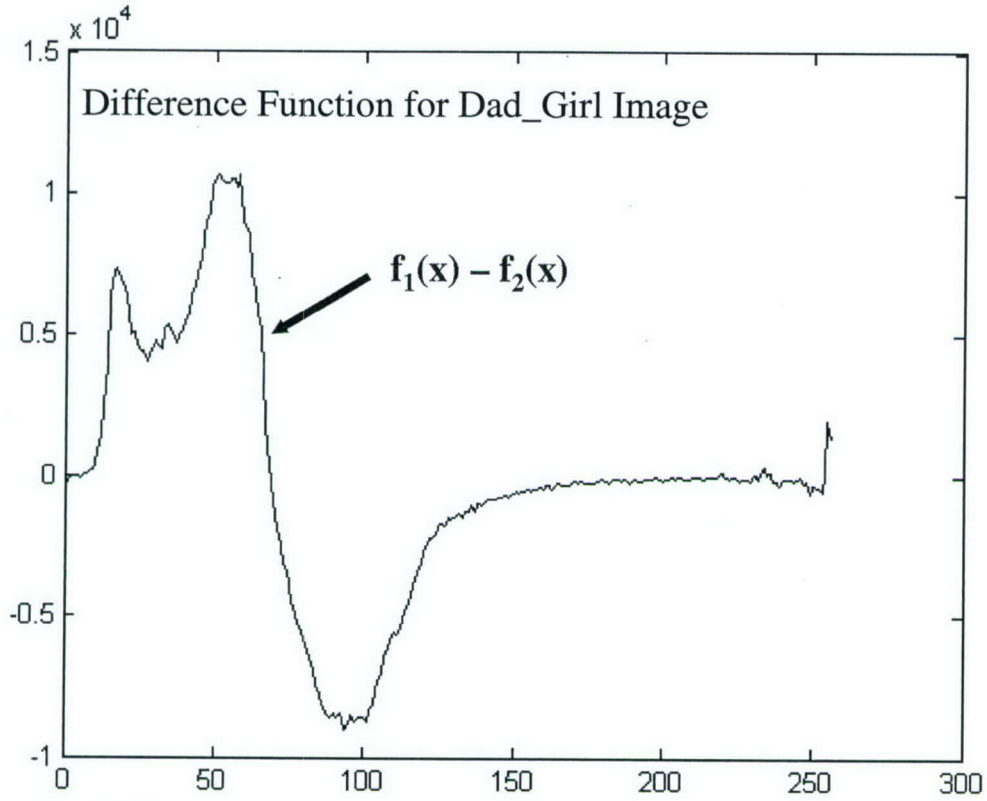

Figure 68 – Difference Function between the original and RetinaX Histograms

We now attempt to emulate the RetineX approach using a linear systems approach. In Figure 67, the input to the linear system will be $f_1(x)$ and the desired output would be $f_2(x)$. That is, we wish to emulate what is accomplished by a simple linear transfer function and we choose the form:

$$Y(s) / F_1(s) = \text{Output / Input} = k_1 (1 + s/\text{alpha}) \qquad (15)$$

Where s is the Laplace transform variable and the two series $f_1(x)$, $f_2(x)$ or $f_1(t)$ or $f_2(t)$ can be considered analogous. Equation (15) is a simple low pass filter of bandwidth alpha radians per second and forward gain of k_1. Really what is desired is to generate a template that the histograms of the revised image will follow that will emulate the algorithm developed by RetineX. We show a number of interesting plots. First a plot of the $f_1(x)$ variable (input) and y(x) for the case $k_1 = 3.1$ and alpha = 2 is displayed next.

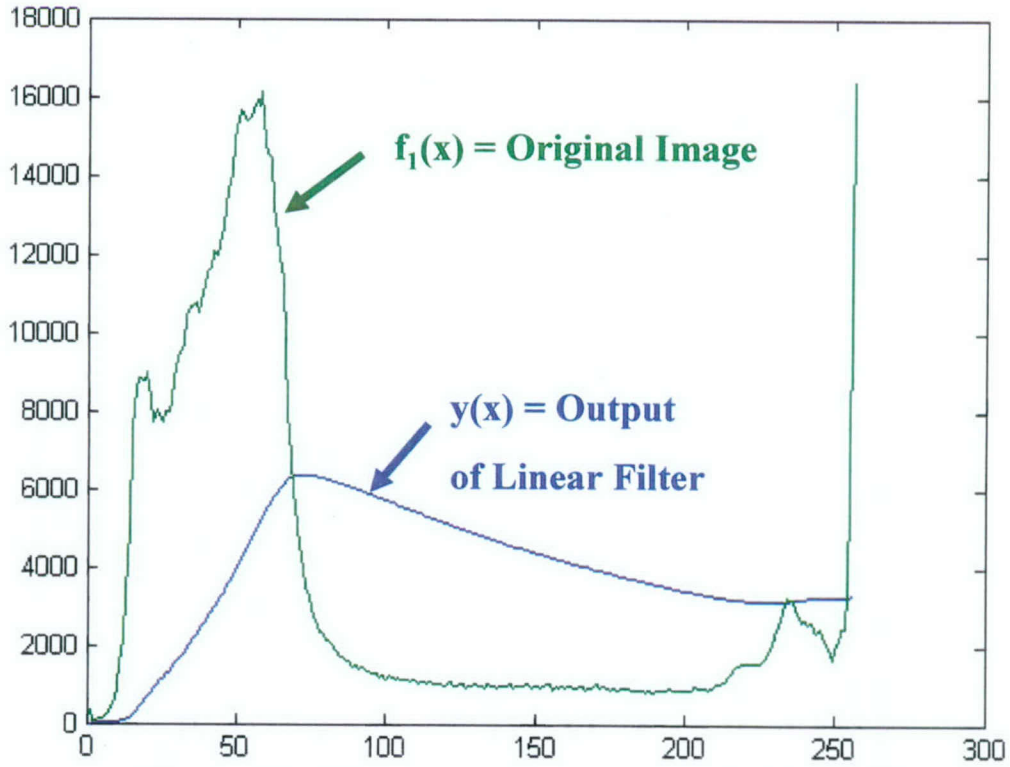

Figure 69– $f_1(x)$ versus the output of the linear filter

Next we show the difference function that results between $f_1(x)$ and $y(x)$. The goal is to emulate the true difference function between $f_1(x)$ and the RetineX algorithm.

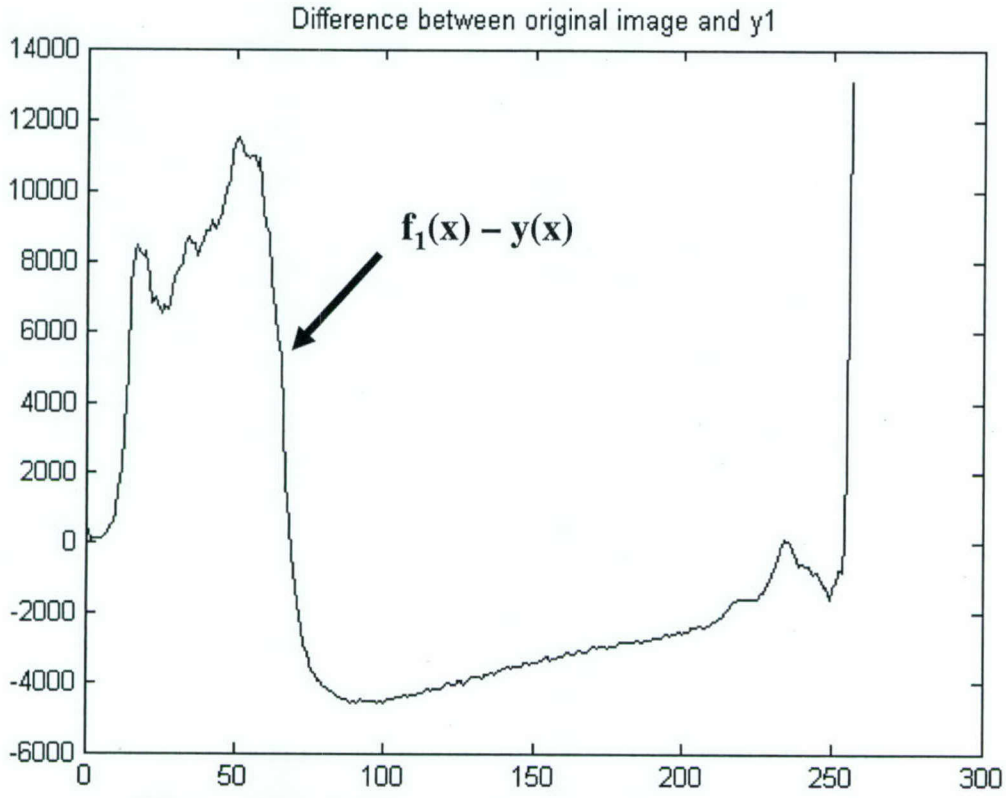

Figure 70 – Difference between $f_1(x)$ and $y(x)$.

A comparison of the two difference functions is now portrayed in Figure 71. The goal is to have similarity or overlap of the two difference functions, indicating that the choice of y(x) was an appropriate linear template.

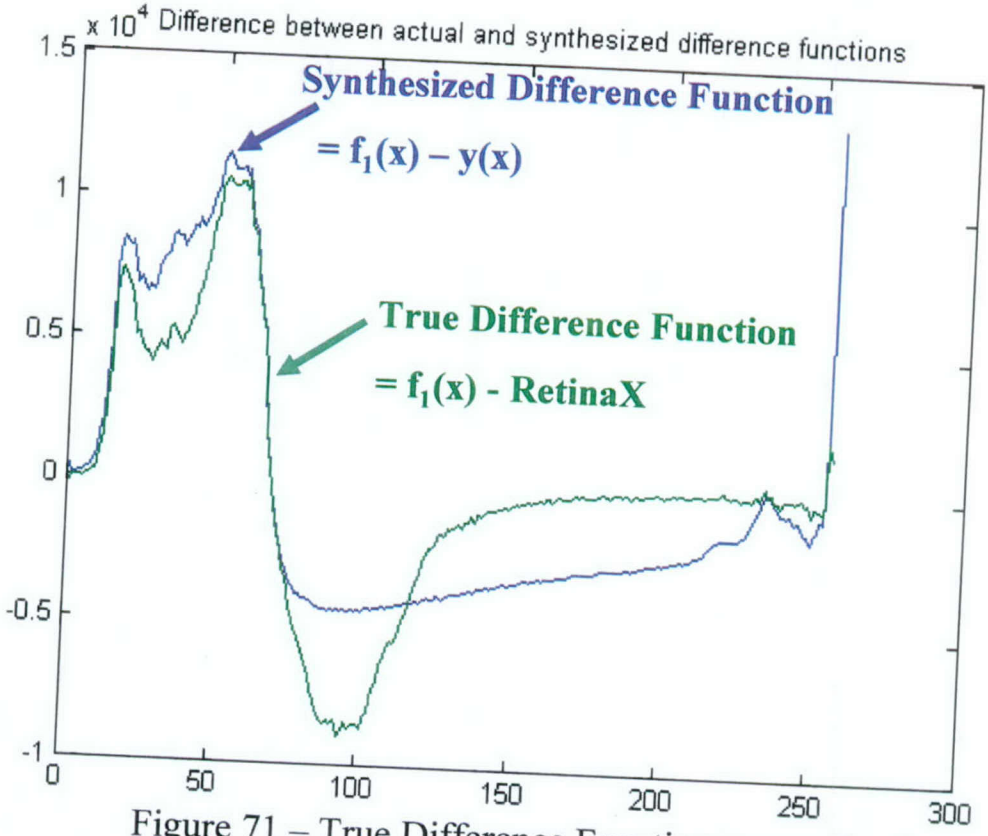

Figure 71 – True Difference Function versus Synthesized

We now show two renderings using this linear framework. Two other variables will be introduced using a simple rule based algorithm based on the following constructs:

Rule 1: If the difference function is positive, lighten all pixels that fall in this category a_1 gray levels.

Rule 2: Stretch the histogram distribution by translating it to the right "stretch" units.

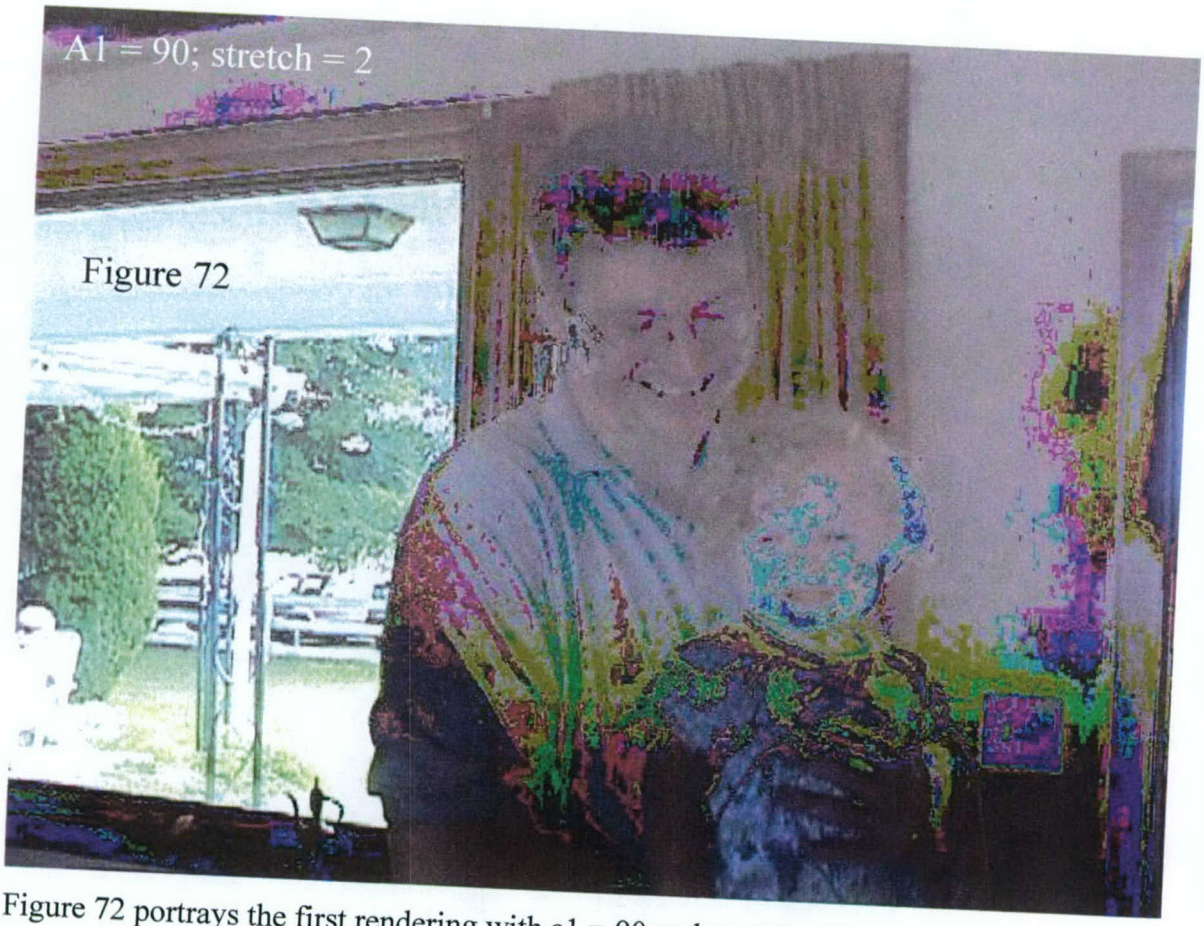

Figure 72 portrays the first rendering with a1 = 90 and stretch = 2.

Figure 73 illustrates the second rendering with a1 = 60 and stretch = 1.

In comparing Figures 72 and 73 to the true RetineX image in Figure 66, it is obvious that the solution of the problem will not be accomplished by just using a linear transformation, such as occurs in equation (15).

THE RATIONALE FOR THE SR APPROACH TO BE CONSIDERED "BIOINSPIRED"

There are three reasons why the technique considered so far may be considered to be based on biological principles or is "bioinspired." They are listed as follows with more details given below;

(1) Sufficient evidence exists that subliminal signals also exist in other biological systems and SR provides an enabling paradigm to detect signals under threshold.

(2) The nonlinear dynamics of the bipotential well (example 2 of SR previously discussed) also can represent a common illusion of visual perception termed the "Decker Cube".

(3) The RetineX theory has analogies to the parabolic templates considered in the SR procedure previously described.

We elaborate on each reason, first for the prior biological evidence:

(1) Prior biological evidence:

As studies in stochastic resonance were discussed by physicists and others, similar dynamic effects were observed in a vast number of biological systems. This theory enabled the description of how creatures could increase their sensitivity and detect subthreshold signals. This was shown for neuronal computing [39], in crayfish [40], insects [41], paddle fish [42], for improving visual acuity [43], and in a variety of other biological systems [44].

A second biological justification for the SR effect is derived as a consequence of the similarity of certain visual illusions to the dynamics of the bipotential well discussed as example 2, previously:

(2) The Similarity of the Decker Cube to the Bipotential Well Problem.

Figure 74 is an illustration of the well-known visual illusion, termed the "Decker Cube". In Figure 74, the dot can be perceived as being either in the front or on the rear of the cube. The human visual perception system will oscillate between the two states of the perception of the dot being either in the front or the back of the cube. This is very similar to the bipotential well in which the ball oscillates between two states. This hints that the nonlinear dynamics of the human visual perception system must have some similarity to the nonlinear dynamics of the bipotential well. Since the bipotential well has nonlinear dynamics that benefit from the SR effect, the generalization is that inherent in the human visual perception system, it must also have such nonlinear dynamics embedded. Thus the SR effect may benefit how humans perceive images.

Analogy to Image Processing

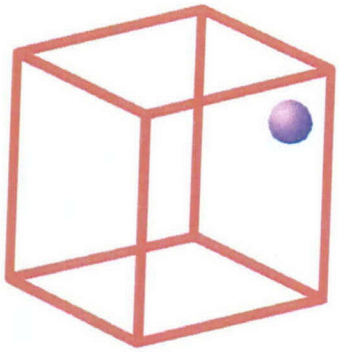

An Example of Visual Bi-stability

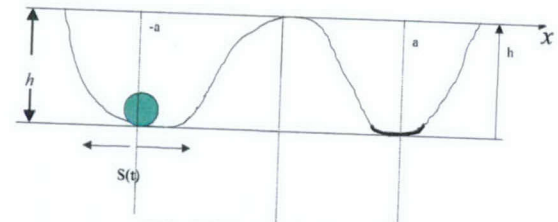

The Bi-Potential Well Problem

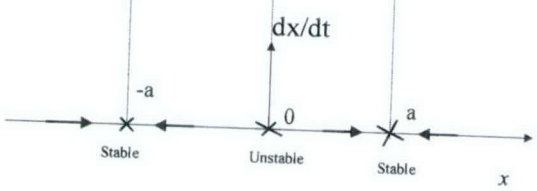

Equilibrium Points for the Physical System

Figure 74 – Relationship between the Decker Cube and The Bipotential Well Problem in Physics

(3)The RetineX Theory of Visual Perception:

As discussed earlier, the RetineX theory was introduced by E. Land as an explanation of how humans process color in a visual image. Its success is without question. It has also been discussed that the RetineX method represents a maximization of the information via the constancy of the color context in the image [38]. As noted earlier [37], in the development of the RetineX theory, the presumption was that the logarithm of the histograms of the picture pixels versus darkness density would be proportional to the form e^{-x^2} where x is the darkness level (normalized to some bit length). Taking the logarithm of the histograms would yield a parabolic relationship between histograms and gray level. This was the procedure used in the SR method in this report. Another interpretation of why a parabolic template was used was because it is also known from optical physics that the light gathering power of the eye is inversely proportional to the square of the distance from the source. This was the original reason why the parabolic rule was employed in this study.

DISCUSSION

Future work can be accomplished in the processing of visual images using computational means. The SR method appears to reduce both Type 1 and the Type 2 error described. A more sophisticated technique must be applied to manipulation of the template for the emulation of the RetineX method.

CONCLUSIONS

Two studies were conducted with computational means to process a visual image. The first method, stochastic resonance, showed the discovery of hidden objects inside the original, compromised image. The second study attempted to emulate the well known image processing software, RetineX. Although the theoretical concept seemed tenable, the results from the second method did not seem outstanding.

REFERENCES

[1] W. Klosgen and J. M. Zytkow, *Handbook of Data Mining and Knowledge Discovery*, Oxford University Press, 2002.

[2] Z. Chen, *Data Mining and Uncertain Reasoning*, John Wiley and Sons, 2001.

[3] J. Mena, *Investigative Data Mining for Security and Criminal Detection*, Elsevier Science, 2001.

[4] B. Thuraisingham, *Web Data Mining and Applications in Business Intelligence and Counter-Terrorism*, CDC Press, 2003.

[5] R. Groth, *Data Mining – Building Competitive Advantage*, Prentice Hall, 2000.

[6] B. Thuraisingham, *Data Mining – Technologies, Techniques, Tools and Trends*, CRC Press, 1999.

[7] U. Fayyad, G. G. Grinstein, and A. Wierse, *Information Visualization in Data Mining and Knowledge Discovery*, Morgan Kaufmann Publishers, Academic Press, 2002.

[8] K. Cios, W. Pedrycz, and R. Swiniarski, *Data Mining – Methods for Knowledge Discovery*, Kluwer Academic Publishers, 1998.

[9] D. Hand, H. Mannila, and P. Smyth, *Principles of Data Mining*, The MIT Press, 2001.

[10] H. Bozdogan, *Statistical Data Mining and Knowledge Discovery*, CRC Press, 2004.

[11] R. Benzi, A. Sutera and A. Vulpiana, "The mechanism of stochastic resonance,", *Journal of Physics*, **A14,** L453-458.

[12] K. Loerincz, Z.Gingl, and L. B. Kiss, "A stochastic resonator is able to greatly improve signal-to-noise ratio," *Physics Letters* **A224**, (1996), pp. 63-67.

[13] L. B. Kiss, "Possible breakthrough: Significant improvement of signal to noise ratio by stochastic resonance," *Chaotic, Fractal and Nonlinear Signal Processing* (AIP Press, NY), 1996, pp. 382-387.

[14] Francois Chapeau-Blondeau, "Input-output gains for signal in noise in stochastic resonance," *Physics Letters,* **A232** (1997), pp. 41-48

[15] Francois Chapeau-Blondeau, "Periodic and Aperiodic Stochastic Resonance with Output Signal-to-noise ratio exceeding that at the input," *International Journal of Bifurcation and Chaos*, **9** (1), (1999), pp. 267-272.

[16] Steven Kay, "Can Detectability be Improved by Adding Noise?", *IEEE Signal Processing Letters*, **7** (1), January, 2000, pp. 8-10.

[17] H.-P. Muller, E. Kraft, A. Ludolph, and S. N. Erne, "New Methods in fMRI Analysis," *IEEE Engineering in Medicine and Biology Magazine*, September/October 2002, pp. 134-142.

[18] E. Bayram, Y. Ge, and C. L. Wyatt, "Confidence-Based Anisotropic Filtering of Magnetic Resonance Images," *IEEE Engineering in Medicine and Biology Magazine*, September/October 2002, pp. 156-160.

[19] B. P. Sutton, D. C. Noll, and J. A. Fessler, "Fast, Iterative Image Reconstruction of MRI in the Presence of Field Inhomogeneities," *IEEE Trans. on Medical Imaging*, **22**(2), Feb. 2003, pp. 178-188.

[20] Z. Xu and A. K. Chan, "Encoding with frames in MRI and analysis of the signal-to- noise ratio," *IEEE Trans. of Medical Imaging*, **21** (4), April, 2002, pp. 332-342.

[21] M. N. Ahmed, S. M. Yamany, N. Mohamed, A. A. Farag, and T. Moriarty, "A modified fuzzy C-Means algorithm for bias field estimation and segmentation of MRI data," *IEEE Trans. on Medical Imaging*," **21** (3), March, 2002, pp. 193-199.

[22] C. Nikou, F. Heitz, J-P Armspach, I-J Namer, and D. Grucker, "Registration of MR/MR and MR/SPECT Brain Images by Fast Stochastic Optimization of Robust Voxel Similarity Measures," *Neuroimage*, **8**, 1998, pp. 30-43.

[23] C-P Lin, W-Y I. Tseng, H-C Cheng, and J-H Chen, "Validation of Diffusion Tensor Magnetic Resonance Axonal Fiber Imaging with Registered Manganese-Enhanced Optic Tracts," *Neuroimage*, **14**, 2001, pp. 1035-1047.

[24] M. Riani and E. Simonotto, "Stochastic Resonance in the Perceptual Interpretation of Ambiguous Figures: A Neural Network Model," *Physical Review Letters*, **72** (19), May 9, 1994, pp. 3120-3123.

[25] E. Simonotto, et al., "MRI studies of visual cortical activity during noise stimulation," *Neurocomputing*, **26-27** (1999), pp. 511-516.

[26] G. P. Harmer, B. R. Davis, and D. Abbott, "A review of stochastic resonance: circuits and measurement," *IEEE Trans. on Instrumentation and Measurement*, **51** (2), April, 2002, pp. 299-309.

[27] F. Vaudelle, J. Gazengel, and G. Rivoire, "Stochastic resonance and noise-enhanced transmission of spatial signals in optics: the case of scattering," *J. Opt. Soc. Am.*, **15** (11), November, 1998, pp. 2674-2680.

[28] B. Kosko and S. Mitaim, "Stochastic resonance in noise threshold neurons," *Neural Networks*, **16** (2003), pp. 755-761.

[29] M. Piana, M. Canfora, and M. Riani, "Role of noise in image processing by the human perceptive system," *Physical Review E*, **62** (1), July, 2000, pp. 1104-1109.

[30] R. Stoop, J. Buchli, G. Keller, and W-H Steeb, "Stochastic resonance in pattern recognition by a holographic neuron model," *Physical Review E*, **67**, 2003, pp. 061918-1-061918-6.

[31] E. Simonotto, M. Riani, C. Seife, M. Roberts, J. Twitty, and F. Moss, "Visual perception of stochastic resonance. *Physical Review Letterers*, **78,** 1997, pp.:1186-1189.

[32] T. Yang, "Adaptively optimizing stochastic resonance in visual systems. *Physics Letters A.*, **245**, 79-86, 1998.

[33] D. W. Repperger, et al., USAF Invention # AFD-0683, "Highly Sensitive Nonlinear Target Recognition Device Based on Principles of Potential Energy and Force," November 13, 2003.

[34] T. M. Cover and J. A. Thomas, "*Elements of Information Theory*," 1991, John Wiley & Sons, Inc.

[35] E. H. Land, "The Retinex Theory of Color Vision," *American Scientist*, **52**, 1964, pp. 247-264.

[36] E. H. Land, "Recent Advances in Retinex Theory and Some Implications for Cortical Computations: Color Vision and the Natural Image," *Proc. of the National Academy of Sciences*, USA, **80,** pp. 5163-5169, August, 1983.

[37] E. H. Land, "An Alternative Technique for the Computaton of the Designator in the Retinex Theory of Color Vision," *Proc. of the National Academy of Sciences*, **83**, pp. 3078-3080, May, 1986.

[38] B. Thompson, Z. Rahman, and S. Park, "A Multiscale Retinex for Improved Performance in Multispectral Image Classification," *Visual Information Processing IX*, S. K. Park, Z. U. Rahman, Editors, *Proceedings of the SPIE*, **4041**, 2000

[39] M. Volgushev and U. T. Eysel, "Noise Makes Sense in Neuronal Computing," *Science*, 8 December, 2000, pp. 1908-1909.

[40] J. K. Douglass, L. Wilkens, E. Pantazelou and F. Moss, "Noise Enhancement of Information Transfer in Crayfish Mechanoreceptors by Stochastic Resonance," *Nature*, **365**, 1993, pp. 337-340.

[41] J. E. Levin and J. P. Miller, "Broadband Neural Encoding in the Cricket Cercal Sensory System Enhanced by Stochastic Resonance," *Nature*, **380**, 1996, pp. 165-168.

[42] D. F. Russell, L. A. Wilkens and F. Moss, "Use of Behavioral Stochastic Resonance by Paddel Fish for Feeding," *Nature*, **402**, 1999, pp. 291-294.

[43] M. H. Henning, J. J. Kerscher, K. Funke and F. Worgotter, "Stochastic Resonance in Visual Cortical Neurons: Does the Eye-Tremor Actually Improve Visual Acuity," *Neurocomputing*, **44-46**, pp. 115-120, 2002.

[44] J. J. Collins, C. C. Chow, and T. T. Imhoff, "Stochastic Resonance without Tuning, *Nature*, **376**, pp 236-238, 1995.

[45] T. S. Parker and L. O. Chua, *Practical Numerical Algorithms for Chaotic Systems*, Springer-Verlag, Chapter 3.

APPENDIX: – TECHNICAL ISSUES REGARDING THE NONLINEAR TARGET DETECTION ALGORITHM

With reference to the physics example (example 2) of SR, the potential energy function V(x) can be expressed as:

$$V(x) = -\tfrac{1}{2} a x^2 + \tfrac{1}{4} b x^4 \qquad (A.1)$$

Where $a > 0$ and $b > 0$.

This satisfies the boundary conditions: $V(0) = 0$, $V(\pm\infty) = +\infty$ (A.2)

From Newtonian dynamics, force is the negative spatial gradient of potential energy, i.e.

$$\text{Force} = -\, d/dx\ V(x) \qquad (A.3)$$

This yields:

$$\text{Force} = a x - b x^3 \qquad (A.4)$$

If the state vector x(t) were velocity and a unit mass M was assumed, it then follows from Newton's second law that in the time domain:

$$d/dt\ x(t) = \text{Force} \qquad (A.5)$$

or

$$d/dt\ x(t) = a x - b x^3 \qquad (A.6)$$

This is the homogenous version of the SR equation. For the forced form of equation (A.6) we have:

$$d/dt\ x(t) = a x - b x^3 + S(t) + \eta(t) \qquad (A.7)$$

where $S(t)$ is the subliminal signal to be identified and $\eta(t)$ is a white Gaussian noise source. The equilibrium points of the homogenous equation (A.6) are of interest.

Equilibrium Points of Equation (A.6):

Please note that the term "equilibrium point" will be considered akin with the terms "fixed point", "singular point", or "steady state point".

For the homogeneous equation (A.6), in steady state, this results in:

$$0 = a\,x\,(1 - b/a\,x^2) \qquad \text{(A.8)}$$

which has roots at x = 0, and $x = \pm \sqrt{\frac{a}{b}}$. Since both a and b are positive, we next demonstrate that the equilibrium point near x = 0 is unstable. Let $\varepsilon > 0$ be small.

To show that x = 0 is an unstable equilibrium point:

For $x = \varepsilon > 0$, equation (A.6) becomes $d/dt\ x(t) \approx a\,(x)\,(1) > 0$. Hence the trajectory diverges to the right away from the equilibrium point x = 0.

For $x = -\varepsilon < 0$, equation (A.6) becomes $d/dt\ x(t) \approx a\,(x)\,(1) < 0$. Hence the trajectory diverges to the left away from the equilibrium point x = 0. Thus x = 0 is an unstable equilibrium point.

To show that x = + a is an stable equilibrium point:

For $x = a + \varepsilon > 0$, equation (A.6) becomes $d/dt\ x(t) \approx a\,(x)\,(1 - [(b/a)\,(a+\varepsilon)]^2) < 0$. Hence the trajectory converges to the left towards the equilibrium point x = a.

For $x = a - \varepsilon > 0$, equation (A.6) becomes $d/dt\ x(t) \approx a\,(x)\,(1 - [(b/a)\,(a-\varepsilon)]^2) > 0$. Hence the trajectory converges to the right towards the equilibrium point x = a. Thus x = a is an stable equilibrium point.

The same arguments apply for x = -a which is also a stable equilibrium point.

We next discuss Lyapunov exponents, which helps clarify the relationship between the SR filter and possible chaotic behavior.

Relationship to Lyapunov Exponents:

Given a nonlinear system with an equilibrium point at x_0 where:

$$\dot{x}(t) = f(x(t)) \qquad \text{(A.9)}$$

Near an equilibrium point (x_0), for y values in the neighborhood of x_0, a Taylor series expansion of $f(y)$ is made:

$$f(y) = f(x_0) + (y - x_0)\frac{df}{dx} + \frac{1}{2}(y - x_0)^2 \frac{d^2 f}{dx^2} + \frac{1}{6}(y - x_0)^3 \frac{d^3 f}{dx^3} + \ldots \qquad \text{(A.10)}$$

where all derivatives are evaluated at $x = x_0$. For the equilibrium point the term $f(x_0)=0$.

Define a new variable $z = y - x_0$, which measures the distance of the trajectory away from the equilibrium point. If we neglect all derivatives of order higher than the first, then z satisfies the following equation:

$$\dot{z}(t) = \frac{df}{dx}\Big|_{x_0} z(t) \qquad \text{(A.11)}$$

which has a solution of the form:

$$z(t) = z(0)\, e^{\lambda t} \qquad \text{(A.12)}$$

where

$$\lambda = \frac{df(x)}{dx}\Big|_{x=x_0} \qquad \text{(A.13)}$$

is the Lyapunov exponent. Thus near the equilibrium point, the trajectories either grow away from (diverge) or converge toward the equilibrium point, depending on the sign of λ. If $\lambda > 0$, then we have divergence of nearby trajectories. If $\lambda < 0$ we have convergence of nearby trajectories. Thus the sign of λ determines this behavior. The magnitude of the value of λ may be a factor on the rate of convergence and divergence of adjacent trajectories. In short, the Lyapunov exponent is the eigenvalue of the Jacobian evaluated at the equilibrium point. This can be viewed as a nonlinear construct borrowing heavily from concepts embedded in linear system theory.

Relationship of the SR Method to Chaos Theory:

It should be made clear that the results presented so far for this SR filter do not put it into the realm of chaotic systems. In short, chaotic systems are globally stable but have local instability near equilibrium points. Without proof we list the following key facts about chaotic systems [45] which clearly show that the SR filter does not fit into this category:

(1) The minimum order of a chaotic system is third order. The SR filter is only a first order nonlinear dynamical system.

(2) For a third order system, a necessary condition for chaotic behavior is that at least one Lyapunov exponent is positive. The sum of the Lyapunov exponents must be negative.

(3) For a fourth or higher order system, the existence of one positive Lyapunov exponent is a sufficient condition for the existence of chaotic behavior.

The Lyapunov Exponents for the SR Filter:

From equation (A.6), the following Lyapunov exponents are easily derived.

At $x = 0$ $\lambda_1 = a$ (A.14)

At $x = \pm \sqrt{\frac{a}{b}}$ $\lambda_2 , \lambda_3 = -2a < 0$ (A.15)

Thus one positive Lyapunov exponent exists, but since the SR filter is only of first order, then it cannot exhibit chaotic behavior. Note also that the sum the three Lyapunov exponents is negative (- a), which ensures a stable system.

Unsolved Technical Problems to be Addressed:

From the prior discussion, a number of interesting problems need to be examined to observe how the performance of the SR filter can be manipulated.

Problem 1:

For the bipotential well problem, the value of threshold h can be stated in terms of the V function, i.e. $h = V(0) - V(a)$ if x has an equilibrium point at $x = a$. There must be a strong relationship between the value of h, the maximum value of $|S(t)|$ and the variance of the noise process $\eta(t)$. Understanding the relationship between these three key variables will enable the user to better understand how to operate at the optimum point in the SR curve of Figure 9. There must be an important dependence between these three variables.

Problem 2:

In the discussion on the RetineX study, it was demonstrated that this algorithm stretched out the pixel distribution from a narrow distribution to more of a full distribution across a wider range of the gray levels. An attempt was made to treat $f_1(x)$ analogous to a time series and $f_2(x)$ as an output time series using linear transfer function analysis. To formulate this as a mathematical problem, let $f_1(x)$ be the original distribution of gray levels, which needs to be stretched, yet maintain the same area. Perform some operation of $f_1(x)$, e.g. a transformation of coordinates or differential equation operation so that:

$$F_2(x) = T [f_1(x)] \quad \text{(A.16)}$$

Where the transformed variable $F_2(x)$ will have approximately the same area as f_1, but have its energy stretched out over the midpoint of the gray level distribution. This maximizes the ability

of humans to perceive images that are too dark and cannot be understood. If the transformation operator T[.] could be a differential equation, then it could be implemented in hardware, thus reducing the computational burden now seen in applying the SR method to image enhancement.

Problem 3:

In chaotic systems, the Lyapunov exponent determines the degree of chaotic behavior. Even though the SR system does not exhibit chaotic behavior, it still has a positive Lyapunov exponent. How does the performance of the system vary as a function of the Lyapunov exponent of the SR system?

Problem 4:

The RetineX method is well known and respected as a standard to enhance image processing. The difference function shown in Figure 68 shows what must be accomplished to realize the same effect as the RetineX method. In an approach similar to problem 2, the goal would be to produce a difference template similar to Figure 68 using linear, or any nonlinear type of transformation on the original distribution of gray levels.

One may pick a particular nonlinear model and find choices of parameters to generate a difference template similar to Figure 68 for a given $f_1(x)$ input function (treating it as a time series or in the spatial domain).

Problem 5:

The questions of what particular SR transformations yield the best SNR is not understood. Using the procedure as described in this report to measure SNR gain as a function of the number of G FLOPS, the Lyapunov exponent λ or any other parameters is an open question. In short, use the SNR as the metric of quality improvement.

Problem 6:

In Figure 9, it is desired to operate at the top of the resonance curve. There must be some way to design system parameters to find the optimal amount of noise power or the optimum number (N) of pixels to be moved for a given image problem. Again, this may depend, specifically, on each image considered.